Estimation of gadolinium concentration in MRI using the recalled echo signal

Georgios   I.Kalaitzakis

Department of Electronics and Computer Engineering
Technical University of Crete

Dissertation Thesis Committee:
Michail Zervakis, Professor (Supervisor)
Konstantinos Marias, Principal Researcher (FORTH)
Konstantinos Balas, Assistant Professor

2014

Abstract

Dynamic Contrast Enhanced Image, is widely used to examine the possible tumors, using Gadolinium based Contrast Agent. The aim of this work, is to estimate pre-contrast spin lattice relaxation time (T_{10}), and the equilibrium magnetization (S_0), in order to measure Gadolinium Concentration. For this reason an analytic method is proposed, to solve a constrained fitting problem, on the experimental data. Semiquantitative parameters, are calculated for both Signal Intensity and Gadolinium Concentration, to examine the perfusion and the possible carcinoma. In order to validate the results, the brain region of Gray and White Matter was used, where we have a more typical behavior (values).

Contents

List Of Figures

List Of Tables

Acknowledgments

Chapter 1

Introduction

1.1 Background

It is a fact, that cancer is a leading cause of death worldwide, accounting for 7.6 million deaths (around 13% of all deaths) in 2008. It is estimated that in 2030, 13.1 million deaths will be caused from cancer worldwide.[3]

In that way, the Magnetic Resonance Imaging (MRI) has become essential to the clinical management of many tumor types. This is because the diagnosis, but also the classification of tumors has benefited from its ability to demonstrate tumor morphology and the relationships of malignant lesions to neighbouring structures. This has lead to improvements in both clinical management and surgical planning, because MRI enables clear delineation of normal anatomical structures and organs, and most of the time clearly delineating and identifying pathological change. Moreover, acquiring multiplanar images or volume acquisitions is valuable for the clinician, to appreciate in a true three dimensional, the tumor and tissue morphology [1].

1.2 MRI-Basic Principles

The MR Imaging, is based upon the measuring of the spatial distribution of nuclei. These nuclei are excited, using a Radiofrequency (RF) pulse and they produce electric signals from their spins. The interval time between those excitation RF pulses, consists the **Repetition Time (TR)**.The angle of the excitation, is called flip angle (**FA**), and is the angle that the nuclei are precessing about, from the direction of the static magnetic field, [4] at a specific frequency(Larmor precession frequency).

These nuclei, in absent of magnetic field, have a random distribution of direction. In the presence of an external magnetic field, their spins, are parallel or anti-parallel with the field. With the application of a RF pulse, the nuclei with the same frequency(Larmor Frequency) as the RF, respond and precess furthermore. With their return to equilibrium state, there is emission of energy. Each of these precessions, create a magnetic field, and the sum of all these fields, is called net magnetization. The net magnetization, as a vector of spinning protons, is consisted by the longitudinal and the transverse component. The longitudinal magnetization, is caused by the difference in the number of spins, in parallel and anti-parallel, and the transverse magnetization, is due to spins getting into phase. Each of these magnetizations, has a relaxation time, a return to equilibrium of net magnetization.[5]

There are two types of relaxation times for those protons. **T1-relaxation time**, which is the spin-lattice relaxation time, and consists the time that is required for the nuclei's longitudinal magnetization to return to thermodynamic equilibrium state(initial state).**T2- relaxation time**, which is the spin-spin relaxation time, and consists the time of nuclei's transverse magnetization, to return to thermodynamic equilibrium state(initial state), as a summation for each nuclei. Each **voxel**, which means the pixel in a specific slice thickness of the image, can be characterized by each relaxation time. [4,5]

The values of T1 relaxation times, depend not only on the kind of tissue, but also on the strength of magnetic field that is applied. On the other hand, the values of T2 relaxation, are more or less, independent from **Magnetic Field (T).** In most cases, a magnetic field of 1-3 Tesla, is being used, and the higher the magnetic field, the higher the T1 values acquired, compared to those of a magnetic field of strength 1.5 T [2].

Another important thing in MRI, are the sequences. The **Spin echo sequence** (**SE**), and the **Gradient Echo Sequence** (**GRE**), are used commonly. In order to explain these sequences, we have to define the **Echo Time (TE)**, which is the interval time between the application of RF pulse, until the peak of the Signal that is produced. The SE is the result, after applying, at first a 90° RF pulse, and then at TE/2 time a 180° RF pulse. Gradient Echo Sequence differs from the Spin Echo Sequence, in the degrees of RF pulse, and in the absence of the second (180°) pulse[4]. Also, another sequence used in diagnostics, [26] is the **Inversion Recovery**, where we have an initial excitation of the protons, with a 180° RF pulse, before the application of the two others (90° and 180°). The interval time, between the 180° pulse, and the 90° pulse, is called **Inversion Time (TI)**.

In the case of GRE, RF pulses of lower angles (most commonly angles lower of 90°) are used. Thusly, that means, we have smaller flip angles of rotation, for the spins. The Gradient Echo precession Sequence, is faster than the Spin Echo Sequence, because the Repetition Time, between the RF pulses is smaller.

Depending on the Repetition time (TR-distance between two successive 90° RF pulses), for a spin echo image, we acquire different contrast. With a low TR (usually lower than 500ms), and low TE, (usually lower than 50ms), we have T1-weighted Image, and with higher TR, and a higher TE, we have a T2-weighted image. In T1-weighted image, areas with long T1, appear dark in the T1W-image, whereas areas with short T1, appear brighter in the T1W-image. On

the other hand, if a higher TR,TE, are chosen, that means we have T2-weighted image. In that case, we have areas with long T2, to appear brighter in the T2W-image, and areas with shorter T2, to appear darker in the T2W-image. [5, 25]

Proportionally, for a Gradient-Echo image, depending on the Flip angle (FA), and TE, we acquire different contrast on image. With a large flip angle(usually larger than 50 °), and a short TE (less than 15ms), we have a T1-weighted image and with a smaller flip angle (40 °), and a larger TE (more than 30ms), we have T2*-weighted image. In this kind of images, TR is usually short(less than 750ms), comparing with the Spin echo image. [25, 26] In a Gradient-Echo image, we see the combined effect of T2 and magnetic field inhomogeneites. This relaxation T2* is known as 'apparent' relaxation time and take into account the magnetic field inhomogeneities [26].

Finally, on the other hand [25, 26] , for a spin echo image, with a combination of long TR(more than 1500ms), and a short TE (less than 40ms), we acquire a Proton Density Image (PD), which is related to the number of hydrogen atoms. In true PD, fluids usually have higher signals. For a gradient echo image, PD images, are the results, of a small flip angle(less than 40 °), and short TE (less than 15ms).

1.3 T1W-Dynamic Enhanced-MRI

In order to improve the results of MRI image, contrast medias are used widely. Most commonly used contrast agents are gadolinium-based. They have the ability to reduce (Paramagnetic Gadolinium-Gd) the spin-lattice relaxation time T1- relaxation time and as a result to enhance the signal intensity in those cases [27].This is significant because most types of lesions and tumors in T1-weighted images have high signal intensity.

With this improvement, we have a new type of MRI, the Dynamic-Contrast Enhanced MRI, which can give us useful information about the administrated contrast agent wash-in, wash-out, but also about tissue perfusion and volume of extravascular-extracellular space[6]. This administration could be oral or itravenous.

Moreover, the distribution of the contrast agent in the body is indicative of certain physiological and pathological processes. Each contrast agent has a relaxivity constant (**r1**), that means the ability to change relaxation times,[27] at a specific concentration.

Thus, instead of acquisition of only one image with enhancement, a series of images is acquired during the distribution of bolus. The kinetics of the contrast agent inside the body leads to a change in Signal Intensity S(t) of the image, at each time point [6].

The behavior and the acquisition of Signal Intensities S(t) over time, are depicted in the figure below.
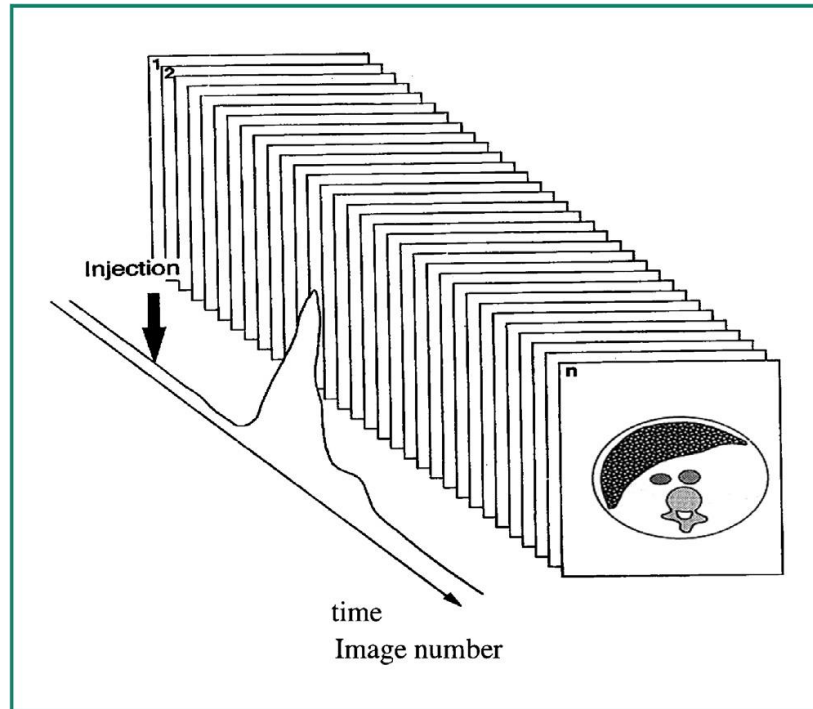
Figure 1.1: Behavior of Signal Intensities S(t) over time. Sequential acquisition dynamic contrast-enhanced imaging from [18]. Acquisition must begin before the start of injection to obtain reference image without contrast agent (baseline). Then continues after the injection.

It can be noticed from the figure above that Signal Intensity S(t) changes over time, and therefore is a function of Contrast Agent concentration in the body, until its total wash out. Furthermore, as we mentioned before the paramagnetic contrast agents, have the ability to reduce the relaxation time T1. So, as the contrast agent is distributed into the body and leaks, the relaxation time T1 changes over time at each voxel and for each time point we have a different relaxation time according to equation 2.2.

There are three typical curves of enhancement for the signal intensity according to bibliography [28]:

- The first type (I) is characterized by persistent enhancement over time.

- The second (II) by a wash-in and then plateau.

- The third (III) by an increased wash-in and then wash-out of the enhancement signal.
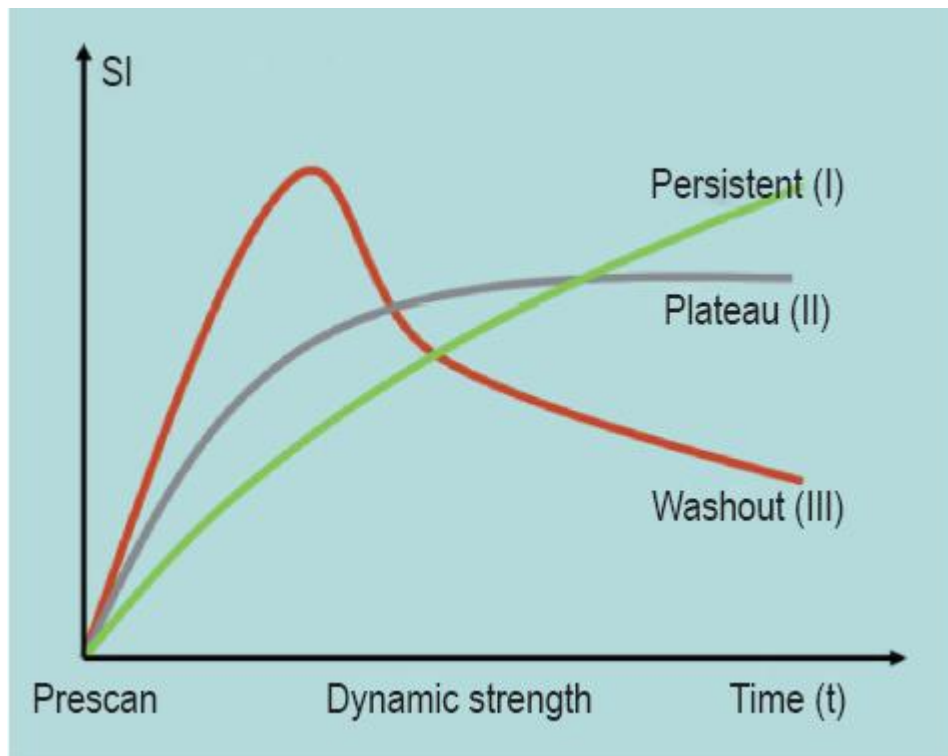
Figure 1.2: The three types of Signal Intensity, theoretically, adapted from [28].

According to the literature [19], the first type of curve (persistent increment), correspond in most cases, to benign lesions. Malignant tumors, are usually reminiscent of type (III) enhancement.

In our data, these three typical curves have the following behavior:
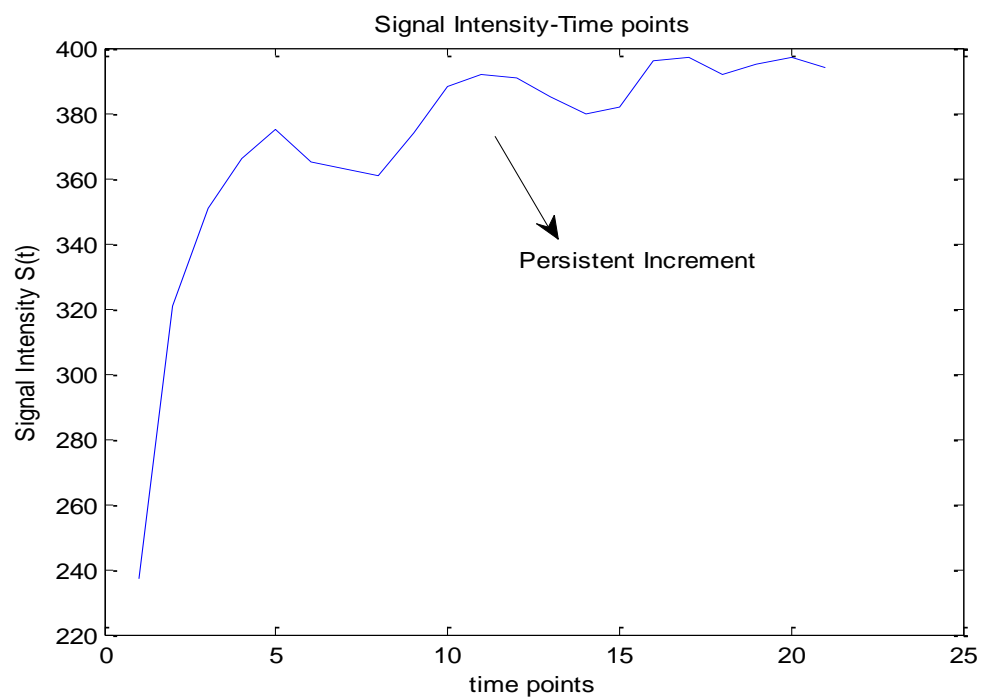
Figure 1.3: Persistent increment (Type I) of Signal Intensity from experimental data
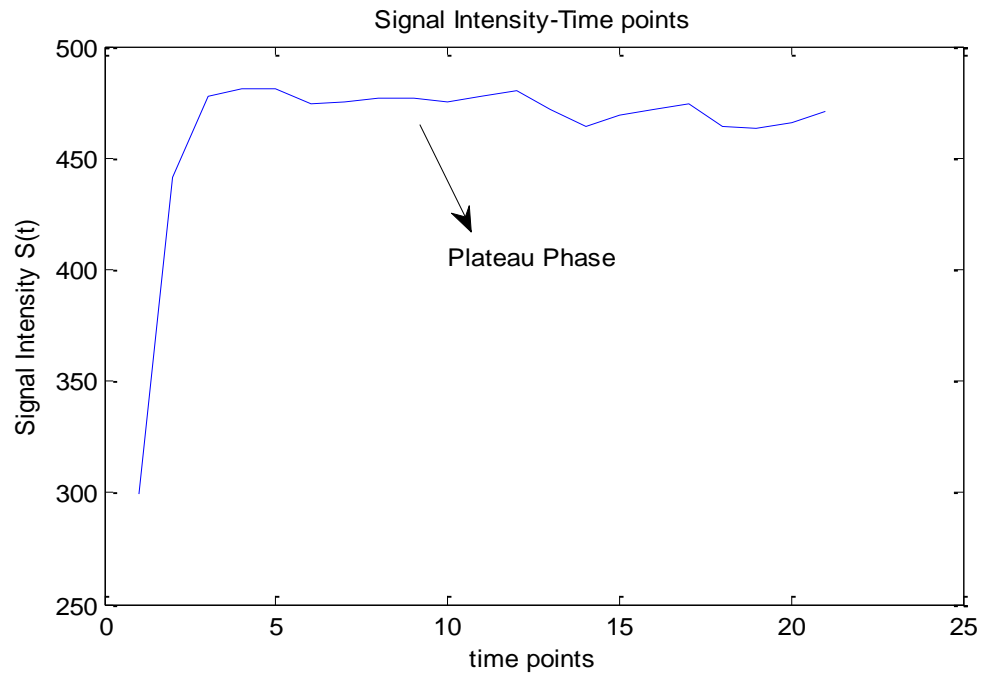
Figure 1.4: Plateau type (II) of Signal Intensity from experimental data
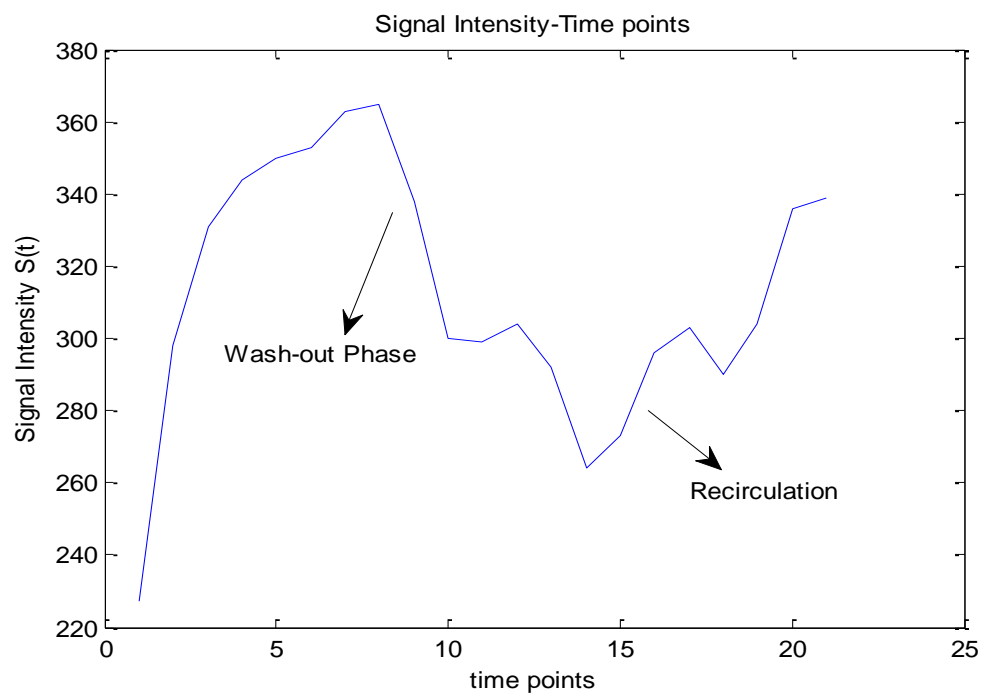
Figure 1.5: Washout type (III) of curve of Signal Intensity from experimental data

1.4 Pharmacokinetic Principles

Tumors can be categorized as malignant, or benign according to their relationship with their neighbouring [11].

More specifically, benign tumors are not cancerous, and they do not invade in neighbouring, so they grow only locally.
On the other hand, malignant tumors, are cancerous. Their growth depend on their ability to stimulate neighbouring cells, in order to initiate formation of new blood vessels inside the tumor, and supply it with oxygen and nutrients, that are essential for its existence.
This is a process, commonly known as angiogenesis [1 ,13].

Basically, angiogenesis is based upon the releasing of molecules, from cancerous tumour cells, that send signals to surrounding normal tissues, in order to activate certain genes, to make proteins, that encourage the growth of new vessels. Consequently, a new blood capillary is formed, simply by the sprouting of an endothelial cell from the wall of an existing vessel, creating some kind of tube between the new vessels, so that the blood can circulate. [1]

The tracer, which in the case of intravenous contrast agent, is crossing the vessel, leaks into the extravascular-extracellular space (EES, leakage space), and by that time we have an increment in the wash-in phase of Signal Intensity. Then it is starting diffusing back into the vasculature, which is observed as a wash-out on the Signal Intensity [1]. In some cases, the contrast agent recirculates, so a second peak is observed, but smaller this time, and is eliminated slowly [18]. Similar behavior, is observed in the Concentration Curve, and can be seen in the figures below (Fig 1.7-1.9).

The above kinetic behavior, is based on Fick's first law, which describes the diffusion of the molecules. According to this, the molecules move from regions with higher concentration, to regions with lower concentration [18]. For these reasons the study of concentration of agent and its changes in time become of particular significance.

The figure below indicates the behavior of the contrast agent molecules, inside the blood vessel and the surrounding extravascular tissue. The Permeability-surface area (PS), is the flow of molecules through the capillary membranes in a certain volume of tissue.[18]
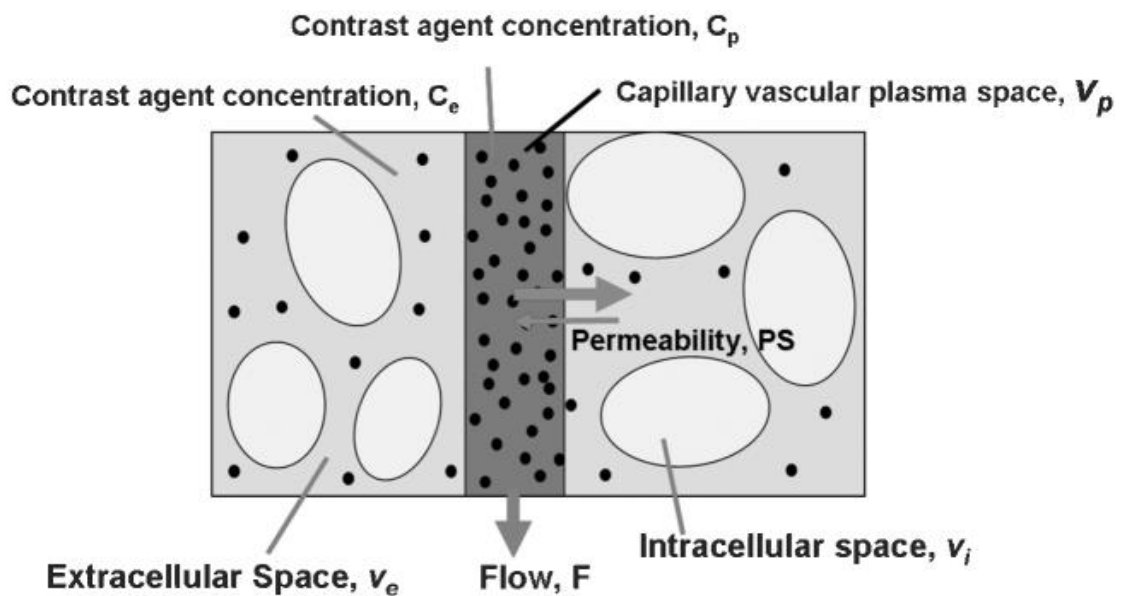
Figure 1.6 Distribution of contrast agent, in an individual voxel of tissue adapted from literature [23]. The bold dots, are the contrast agent's molecules. The leakage of these molecules, is determined by the concentration difference between the plasma, v_p and the extracellular space, v_e, and also by the permeability and surface area of the capillary endothelia, PS. The available contrast agent does not leak into the intracellular space, v_i. [24]

More specifically, the three typical curves of Gadolinium Concentration, relative to the Signal Intensity Curves of Figures 1.3-1.5 are:
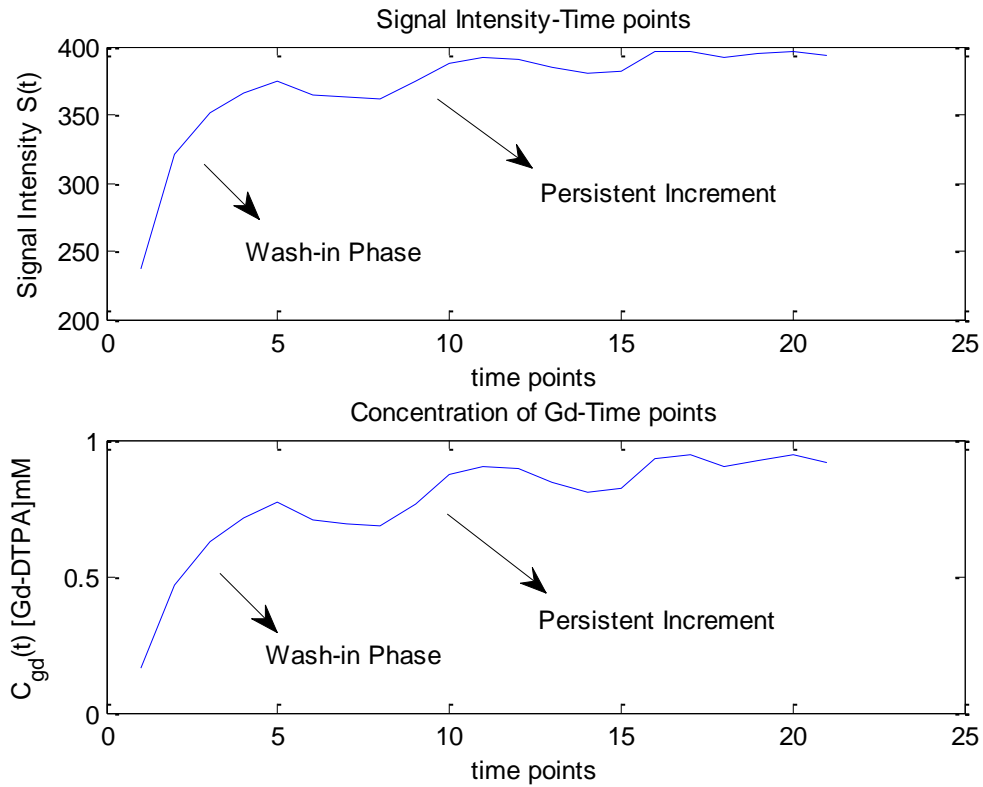
Figure 1.7: Estimated Curve (Type I) of Gadolinium Concentration with the optimal S0=3522, and T10=0.9s. The first figure correspond to the experimental Signal Intensities S(t) over time, and the second figure is the Concentration over time C(t), extracted from this task. In this type of curve, while the molecules of contrast agent leak intro the EES space, we have an increment in the signal of both Signal Intensity S(t) and Gadolinium Concentration C(t), which starts as a wash-in and has persistent increment. This increment now, continues persistently, because the leakage is continuous. The capacitance of EES in this kind of tissues is increased.
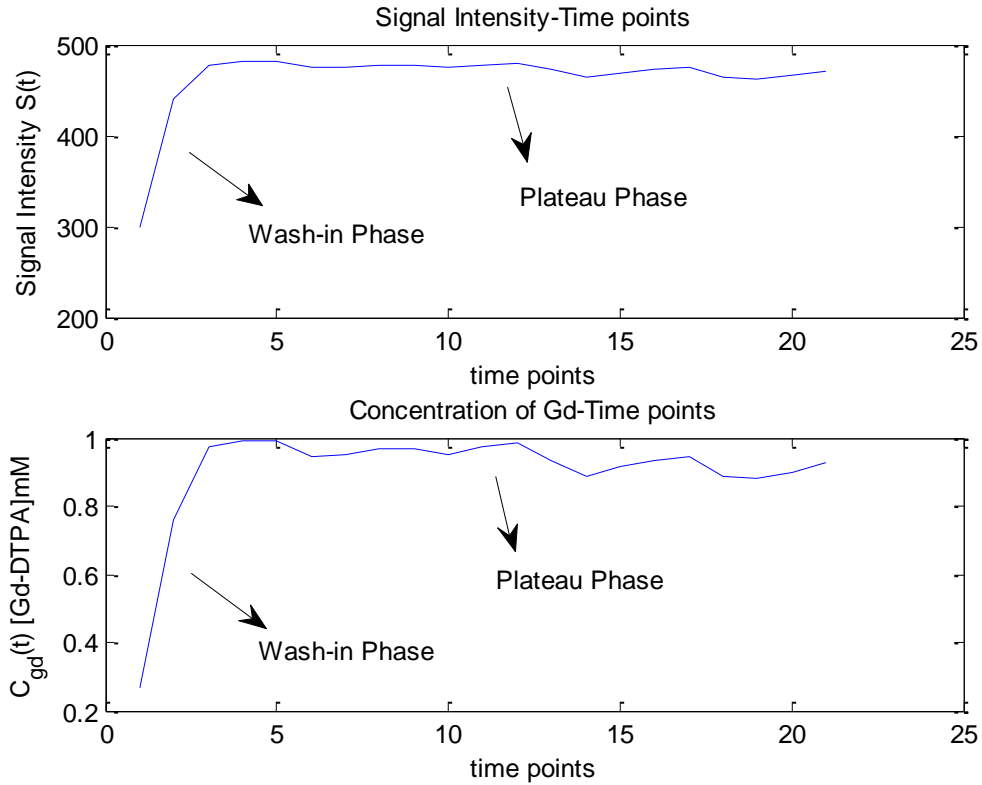
Figure 1.8: Estimated Curve (Type II) of Gadolinium Concentration with the optimal S0=4299, and T10=1.3s. The first figure correspond to the experimental Signal Intensities S(t) over time, and the second figure is the Concentration over time C(t), extracted from this task. We can notice an early entry of the molecules of contrast agent, into the Extravascular-Extracellular space, which is observed as a wash-in phase, and then for the rest time points, a stable phase, with no particular reaction, which [18] is relative to the capacitance (reservoir effect) of the EES space. The contrast agent is eliminated later from EES, when the concentration of contrast agent in the plasma becomes lower than that in the EES, according to Fick's first law, stated before.
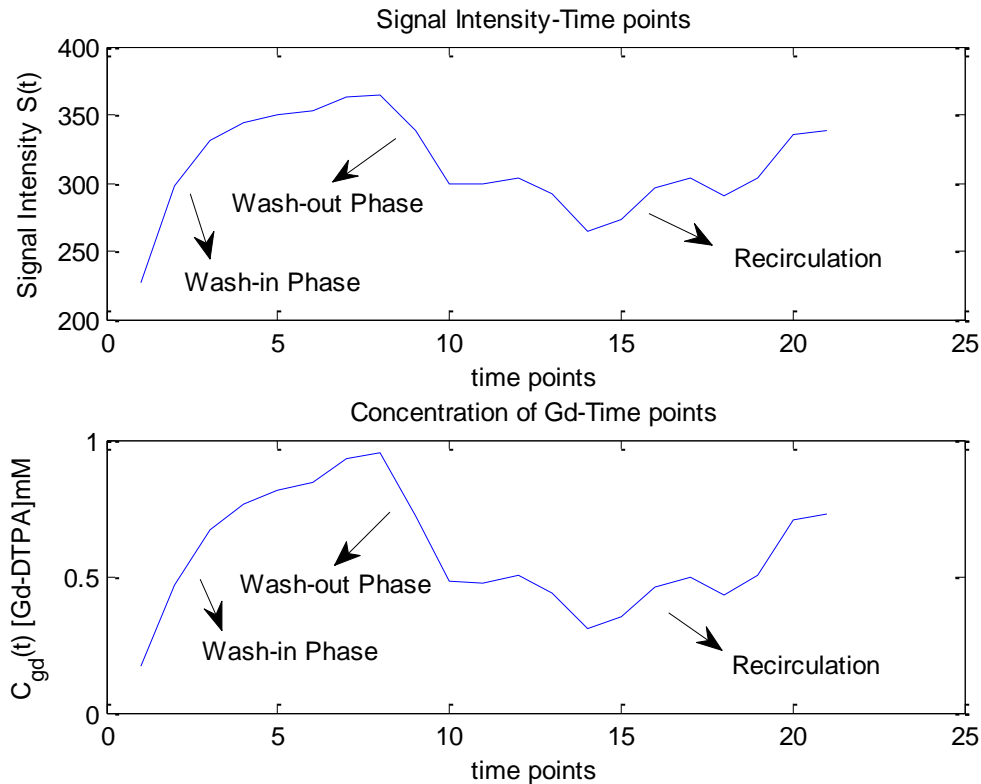
Figure 1.9: Estimated Curve (Type III) of Gadolinium Concentration with the optimal S0=3202, and T10=0.8s. The first figure correspond to the experimental Signal Intensities S(t) over time, and the second figure is the Concentration over time C(t), extracted from this task. There is a leakage of contrast agent molecules, through capillary wall, which is observed as a wash-in phase. After some time points, a wash-out is noticed, which is equivalent to the elimination of contrast agent. The contrast agent is not immediately eliminated, so a second lower peak is observed, because of the recirculation. So [18] after reaching the peak, the enhancement rapidly decreases during evacuation of the molecules of contrast agent derived from bolus. Then, the contrast agent recirculates and is slowly eliminated.

1.4 Problem and Thesis Contribution

The main task of this work, was to measure the gadolinium concentration, by estimating the pre-contrast agent's T_{10}-relaxation time, and S_0 magnetization at equilibrium state. In the related studies, as cited in section 2.1.1, this estimation is done more or less, without using any constraints about the values of these parameters, only boundary conditions for their range. In this work, these parameters are calculated, so that the calculated concentration of contrast agent (CA), which is a parameter of T_{10} and S_0, is in the range of 0-1 mM, in order to be in a real life range of values and having the same range for each different regions. To this end, additional nonlinear constraints, which are described in section 3.2, are included.

1.5 Outline Of Thesis

In Chapter 2, "*Definition of the Problem*", we discuss the Thesis's main task, and the problem of pre-contrast agent T_1- relaxation time and magnetization at equilibrium state S_0 estimation, and thus the estimation of gadolinium concentration from the time of the arrival of Contrast Agent(CA). Also, some related works, and analytical optimization methods, are cited.

In Chapter 3,"*Concentration Estimation Method*", we describe the optimization problem, that we encounter, the constraints and the method that we used in this study, measuring the concentration of contrast media in tissue.

Chapter 4,"*Perfusion Estimation Methods*", is about the approaches to estimate the distribution of Contrast Agent (CA), which leads to the distribution of blood in tissue.

In Chapter 5, "*Results*", we cite the results we gained, for both concentration-optimization problem, perfusion descriptors and the validation task.

In Chapter 6, "*Conclusion & Future Work*", we sum up the work that is done, and also we suggest some future work, which may be interesting, and significant to be done.

Chapter 2

Definition of the Problem

The main task of this work, was to measure the gadolinium concentration, by estimating the pre-contrast agent's T_{10}- relaxation time, and S_0 magnetization at equilibrium state. For this reason, we are solving a non-linear constrained optimization problem, to find the optimal T_{10} and S_0 . More about the optimization problem in Chapter 3.

Following the extraction of concentration, we are examining the perfusion phenomenon. Two main ways to measure the perfusion in the tissue, are commonly used. Semi-quantitative parameters, which are based upon the Signal Intensity or the Gadolinium Intensity, without taking into account the physiology of the tissue, and the pharmacokinetic parameters, which are measuring also the Concentration in plasma, also known as AIF(Arterial Input Function). [11] In this study, we are measuring Semiquantitative Parameters, based upon the Signal Intensity, but also based upon the Gadolinium Intensity.

2.1 Concentration Descriptors

Depending on the relationship between the Signal Intensity and concentration of Contrast Agent (CA), extraction of C_{gd} is possible. This relationship could be linear or nonlinear, but it has been reported that non-linear approximation has greater accuracy. [6,10]

2.1.1 The State of Art approaches

In some studies, linear relationship between the change of signal intensity and the contrast agent is assumed [6,9]:

$$\frac{S_{obs}(t) - S0}{S0} = \delta \cdot [C(t)] \tag{2.1}$$

where S_{obs}, is the observed Signal Intensities S(t), in the same logic of 1.3 where we discussed that the kinetics of the contrast agent inside the body can be depicted as a change in Signal Intensity S(t) of image, at each time point [6].

S_0 is the signal without Contrast Agent, [C(t)] is the concentration of Contrast Agent over time, and δ is constant of proportionality which is a function of various tissue, field and sequence parameters.

Thus, with this approximation knowing for each pixel, only the Signal Intensities S(t) over time and the value of Signal Intensity in absence of contrast agent S_0, we can measure the concentration of contrast agent C(t) over time.

Assumptions of linear approach

This linear relationship, gives accurate results, only on a limited range of contrast agent's concentration. Also, this relationship shows to be a good approximation, using a Repetition Time (TR) up to 500ms in the sequence used experimentally. It is assumed Repetition Time is approximately equal to the T1 of the ROI and that the relaxation rate $\frac{1}{T1}$ is independent of time. Consequently, this approximation is restrictive, and nonlinearity is essential for better accuracy on results and a wider range of concentration.[6,8,9,12].

Assumptions of nonlinear approach

In the nonlinearity case, in order to acquire real information, [11] the signal intensities S(t) are converted into spin-lattice relaxation time T1(t) (equation 2.2 below) and the spin-lattice relaxation time into concentration C(t) (equation 2.3 below), by estimating pre-contrast spin-lattice relaxation time(T_{10}), and equilibrium magnetization S_0. The measurement of T_{10} is achieved usually, using variable flip angle gradient echo sequences, with a constant Repetition Time, in most cases. [12, 16, 20]. It is assumed that T2* relaxation time (section 1.2) is much bigger than Echo Time and is not included in the equations (2.2, 2.3) [8]. Other way to measure T_{10}, is using variable saturation techniques, like images, with different Inversion Times.[12, 16].

Furthermore, a linearization of the non-linear approximation has been proposed in the literature [14] (DESPOT1 algorithm), with only two flip angles, by estimating T_{10} and S_0, using a constrained gradient descent optimization.

Some other works, estimate the concentration in tissue, from the concentration in plasma, also known as AIF (Arterial Input Function)[17].

T1(t) relaxation and Signal Intensity S(t) over time

As mentioned in section 1.2 and as it seems in figure 1.1, the kinetics of the contrast agent inside the body can be depicted as a change in Signal Intensity S(t) of image, at each time point [6]. Furthermore, the paramagnetic contrast agents, have the ability to reduce the relaxation time T1. So, as the contrast agent moves and leaks into the body, the relaxation time T1 changes over time for each voxel. Consequently, the relaxation time T1 of each voxel is a function of time and for each time point we have a different relaxation time.

Thus, the spin-lattice relaxation time T1(t) can be calculated [6] over time from the equation:

$$\frac{1}{\text{T1}(t)} = -\frac{1}{TR} ln \left(\frac{sin\theta - {S(t)}/{\text{S0}}}{sin\theta - cos\theta \cdot \frac{S(t)}{\text{S0}}} \right) \tag{2.2}$$

where S(t) is the Signal Intensity over time, from the moment of arrival of the contrast agent in tissue, S_0 is the equilibrium magnetization, ϑ is the angle of excitation (flip angle) for the nuclei, and TR is the repetition time, as an interval time between the application of the RF pulses.

Concentration C(t) over time

More specifically, in the tasks, in which the nonlinearity between the contrast agent (CA), and the Signal Intensity S(t), is taken into account, [6] the relationship between the CA, and the spin-lattice relaxation time $T_1(t)$ is:

$$\frac{1}{\text{T1}(t)} = \frac{1}{\text{T10}} + \text{r1} \cdot [\text{C(t)}] \tag{2.3}$$

where T_{10} is the pre-contrast agent relaxation time, r_1 is the relaxivity of the contrast agent, and [C(t)] is the concentration over time.

Parameter Estimation Using different Inversion Times

In these tasks [12, 16], in order to determine pre-contrast spin lattice relaxation times T_{10}, and equilibrium magnetization S_0, Inversion Recovery sequence imaging, is applied, using variable times of inversion (TI). Consequently, the estimation of those two parameters, is achieved solving the least squares fitting problem:

$$S(TI) = \text{S0} \cdot (1 - 2e^{\frac{-TI}{T10}} + e^{\frac{-TR}{T10}}) \tag{2.4}$$

Thus, the estimated signal intensities, are fitted on the experimental signal data, for the optimal values of S_0 and T_{10}. Following the parameter estimation, the measurement of concentration, is achieved from 2.2, where $T1(i)$ is the T_1 time at a given gadolinium concentration. Using true IR sequence, inversion of positive values of the signal prior the null point occurs, and the problem is addressed by modulus IR sequences.

An example of an Inversion Recovery Sequence, using different Inversion times is described in figure 2.1:
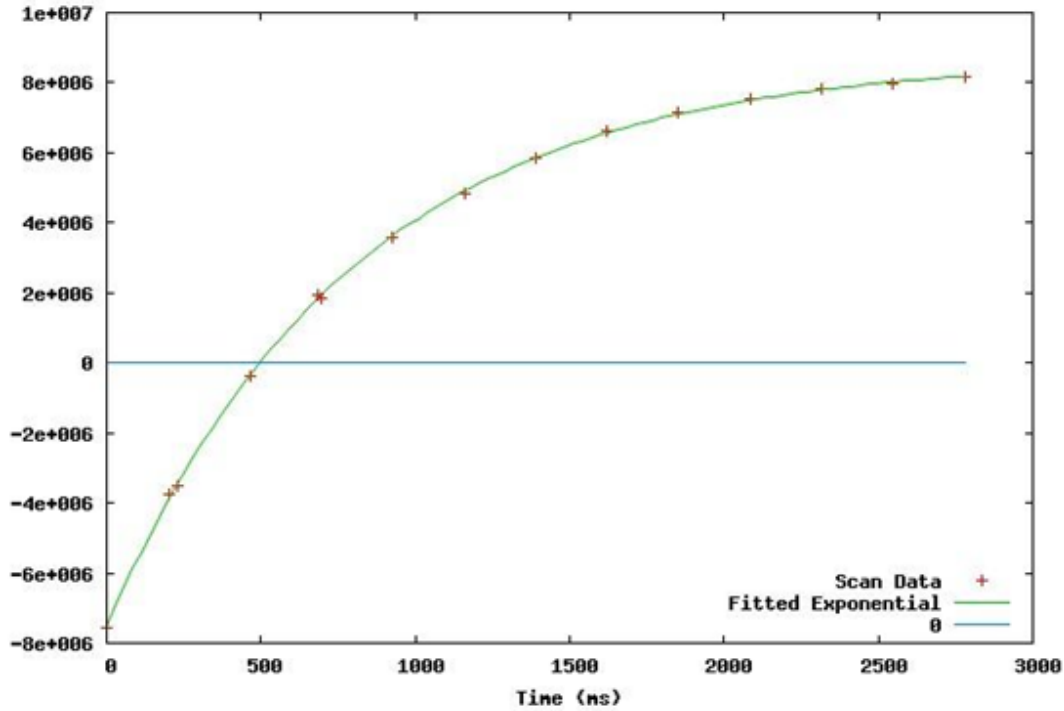
Figure 2.1: A typical curve fitting example using Inversion Recovery Sequence equation (2.4), adapted from [40]

The basic concept is based upon the Inversion Recovery Sequence. As described in section 1.2, in this type of sequence we have an initial excitation of the protons, with a 180° RF pulse, before the application of the two others (90° and 180°). The interval time, between the 180° pulse, and the 90° pulse, is called Inversion Time (TI). Thus, changing Inversion Times (Time axis) we acquire different contrast value (Scan Data). Using the 2.4 equation, we find the best curve (Fitted Exponential) that is closest to the data points, by estimating T10 and S0.

The initial usage of a 180° RF inversion wave flips longitudinal magnetization in the opposite direction (negative) and due to longitudinal relaxation, longitudinal magnetization will increase as it returns to its initial value, passing through null value [38].

Parameter Estimation Using different Flip Angles

In this field [12,16,20] , the estimation of the pre-contrast relaxation time (T_{10}) and the equilibrium magnetization (S_0), is accomplished using variable flip angle gradient echo acquisitions, with a constant Repetition Time (TR). More specifically, the mathematical equivalent of this sequence is:

$$S1(a) = S_0 \frac{sina(1-e^{-TR/T_{10}})}{1-cosa \cdot e^{-TR/T_{10}}}$$
(2.5)

where a is the different flip angle, usually angles lower than 90°. Thusly, the problem is similar to the previous method, as an estimation of two parameters (S_0 and T_{10}), solving the least square fitting problem, on the experimental data.

The concentration, is derived again from the equation 2.2.

It is assumed that T2* relaxation time is much bigger than Echo Time and is not included in the equation [8].

Parameter Estimation Using the Basic DESPOT1 algorithm

In this method [14, 21], a linearization of the non-linear expression of the spoiled gradient echo sequence is used. The algorithm, uses a gradient echo sequence:

$$S1(a) = S_0 \frac{sina(1-e^{-TR/T_{10}})}{1-cosa \cdot e^{-TR/T_{10}}}$$

which is reformulated as a simple linear equation:

$$Y = aX + b \qquad\qquad (2.6)$$

Which is parameterized as $Y = \frac{S1(a)}{sina}$, $X = \frac{S1(a)}{tana}$, $a = e^{-TR/T_{10}}$, $b = S_0 \cdot (1 - e^{-TR/T_{10}})$

Thus, the parameters are extracted from 2.6 as:

$$T10 = -\frac{TR}{lna}, S0 = \frac{b}{1-a}$$

So, the calculation of T10 and S0, is achieved, increasing a, until the optimal fit to the experimental data.

Parameter Estimation Using the Optimized DESPOT1 algorithm

This method [14], uses a constrained gradient descent optimization, in order to find the optimal values of T10 and S0, by including the estimation of $\vartheta 1$ and $\vartheta 2$ in the minimization function. The problem is defined as the minimization of the distance function:

$$\operatorname*{argmin}_{(\vartheta,\ T10,\ S0)} [\lambda|\vartheta - \theta|^2 + (1-\lambda)|S_\vartheta - S_\theta|^2]$$

with $\vartheta = [\vartheta 1, \vartheta 2]$, $\theta = [\theta 1, \theta 2]$, $S_\vartheta = [S_{\vartheta 1}, S_{\vartheta 2}]$ and $S_\theta = [S_{\theta 1}, S_{\theta 2}]$

S_θ: are the experimental Intensities
S_ϑ: are the estimated Intensities
θ: are the prescribed flip angles
ϑ: are the estimated flip angles
λ: scale factor to balance the 2 terms in the distance function

Thus, the algorithm starts from the values (T10=1, S0=0, $\vartheta 1 = \theta 1$, $\vartheta 2 = \theta 2$), and the optimal values that minimize the distance function, are calculated iteratively.

Parameter Estimation Using Arterial Input Function

Based on physiological parameters, [22] specifically in the brain region, the tissue is modeled as a well-mixed compartment, parameterized by:

$$C(t) = \frac{p}{k_H} \cdot CBF \cdot \int_0^t AIF(\tau) \cdot e^{-(t-\tau)/MTT} \, d\tau \qquad\qquad (2.7)$$

where p is the tissue brain density(set to 1 mL/g) and $k_H = (1 - H_{art})/(1 - H_{cap})$ the difference in hematocrit (H) between capillaries and large vessels, CBF(Cerebral Blood Flow) is chosen as a physiological parameter(e.g 60 mL/100g/min), and MTT stands for Mean Transmit Time. The AIF is taken from a vascular model of the human vasculature.

2.1.2 Analytical Optimization Methods

As described above, our problem is a nonlinear constrained problem. The general constrained optimization problem is [33: pg 58]:

$$\text{Minimize} \qquad f(x)$$
$$\text{such that} \qquad g_j(x) \le 0, j = 1,2, \dots, m$$
$$h_j(x) = 0, j = 1,2, \dots, r$$

Some typical methods of analytical optimization are:

Penalty Function Method

The main formulation of this method is [33: pg 58]:

$$\text{Minimize} \qquad P(x)$$

Where

$$P(x, \rho, \beta) = f(x) + \sum_{j=1}^{r} p_j h_j^2(x) + \sum_{j=1}^{m} \beta_j g_j^2(x).$$

and where the components of the penalty parameter vectors ρ and β, are given by:

$$\rho_j \gg 0, \qquad \beta_j = \begin{cases} 0 & if \ g_j(x) \le 0 \\ \mu_j \gg 0 & if \ g_j(x) > 0 \end{cases}$$

The parameters, ρ and β, are called penalty parameters, $P(x, \rho, \beta)$ is the penalty function, and the solution of the problem is $x^*(\rho, \beta)$.

The variable $\rho_j \equiv constant \equiv \rho$, for all j, and also most of the time, $\mu_j \equiv \rho$, for all j such that $g_j(x) > 0$. Typically, the penalty parameter p is set at $p = 10^4$.

This method, belongs in the class of external methods, because it converges externally from the infeasible region. This is because, while the constraint is violated, we increase its penalty parameter, and the optimal solution will be found when $\lim_{p \to \infty} x^*(p) = x^*$.

Gradient Projection Method

The main idea of this method, [34] [33 pg:81-88] is that we know some vector x' that satisfies our constraints. Thusly, we are examining in some direction s, which is the projection of the steepest descent onto the constraint, so that it leads to another x'. This new vector, also satisfies our constraint, but is closest to the minimum. This is repeated until we find the optimum solution. This way, this optimization method is geometrically analytical.

The method is based on the idea, that we are constructing a sequence of feasible points, finding a path, that leads to the optimal value. Examining the negative (sign) gradient in an initial known feasible point, we are constructing a projection, onto the constraint, in order to find the path to the optimal value. Thusly, each time, we are constructing, a projection map, having a sequence of feasible points, and based on them, we are searching the optimal solution. If there is a violation of constraints, in some point of x' in the construction of the projection, then we are searching a point of intersection with the initial constraint, in order to make a new constraint, and then to construct the projection.

Lagrange Multipliers Method

The Lagrange multipliers method allows only equality constraints, and in order to include inequality constraints, we use the Karush-Kunh Tucker conditions to generalize them, as it will be discussed later.

The basic use of Lagrange Multipliers in our work [32,35], is that they consist the criterion for parallelism in our constraint. In order, to minimize our cost function, with the given constraint, it is demanded that the vector of cost function's gradient (for one equality constraint), $\nabla f(\bar{x})$ is parallel (or antiparallel-change in the sign of λ) to the gradient of our constraint $\nabla h(\bar{x})$ (equivalently $\nabla f(\bar{x})$, $\nabla h(\bar{x})$ orthogonal on our constraint surface $h(\bar{x})=0$). Consequently, in general the optimal value satisfies the linear combination of:

$$\nabla f(\bar{x}) + \sum_{j=1}^{r} \lambda_j \nabla h_j(x) = 0.$$

which is known as the condition of Lagrange Multipliers. Thus, $\nabla f(\bar{x}) + \sum_{j=1}^{r} \lambda_j h_j(x) = 0$, and defining the Lagrangian we gain:

$$L(x, \lambda, \mu) = f(x) + \sum_{j=1}^{r} \lambda_j h_j(x).$$

The Lagrange Multipliers, could be positive or negative, if the gradients are parallel or antiparallel (for one equality constraint).

Thus, we are searching for critical points. The feasible point, that means the point that satisfies our constraints, must satisfy the criterion of linear combination, with respect to each one of our variable.

The figure below explains the above idea, for two equality constraints.
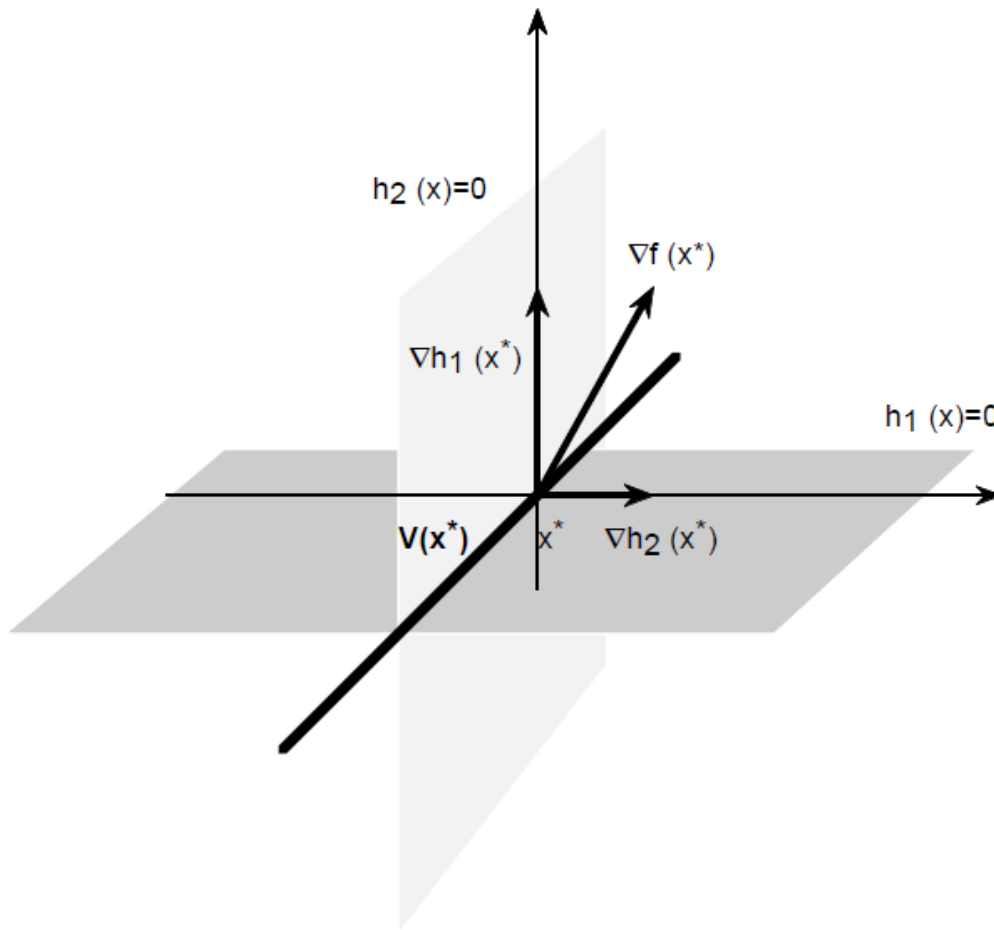
Figure 2.2: Graphical explanation of Lagrange Multipliers with two equalities constraints, h1(x)=0, h2(x)=0. In the optimal solution x*, the gradient of ∇f(x), can be expressed as a linear combination of ∇h1(x) and ∇h2(x). Source:[37]

Lagrange Multipliers with Karush-Kuhn Tucker Conditions

The Karush-Kunh Tucker Conditions, [35] generalize the method of Lagrange multipliers, to handle inequality constraints, which as stated before, allows only equality constraints.

The inequality constraint, is handled as an equality constraint in the form of Lagrangian, and with the conditions below, we are examining if the solution is on the boundary of the constraint, or in the interior of the constraint. According to the method above, for one inequality constraint, it is demanded that the vector of cost function's gradient, $\nabla f(\bar{x})$ is parallel (or antiparallel-change in the sign of μ) to the gradient of our constraint $\nabla g(\bar{x})$ (equivalently $\nabla f(\bar{x})$, $\nabla g(\bar{x})$ orthogonal on our constraint surface $g(\bar{x}) \leq 0$). Thusly, in general the optimal value must satisfies the linear combination of:

$$\nabla f(\bar{x}) + \sum_{j=1}^{r} \lambda_j \nabla h_j(x) + \sum_{j=1}^{m} \mu_j \nabla g_j(x) = 0.$$

and the Lagrangian is:

$$L(x, \lambda, \mu) = f(x) + \sum_{j=1}^{r} \lambda_j h_j(x) + \sum_{j=1}^{m} \mu_j g_j(x).$$

The conditions below, are known as Karush-Kunh Tucker Conditions (KKT), and the solution must satisfy those, in order to be optimal. With this way, we are examining if the optimal solution is inside the space of constraint (μ=0), or in the boundary($g(x) = 0, \mu \neq 0$). Consequently, we have two cases :

- Inactive Constraint($\mu_j = 0$): The optimal point, lies in the region of $g_j(x) < 0, j = 1,2, \dots, m$

- Active Constraint: The optimal point, lies on the boundary $g_j(x) = 0, j = 1,2, \dots, m$

Thusly, the conditions (KKT conditions) for the optimal solution $\bar{x}$ are [30:pg 243-244]:

- Stationary Conditions $\nabla f(\bar{x}) + \sum_{j=1}^{r} \lambda_j \nabla h(\bar{x}) + \sum_{j=1}^{m} \mu_j \nabla g(\bar{x}) = 0$

- Complementary Slackness Conditions $\lambda_i h_i(\bar{x}) = 0$, $\mu_j g_j(\bar{x}) = 0$, $\lambda_i, \mu_j \geq 0$, i = $1,2, \dots, r, j = 1,2, \dots, m$

Consequently, we test all the cases, for each constraint, as it will be described in section 3.3.

The sign of Lagrange Multiplier, [35] in the case of inequalities, is important, because in the case of minimization, the function $f(x)$, will have a minimum at x*, if the direction of the steepest descent for $f(x)$ at x*, is oriented away from the region, $g_j(x) < 0, j = 1,2, \dots, m.$, that means the gradient of $f(x)$ being oriented towards the region of $g_j(x) < 0, j = 1,2, \dots, m..$

Considering that $-\nabla g(\bar{x})$ points in the direction of the region $g_j(x) < 0, j = 1,2, \dots, m$, so it is required for minimization of $f(x)$ that:

$$\nabla f(\bar{x}) = -\sum_{j=1}^{r} \lambda_j \nabla h_j(x) - \sum_{j=1}^{m} \mu_j \nabla g_j(x), \text{ for } \lambda_i, \mu_j \geq 0$$
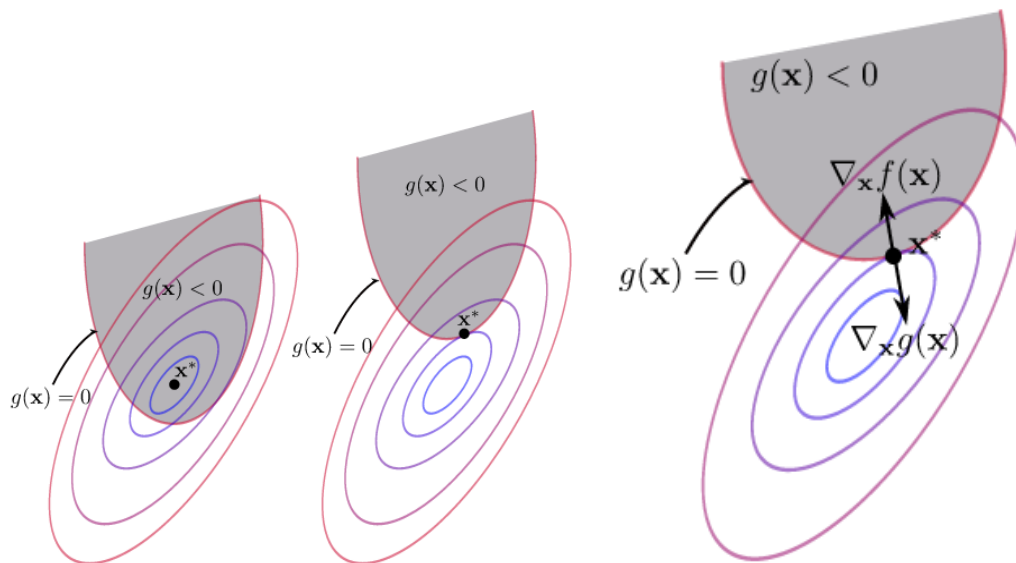
**Figure 2.3: Graphical Explanation of Karush-Kuhn Tucker Conditions for inequalities.
Source: [36]**
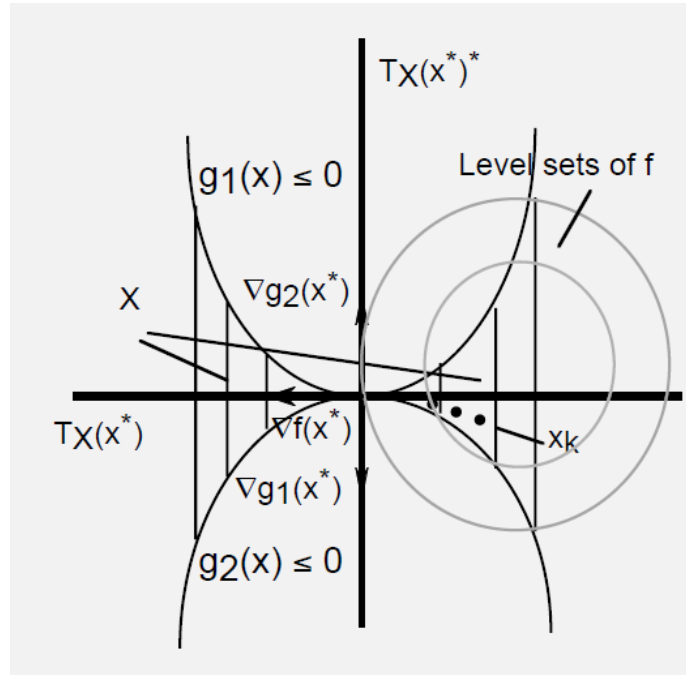
Figure 2.4: Graphical Explanation of Karush-Kuhn Tucker Conditions for two inequalities and a set of x∈ *X*. Source: [37]

In our problem, the functions that consist the constraints, are nonlinear with increased complexity. Thusly, a geometrically analytical method, as the gradient projection method, is not preferable. Also, the penalty function method, is not suitable in our case, because it is based on a directly mathematical approach, increasing the penalty parameter each time, and considering the nonlinearity of the constraint, the complexity is increased. Thus, the analytical solution that is proposed, for our problem, is based on Lagrange multipliers, and taking into account, that our constraints are inequalities, we use Karush-Kuhn Tucker conditions.

2.1.3 Proposed Approach

An analytical solution, based on Lagrange Multipliers with KKT conditions, is proposed, taking into account the nonlinearity, to extract the contrast agent's concentration in the range of 0-1mM, by estimating the pre-contrast relaxation time (T_{10}) and the equilibrium magnetization (S_0), as a result of solving an optimization problem, which will be discussed in Chapter 3. In order to obtain pre-contrast T1 values, we used the spoiled gradient echo recalled signal, with different flip angles.

2.2 Perfusion Descriptors

Describing blood distribution of the contrast agent is essential, in order to separate the possible angiogenesis, from the normal areas. High perfusion, means high needs for blood. Tumors have high needs for blood, in order to grow and angiogenesis plays a critical role in the process of cancer progression.[8]

First of all, as we mentioned in Section 1.3 we can extract information about tumor indirectly, from the Signal-Intensity curve. The DCE-MRI gives us images for each time point of the life of CA in the Tissue Of Interest (TOI). The other way and more quantitative is to measure the gadolinium concentration in the tissue, and then to calculate pharmacokinetics parameters, which take into account the concentration in plasma, which is known as Arterial Input Function.[11].

In this task we compute semi-quantitative parameters, using the Signal Intensity but also the Gadolinium Concentration. In DCE-MRI, these parameters are lack of specificity and particular detection of tumor areas, but we can have a quantitative information about the possible abnormalities. Using only Signal Intensities, we have limitations, because they do not reflect contrast agent concentration in the TOI, and they can be influenced by scanner settings, such as gain or scaling factors [11]. We used the parameters IAUC(Initial Area Under the Curve), FAUC (Final Area Under the Curve) and AUCR(Area Under the Curve Ratio), as proposed in the literature[7], based upon the Signal Intensity, but also upon the estimated Gadolinium Concentration. Furthermore, additional parameters [6], calculated are the Maximum Signal Intensity, Maximum Intensity Time Ratio, Gradient Wash-in and [19, 29]AUC(Area Under the whole curve), from the Signal intensity curve, and from the Gadolinium Concentration curve .

The meaning and the mathematical equivalent of those parameters are explained in Chapter 4.

The following block diagram summarizes all the workflow from image acquisition to computing the Gd concentration [24].
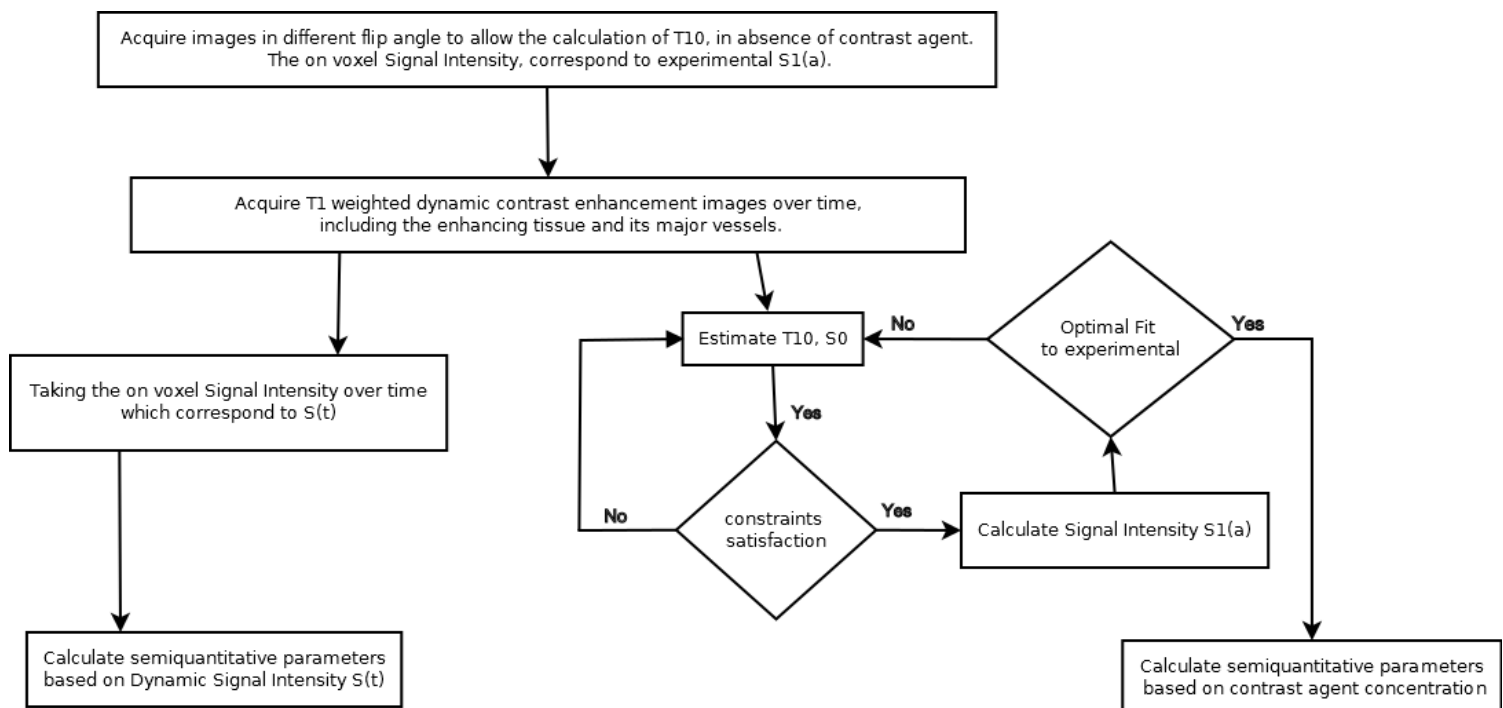
Figure 2.5: Block diagram with the steps of the work

Chapter 3

Concentration Estimation Method

The measurement of the pre-contrast spin-lattice relaxation time (T_{10}), the equilibrium magnetization (S_0) and thusly the contrast agent concentration are calculated for each voxel. Consequently, a map of parameters is formed.

3.1 Measuring Contrast Agent Concentration

As we mentioned in section 2.1.1, in this work, we took into account the nonlinearity relationship between the contrast agent, and the Signal Intensity.

In theory [6], the gradient recalled echo signal, by variable flip angle, prior to the injection is given by the equation, in 2.5

$$S1(a) = S_0 \frac{sina(1 - e^{-TR/T_{10}})}{1 - cosa \cdot e^{-TR/T_{10}}}$$

(3.1.1)

where S_1, is the signal prior to the injection, in the different flip angles, a is the variable flip angle that is used. In this study, our flip angles are 5° 10° 15° 20° 25° 30 ° 60°, S_0 is the magnetization equilibrium, and TR is the Repetition Time, which in this study is 0.0051s for the data of cervix, and 0.0069s for the data of brain used.

Also, as stated in section 1.3, the relaxation times (T1), are a function of time, from the moment of the injection of contrast agent in the body. Thusly, from [6], we have:

$$\frac{1}{T1(t)} = -\frac{1}{TR} ln \left(\frac{sin\theta - S(t)/S0}{sin\theta - cos\theta \cdot \frac{S(t)}{S0}} \right)$$

(3.1.2)

where S is the Signal Intensity over time, from the moment of arrival of the contrast agent in tissue, S_0 is the equilibrium magnetization, ϑ is the angle of excitation (flip angle) for the nuclei, and TR is the repetition time, as an interval time between the application of the RF pulses.

Another significant equation is the following, where Concentration of contrast agent is calculated [6] :

$$C_{gd}(\text{t}) = \frac{1}{r1} \cdot \left(\frac{1}{T1(t)} - \frac{1}{T10} \right) \tag{3.1.3}$$

We sum up the variables:

S(t)	Vector of Signal Intensities (Dynamic), as a function of time, for a specific voxel, without baseline, from the time of arrival in tissue.
$S_1(a)$	Vector of Signal Intensities, for different flip angle, for a specific voxel. Not varying with time.
$C_{gd}(\text{t})$	Concentration of Contrast Agent (CA), in tissue, vector over time.
r_1	Relaxivity constant of Gd-DTPA, r_1=4.59, and r_1=5.2 for Gd-BT-DO3A.
a	The different flip angle, we use for the Signal Intensity S_1, [5° 10° 15° 20° 25° 30 ° 60°].
θ	Flip angle for the Dynamic Intensities S(t), 10° (0.1745 rad) in this study.
TR	Repetition Time, 0.0051s for the cervix data, and 0.0069s for the brain data.
S_0	Equilibrium Magnetization. Parameter for estimation.
T_{10}	Pre-contrast spin-lattice relaxation time, in absence of CA. Parameter for estimation.
$T_1(t)$	Spin-lattice relaxation time, as a function of time, from the time point of the arrival of CA, in the tissue.

Table 3.1: The working quantities and vectors of optimization problem

3.2 Optimization Problem and Constraints

The main problem, is to extract the values of S_0 and T_{10}, so that the estimated S_1 signal, is fitted on the S_1 experimental data points, for each voxel. Therefore, we must minimize the prediction error, comparing with the experimental data in different flip angles. In this case we choose the least square error:

$$min\left\{ \sum_a \left(S1(a) - S1_{exp}(a) \right)^2 \right\} \tag{3.2.1}$$

The choice of least square error, comparing to absolute prediction error, is justified by the fact, that in the first case, we put small weight on small residuals, while on the other hand with absolute prediction error, most weight is given on small residuals and the least weight on large residuals. [30: pg 296]

Furthermore, using absolute prediction error, our function is not differentiate, which is not preferable, because the analytic optimization method we use, is based on differentiation.

The estimated S_0 and T_{10}, must satisfy the following constraints:

- **$0.2 < T_{10} < 1.8$** $\hspace{4cm}$ (3.2.A)

- $0 < C_{gd}(t) < 1$

Extracting constraint for $C_{gd}(t) > 0$:

$$C_{gd}(t) = \frac{1}{r1} \cdot \left(\frac{1}{T1(t)} - \frac{1}{T10} \right)$$

We define, to simplify our calculations, $R1(t) = \frac{1}{T1(t)}$ και $R_{10} = \frac{1}{T10}$, and in order to extract positive concentration, the following inequality, must be satisfied

$$C_{gd}(t) > 0 \leftrightarrow$$

$$\frac{1}{r1} \cdot \left(\frac{1}{T1(t)} - \frac{1}{T10} \right) > 0 \leftrightarrow$$

$$\left(\frac{1}{T1(t)} - \frac{1}{T10} \right) > 0 \leftrightarrow$$

$$\frac{1}{T1(t)} > \frac{1}{T10} \leftrightarrow$$

$$R1(t) > R10 \text{ and } \frac{1}{T1(t)} > 0$$

But from constraint 3.2.A, we have $0.2 < T10 < 1.8$, so $T10 > 0$. Thusly, $\frac{1}{T10} > 0$ and then $R10 > 0$. Consequently, the constraint $\frac{1}{T1(t)} > 0$ is satisfied and there is no need to be cited.

Therefore, it only requires $R1(t) > R10$.

At this point, we are extracting the essential inequality, for T_{10} and S_0, so that the inequality $R1 > R10$, is satisfied.

$$R1(t) > R10 \leftrightarrow$$

$$\frac{1}{T1(t)} > \frac{1}{T10} \leftrightarrow$$

$$-\frac{1}{TR} \ln \left(\frac{sin\theta - S(t)/S0}{sin\theta - cos\theta \cdot \frac{S(t)}{S0}} \right) > \frac{1}{T10} \leftrightarrow$$

The variable S(t), is a vector of time. Consequently, this criterion, must be satisfied for each element of the vector. So, let S_k, the examined element, it must satisfy the following:

$$\ln \left(\frac{sin\theta - S_k/S0}{sin\theta - cos\theta \cdot \frac{S_k}{S0}} \right) < -\frac{TR}{T10} \leftrightarrow$$

$$\boxed{\left(\frac{sin\theta - S_k/S0}{sin\theta - cos\theta \cdot \frac{S_k}{S0}} \right) < e^{-\frac{TR}{T10}}}$$

(3.2. B)

$$\forall S_k \in S$$

At this point, we have extracted the constraints, which satisfy the inequality $C_{gd}(t) > 0$. The next constraint, which must be satisfied is $C_{gd}(t) < 1$.

Extracting constraint for $C_{gd}(t) < 1$:

An additional constraint, which must be added, is to the upper bound of values, of Contrast Agent. So, we are extracting the essential inequality for T_{10}, and S_0, for which the maximum value of concentration, does not exceed an upper bound which is parameterized. For this study, the upper bound for the Concentration of Contrast agent, is set to 1mM.

More specifically,

$$C_{gd}(t) < C_{max}$$

$$\frac{1}{r1}\left(\frac{1}{T1(t)} - \frac{1}{T10}\right) < Max$$

We define the variable: **M=Max*r1**

$$\left(\frac{1}{T1(t)} - \frac{1}{T10}\right) < M$$

$$-\frac{1}{TR}\ln\left(\frac{sin\theta - S(t)/S0}{sin\theta - cos\theta \cdot \frac{S(t)}{S0}}\right) - \frac{1}{T10} < M$$

$$-\frac{1}{TR} \cdot \ln\left(\frac{sin\theta - S(t)/S0}{sin\theta - cos\theta \cdot \frac{S(t)}{S0}}\right) < M + \frac{1}{T10}$$

$$\ln\left(\frac{sin\theta - S(t)/S0}{sin\theta - cos\theta \cdot \frac{S(t)}{S0}}\right) > -M \cdot TR - \frac{TR}{T10}$$

The variable S(t), is a vector of time. Consequently, this criterion, must be satisfied for each element of the vector. So, let S_k, the examined element, it must satisfy the following:

$$\ln\left(\frac{sin\theta - S_k/S0}{sin\theta - cos\theta \cdot \frac{S_k}{S0}}\right) > -M \cdot TR - \frac{TR}{T10}$$

$$\boxed{\left(\frac{sin\theta - S_k/S0}{sin\theta - cos\theta \cdot \frac{S_k}{S0}}\right) > e^{-M \cdot TR - \frac{TR}{T10}}}$$

$$(3.2.\,C)$$

$$\forall S_k \in S$$

<u>To sum up, we have the following three inequalities constraints</u>:

- $0.2 < T10 < 1.8$ derived from 3.2.A

- $\frac{sin\theta - S_k/S0}{sin\theta - cos\theta \cdot \frac{S_k}{S0}} < e^{-\frac{TR}{T10}}, \forall S_k \in S$ derived from 3.2.B

- $\frac{sin\theta - S_k/x}{sin\theta - cos\theta \cdot \frac{S_k}{x}} > e^{-M \cdot TR - \frac{TR}{T10}}, \forall S_k \in S$ derived from 3.2.C

Therefore, the (**3.2A**), (**3.2.B**), (**3.2.C**) ,are our inequalities, and we are solving the optimization problem, finding x=S0 and y=$T10$ that satisfy those constraints. We set y=$T10$, and not $y = \frac{TR}{T10}$, because it is preferable for the solution to be parameterized, and Repetition Time (TR) may changes between medical incidents.

Consequently, our problem is the minimization of the prediction error:

$$\min\left\{\sum_a \left(S1(a) - S1_{exp}(a)\right)^2\right\} \tag{3.2.2}$$

with $S1(a) = x \cdot \dfrac{sina\cdot(1-e^{-\frac{TR}{y}})}{1-cosa\cdot e^{-\frac{TR}{y}}}$, while satisfying the following: (3.2.3)

- $0.2 < y < 1.8$ (3.2.D)

- $\dfrac{sin\theta - S_k/x}{sin\theta - cos\theta \cdot \frac{S_k}{x}} < e^{-\frac{TR}{y}}$, $\forall S_k \in S$ (3.2.E)

- $\dfrac{sin\theta - S_k/x}{sin\theta - cos\theta \cdot \frac{S_k}{x}} > e^{-M\cdot TR - \frac{TR}{y}}$, $\forall S_k \in S$ (3.2.F)

3.3 Estimation of T_{10}, S_0 via Lagrange Multipliers and Karush-Kunh Tucker Conditions (KKT Conditions)

As we mentioned above (section 2.1.3), in this work we used the Lagrange Multipliers method, and because of the nonlinear inequalities, we used the KKT conditions, in order to find the optimal solution. Our problem, does not require equality constraints.

From 3.2.2 and 3.2.3, if we define d= $S1_{exp}$(a) and set $\varphi = \sum_a \left(x \cdot \dfrac{sina \cdot \left(1-e^{-\frac{TR}{y}}\right)}{1-cosa \cdot e^{-\frac{TR}{y}}} - d \right)^2$ for the

main criterion of 3.2.1, we obtain the Lagrange criterion including the inequalities (3.2.D, 3.2.E, 3.2.F):

$L(x, y, \mu1, \mu2) = \varphi + \sum_i \mu1i \left(-\dfrac{sin\theta - \text{Si}/x}{sin\theta - cos\theta \cdot \frac{\text{Si}}{x}} + e^{-\frac{TR}{y}} \right) + \sum_i \mu2i \cdot \left(\dfrac{sin\theta - \text{Si}/\text{x}}{sin\theta - cos\theta \cdot \frac{\text{Si}}{\text{x}}} - e^{-M \cdot TR - \frac{TR}{y}} \right) + \mu3(0.2 - y) + \mu4(y - 1.8)$

$$L(x, y, \mu1, \mu2, \mu3, \mu4) = \sum_a \left(x \cdot \dfrac{sina \cdot \left(1-e^{-\frac{TR}{y}}\right)}{1-cosa \cdot e^{-\frac{TR}{y}}} - d \right)^2 + \sum_i \mu1_i \left(\dfrac{sin\theta - \text{Si}/x}{sin\theta - cos\theta \cdot \frac{\text{Si}}{x}} - e^{-\frac{TR}{y}} \right) + \sum_i \mu2_i \left(-\dfrac{sin\theta - \text{Si}/\text{x}}{sin\theta - cos\theta \cdot \frac{\text{Si}}{\text{x}}} + e^{-M \cdot TR - \frac{TR}{y}} \right) + \mu3 \cdot (0.2 - y) + \mu4 \cdot (y - 1.8)$$

The conditions, resulting from KKT (Karush-Kunh-Tucker), examining the derivatives, with respect to x and y, we gain: (for simplicity, we set S(t)= Si for a specific element of $S(t)$)

- $\dfrac{\vartheta L}{\vartheta x} = 2 \left(\dfrac{x \cdot sina\left(1-e^{-\frac{TR}{y}}\right)}{1-cosa \cdot e^{-\frac{TR}{y}}} - d \right) \left(\dfrac{sina\left(1-e^{-\frac{TR}{y}}\right)}{1-cosa \cdot e^{-\frac{TR}{y}}} \right) + \sum_i \mu1_i \left(\dfrac{S_i}{\left(sin\theta - \frac{cos\theta \cdot S_i}{x}\right)x^2} + \dfrac{cos\theta \cdot S_i\left(\frac{S_i}{x} - sin\theta\right)}{x^2\left(sin\theta - \frac{cos\theta \cdot S_i}{x}\right)^2} \right) + \sum_i \mu2_i \cdot \left(-\dfrac{S_i}{x^2\left(sin\theta - \frac{cos\theta \cdot S_i}{x}\right)^2} - \dfrac{cos\theta \cdot S_i\left(\frac{S_i}{x} - sin\theta\right)}{x^2\left(sin\theta - \frac{cos\theta \cdot S_i}{x}\right)^2} \right)$

- $\dfrac{\vartheta L}{\vartheta y} = 2 \left(\dfrac{x \cdot sina\left(1-e^{-\frac{TR}{y}}\right)}{1-cosa \cdot e^{-\frac{TR}{y}}} - d \right) \cdot \left(\dfrac{cosa \cdot TR \cdot \left(1-e^{-\frac{TR}{y}}\right) \cdot sina \cdot x \cdot e^{-\frac{TR}{y}}}{y^2 \cdot \left(1-cosa \cdot e^{-\frac{TR}{y}}\right)^2} - \dfrac{sina \cdot x \cdot TR \cdot e^{-\frac{TR}{y}}}{y^2 \cdot \left(1-cosa \cdot e^{-\frac{TR}{y}}\right)} \right) - \sum_i \mu1_i \left(\dfrac{TR \cdot e^{-\frac{TR}{y}}}{y^2} \right) + \sum_i \mu2_i \left(\dfrac{TR \cdot e^{-M \cdot TR - \frac{TR}{y}}}{y^2} \right) - \mu3 + \mu4$

And also, the Complementary Conditions to be satisfied:

- $\sum_i \mu 1_i \left(\dfrac{sin\theta - {}^{Si}/_x}{sin\theta - cos\theta \cdot \frac{Si}{x}} - e^{-\frac{TR}{y}} \right) = 0$ (3.2.2)

- $\sum_i \mu 2_i \left(-\dfrac{sin\theta - {}^{Si}/_x}{sin\theta - cos\theta \cdot \frac{Si}{x}} + e^{-M \cdot TR - \frac{TR}{y}} \right) = 0$ (3.2.3)

- $\mu 3 \cdot (0.2 - y) = 0$

- $\mu 4 \cdot (y - 1.8) = 0$

- $0.2 - y \leq 0$

- $y - 1.8 \leq 0$

- $\mu 1, \mu 2, \mu 3, \mu 4 \geq 0$

We set our derivatives equal to zero, and using the above Complementary Conditions we try to solve our problem, by checking all the cases.

The main idea, is that when we set a multiplier equal to zero, then we are searching for the optimal solution-critical point, inside the space that the constraint define, but when we set the constraint to zero, then we are searching for the optimal values in the bounds. Thusly, for the boundaries, we need to test along the bound of 3.2.E constraint and the line y between 0.2 and 1.8, and also along the bound of 3.2.F constraint and the line y between 0.2 and 1.8, in order to check our several distinct regions. As a consequence, in each case, we solve a system of equations, finding x,y, and we choose the optimal solution, among all, that satisfies the constraints and minimizes the prediction error. The derivatives, and the solution of the equations were calculated on Matlab, and Maple.

To sum up, a nonlinear constrained optimization problem is solved for each voxel, based on the method above. The results, of the optimization problem are cited in Chapter 5.

After due consideration, from the whole vector of S, it is only required to examine its minimum and maximum value, in order to satisfy the inequalities (3.2.E, 3.2.F). More specifically, for the inequality 3.2.E, it is only required that the minimum element of S, satisfies the inequality, because the fraction at that point reaches its maximum value. So, if the maximum value of fraction is lower than $e^{-\frac{TR}{y}}$, then the rest elements of S vector will satisfy the inequality. Commonly, for the inequality 3.2.F, it is only demanded, that the maximum element of S, satisfies the inequality, because the fraction at that point, reaches its minimum value. Thus, if the minimum value of fraction, is bigger than $e^{-M \cdot TR - \frac{TR}{y}}$, then the rest elements of S vector will satisfy the inequality. Consequently, the inequalities constraints 3.2.E and 3.2.F become:

- $\dfrac{sin\theta - {}^{Smin}/_x}{sin\theta - cos\theta \cdot \frac{Smin}{x}} < e^{-\frac{TR}{y}}$ (3.2.G)

- $\dfrac{sin\theta - {}^{Smax}/_x}{sin\theta - cos\theta \cdot \frac{Smax}{x}} > e^{-M \cdot TR - \frac{TR}{y}}$ (3.2.H)

And thus the Complementary Conditions 3.2.2 and 3.2.3 become:

- $\mu 1 \left(\dfrac{sin\theta - {}^{Smin}/_x}{sin\theta - cos\theta \cdot \frac{Smin}{x}} - e^{-\frac{TR}{y}} \right) = 0$ (3.2.4)

- $\mu 2 \left(-\dfrac{sin\theta - {}^{Smax}/_x}{sin\theta - cos\theta \cdot \frac{Smax}{x}} + e^{-M \cdot TR - \frac{TR}{y}} \right) = 0$ (3.2.5)

The Lagrangian now has the form:

$$L(x, y, \mu1, \mu2, \mu3, \mu4) = \sum_a \left(x \cdot \frac{sina\cdot\left(1-e^{-\frac{TR}{y}}\right)}{1-cosa\cdot e^{-\frac{TR}{y}}} - d \right)^2 + \mu1\left(\frac{sin\theta - {S_{min}}/{x}}{sin\theta - cos\theta\cdot\frac{S_{min}}{x}} - e^{-\frac{TR}{y}} \right) +$$

$$\mu2\left(-\frac{sin\theta - {S_{max}}/{x}}{sin\theta - cos\theta\cdot\frac{S_{max}}{x}} + e^{-M\cdot TR - \frac{TR}{y}} \right) + \mu3\cdot(0.2 - y) + \mu4\cdot(y-1.8)$$

Therefore, we demand the derivatives to be equal to zero and the Complementary conditions to be satisfied for $S = [S_{max}\ S_{min}]$, and not the whole vector of S(t).

- $$\frac{\partial L}{\partial x} = 2\left(\frac{x\cdot sina\left(1-e^{-\frac{TR}{y}}\right)}{1-cosa\cdot e^{-\frac{TR}{y}}} - d \right)\left(\frac{sina\left(1-e^{-\frac{TR}{y}}\right)}{1-cosa\cdot e^{-\frac{TR}{y}}} \right) + \mu1\left(\frac{S_{min}}{\left(sin\theta - \frac{cos\theta\cdot S_{min}}{x}\right)x^2} + \right.$$

$$\left. \frac{cos\theta\cdot S_{min}\left(\frac{S_{min}}{x} - sin\theta\right)}{x^2\left(sin\theta - \frac{cos\theta\cdot S_{min}}{x}\right)^2} \right) + \mu2\cdot\left(-\frac{S_{max}}{x^2\left(sin\theta - \frac{cos\theta\cdot S_{max}}{x}\right)^2} - \frac{cos\theta\cdot S_{max}\left(\frac{S_{max}}{x} - sin\theta\right)}{x^2\left(sin\theta - \frac{cos\theta\cdot S_{max}}{x}\right)^2} \right)$$

- $$\frac{\partial L}{\partial y} = 2\left(\frac{x\cdot sina\left(1-e^{-\frac{TR}{y}}\right)}{1-cosa\cdot e^{-\frac{TR}{y}}} - d \right)\cdot\left(\frac{cosa\cdot TR\cdot\left(1-e^{-\frac{TR}{y}}\right)\cdot sina\cdot x\cdot e^{-\frac{TR}{y}}}{y^2\cdot\left(1-cosa\cdot e^{-\frac{TR}{y}}\right)^2} - \frac{sina\cdot x\cdot TR\cdot e^{-\frac{TR}{y}}}{y^2\cdot\left(1-cosa\cdot e^{-\frac{TR}{y}}\right)} \right) -$$

$$\mu1\left(\frac{TR\cdot e^{-\frac{TR}{y}}}{y^2} \right) + \mu2\left(\frac{TR\cdot e^{-M\cdot TR - \frac{TR}{y}}}{y^2} \right) - \mu3 + \mu4$$

Thus, examining all the cases (bounds of constraints, interior-critical points, bound of 3.2.G constraint: $x = \frac{S_{min}\cdot\left(-1+e^{\frac{-TR}{y}}\cdot cos\vartheta\right)}{sin\vartheta\cdot\left(-1+e^{\frac{-TR}{y}}\right)}$, for y between 0.2 and 1.8, bound of 3.2.H constraint:

$x = \frac{S_{max}\cdot\left(-1+e^{\frac{-TR\cdot(M\cdot y+1)}{y}}\cdot cos\vartheta\right)}{sin\vartheta\cdot\left(-1+e^{\frac{-TR\cdot(M\cdot y+1)}{y}}\right)}$, for y between 0.2 and 1.8), based on the main idea we

mentioned above, we choose the optimal solution, among all, that satisfies the constraints and minimizes the prediction error.

The cases are summarized below:

1. $\mu1=0$, $\mu2=0$, $\mu3=0,\mu4=0$. All constraints are inactive.

2. $\mu2=0$, $\mu3=0$, $\mu4=0$ and $\frac{sin\theta - {S_{min}}/{x}}{sin\theta - cos\theta\cdot\frac{S_{min}}{x}} - e^{-\frac{TR}{y}} = 0$. Finding the optimal value in the bound of 3.2.G constraint and interior point of the 3.2.D line.

3. $\mu1=0$, $\mu3=0$, $\mu4=0$ and $-\frac{sin\theta - {S_{max}}/{x}}{sin\theta - cos\theta\cdot\frac{S_{max}}{x}} + e^{-M\cdot TR - \frac{TR}{y}} = 0$. Finding the optimal value in the bound of 3.2.H constraint and interior point of the 3.2.D line.

4. $\frac{sin\theta - {S_{min}}/{x}}{sin\theta - cos\theta\cdot\frac{S_{min}}{x}} - e^{-\frac{TR}{y}} = 0, -\frac{sin\theta - {S_{max}}/{x}}{sin\theta - cos\theta\cdot\frac{S_{max}}{x}} + e^{-M\cdot TR - \frac{TR}{y}} = 0$ $\mu3=0$ $\mu4=0$ which is absurd.

5. $\dfrac{sin\theta - ^{S_{min}}/_x}{sin\theta - cos\theta \cdot \frac{S_{min}}{x}} - e^{-\frac{TR}{y}} = 0$ $\mu2{=}0$ $\mu3{=}0$ and **y=1.8**. Finding the optimal value in the
bound of 3.2.G constraint and upper bound of line 3.2.D

6. $\dfrac{sin\theta - ^{S_{min}}/_x}{sin\theta - cos\theta \cdot \frac{S_{min}}{x}} - e^{-\frac{TR}{y}} = 0$ $\mu2{=}0$ **y=0.2** and $\mu4{=}0$. Finding the optimal value in the
bound of 3.2.G constraint and lower bound of line 3.2.D

7. $-\dfrac{sin\theta - ^{S_{max}}/_x}{sin\theta - cos\theta \cdot \frac{S_{max}}{x}} + e^{-M \cdot TR - \frac{TR}{y}} = 0$ $\mu1{=}0$ $\mu3{=}0$ and **y=1.8**. Finding the optimal value in
the bound of 3.2.H constraint and upper bound of line 3.2.D

8. $-\dfrac{sin\theta - ^{S_{max}}/_x}{sin\theta - cos\theta \cdot \frac{S_{max}}{x}} + e^{-M \cdot TR - \frac{TR}{y}} = 0$ $\mu1{=}0$ **y=0.2** and $\mu4{=}0$. Finding the optimal value in
the bound of 3.2.H constraint and lower bound of line 3.2.D

9. $\dfrac{sin\theta - ^{S_{min}}/_x}{sin\theta - cos\theta \cdot \frac{S_{min}}{x}} - e^{-\frac{TR}{y}} = 0$ $-\dfrac{sin\theta - ^{S_{max}}/_x}{sin\theta - cos\theta \cdot \frac{S_{max}}{x}} + e^{-M \cdot TR - \frac{TR}{y}} = 0$ y=0.2 and $\mu4{=}0$ which
is absurd.

10. $\dfrac{sin\theta - ^{S_{min}}/_x}{sin\theta - cos\theta \cdot \frac{S_{min}}{x}} - e^{-\frac{TR}{y}} = 0$ $-\dfrac{sin\theta - ^{S_{max}}/_x}{sin\theta - cos\theta \cdot \frac{S_{max}}{x}} + e^{-M \cdot TR - \frac{TR}{y}} = 0$ $\mu3{=}0$ and y=1.8
which is absurd.

11. $\mu1{=}0$ $\mu2{=}0$ **y=0.2** and $\mu4{=}0$. The only active constraint is the lower bound of 3.2.D

12. $\mu1{=}0$ $\mu2{=}0$ $\mu3{=}0$ and **y=1.8**. The only active constraint is the upper bound of 3.2.D

13. $\mu1{=}0$ $\mu2{=}0$ y=0.2 y=1.8 which is absurd.

14. $\dfrac{sin\theta - ^{S_{min}}/_x}{sin\theta - cos\theta \cdot \frac{S_{min}}{x}} - e^{-\frac{TR}{y}} = 0$ $\mu2{=}0$ y=0.2 and y=1.8 which is absurd.

15. $\mu1{=}0$ $-\dfrac{sin\theta - ^{S_{max}}/_x}{sin\theta - cos\theta \cdot \frac{S_{max}}{x}} + e^{-M \cdot TR - \frac{TR}{y}} = 0$ y=0.2 and y=1.8 which is absurd.

16. $\dfrac{sin\theta - ^{S_{min}}/_x}{sin\theta - cos\theta \cdot \frac{S_{min}}{x}} - e^{-\frac{TR}{y}} = 0$ $-\dfrac{sin\theta - ^{S_{max}}/_x}{sin\theta - cos\theta \cdot \frac{S_{max}}{x}} + e^{-M \cdot TR - \frac{TR}{y}} = 0$ y=0.2 and y=1.8
which is absurd.

It must be noticed that when we set to zero the multipliers $\mu3, \mu4$ then we are searching for
the optimal values for y between 0.2 and 1.8 for the x of the examined case.

Chapter 4

Perfusion Estimation Methods

The following descriptors are computed on the Region Of Interest (ROI). Consequently, these parameters, are calculated for each voxel, and therefore we have created a map, for each one of the following parameters. Some of these, are based upon both Signal Intensity and Gadolinium Concentration, and some others only on Signal Intensity.

These parameters belong in the category of semiquantitative descriptors of perfusion phenomenon, because they do not take into account the concentration in plasma, which is known as Arterial Input Function [11]. As we mentioned in section 2.2 the perfusion phenomenon, is equivalent to high needs for blood and considering that tumors require high amounts of blood supplies, in order to exist and to progress beyond its size limit, the cells must multiply, so angiogenesis plays a critical role in the process of cancer progression [8].

The semiquantitative parameters consist an indirectly method to extract information about the blood distribution, the possible tumor area and we examine the parameters below in order to discuss their results and decide which of these give satisfying results, where diagnosis could be possible.

Maximum Signal Intensity

We are measuring the maximum Signal intensity over time [6], from

$$S_{max} = \max S(t)$$

The extracted parametric map (figure 5.5), gives the level of signal intensity with the largest enhancement by the contrast media on each voxel.

Maximum Intensity Time Ratio

We are calculating [6], the maximum ratio from the baseline intensity, until the peak of the enhancement for the first time, to the interval time, in those time points, for both Signal Intensity, and Gadolinium Concentration:

$$MITR = \frac{S_{max} - S1}{t_{max}} \quad \text{and} \quad MITR = \frac{C_{max} - C1}{t_{max}}$$

Thus, the extracted parametric map in the figure 5.7 indicates the ratio of maximal signal change $S_{max} - S1$ to the interval time t_{max}.

The graphical equivalent is described in the figure 4.3.

Gradient Wash-in

The best line for the wash-in phase is estimated [6], for the Signal Intensities, but also for the Concentration Curve. The Wash-in phase ends when the Intensity reach its maximum value. This estimation, measures the gradient, by solving a linear fit problem on the wash-in phase:

$$[a_{in}\ b_{in}] = \arg\min \sum_{t\max}\|a + b \cdot t - S(t)\|_2^2$$

Where b_{in}, is the parameter that describes the wash-in gradient and $t_{\max}$ is the time of peak. Similarly, for the concentration curve:

$$[a_{in}\ b_{in}] = \arg\min \sum_{t\max}\|a + b \cdot t - C(t)\|_2^2$$

The slope of the line, describes the parametric wash-in map for each voxel that is created (figure 5.6). The fit of the line is described in the figures 4.2.

Area Under the Curve

We are performing an integration, [19, 29] in the whole area under the curve, both for Signal Intensity and Gadolinium Curve.

$$\text{AUC}=\int_0^{end} S(t)dt \qquad \text{and} \qquad \text{AUC}=\int_0^{end} C(t)dt$$

The calculation of the integral, was performed using Trapezoidal Rule.

In the parametric map of Area Under the Curve (figure 5.8), the result of the above integration correspond to the absorption of contrast media in each voxel.

Initial Area Under the Curve

We are examining, for each curve (Dynamic Intensity or Gadolinium Concentration), the wash-in phase, the phase until the curve reaches its maximum value, and we integrate this area, using Trapezoidal Rule. This parameter, informs us about the permeability and the speed of the enhancement.[7]

$$\text{IAUC}=\int_0^{max} S(t)dt \qquad \text{and} \qquad \text{IAUC}=\int_0^{max} C(t)dt$$

The parametric map of Initial Area Under the Curve (figure 5.9) contains the result of integration for each voxel that corresponds to the initial arrival of contrast agent that reflects blood flow, vascular permeability and the fraction of interstitial space [7].

The graphical equivalent is described in the figure 4.3.

Final Area Under the Curve

Respectively, for the wash-out phase, from the maximum value of Intensity, until the complete wash-out of the signal, we perform an integration for this area. This parameter, does not seem to provide enough information, but is essential for the measurement of the descriptor below (AUCR). [7]

$$\text{FAUC}=\int_{max}^{end} S(t)dt \quad \text{and} \quad \text{FAUC}=\int_{max}^{end} C(t)dt$$

In the parametric map of Final Area Under the Curve, in figure 5.10 each voxel contains the result of the above integration which correspond to the size of Extravascular Extracellular Space (EES) and indicates the wash-out phase.

The graphical equivalent is described in the figure 4.3.

Area Under the Curve Ratio

The mathematical equivalent for this parameter, is quotient of the Initial Area Under the Curve, and the Final Area Under the Curve:

$$AUCR = \frac{IAUC}{FAUC}$$

for both Signal Intensity, and Gadolinium Concentration.

In this parametric map (figure 5.11), pixels with considerably different intensity, are considered of higher interest [7] and of areas possibly pathological.

The graphical equivalent is described in the figure 4.3.

As it is observed (section 5.3), in the cases that we calculate parameters for both Signal Intensity and Gadolinium Concentration, the results including the discrimination of different contrast on image and the discrimination between the normal areas and possible carcinoma are almost the same.

The figures below indicate the graphical equivalent of those parameters:
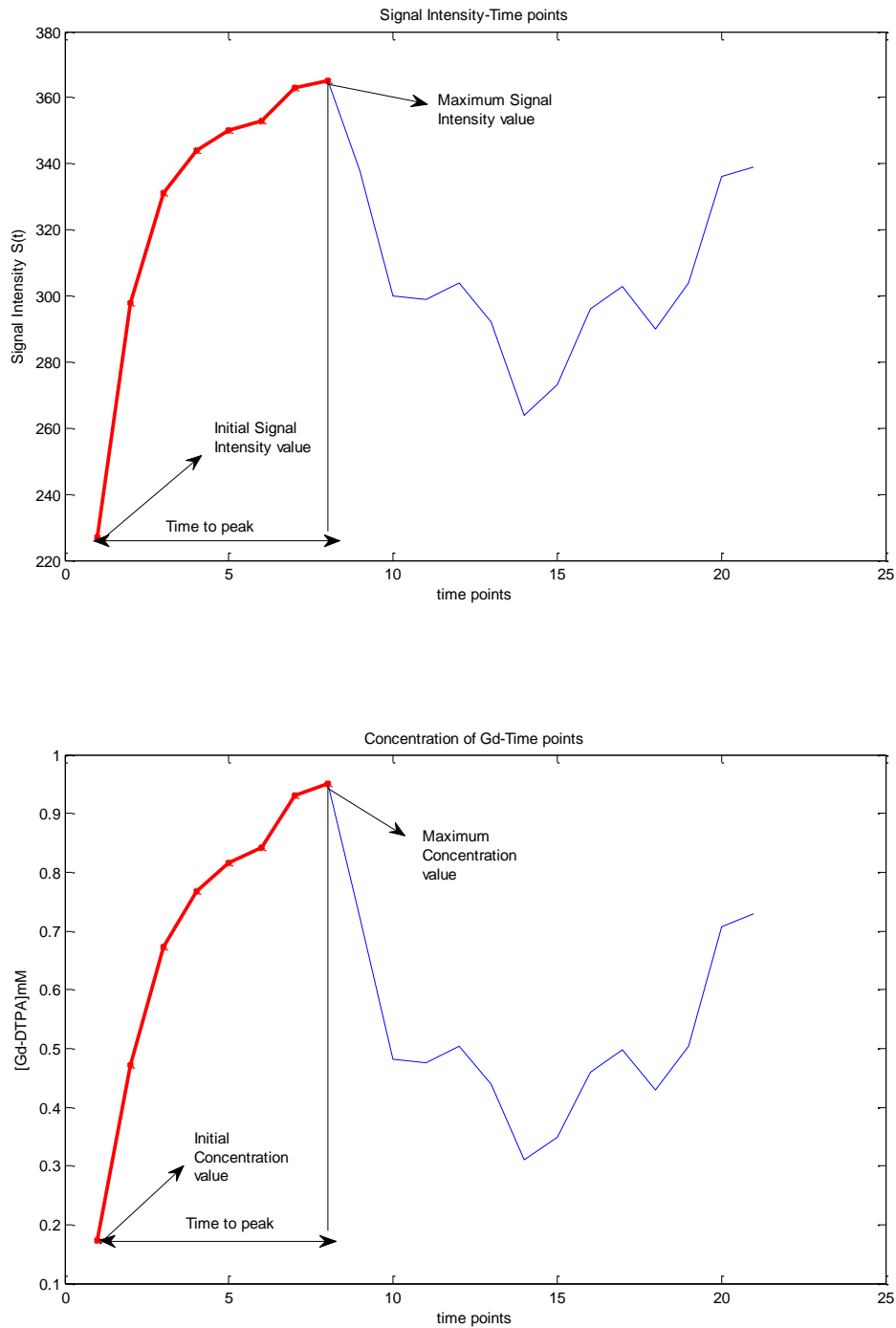
Figure 4.1: Explanation of Maximum Signal Intensity, and Maximum Intensity Time Ratio, for both Signal Intensity and Gadolinium Concentration.

Furthermore, an example of Wash-in gradient for a specific voxel, for both Signal Intensity and Gadolinium Concentration is given:

The slope of the line, describes the parametric wash-in map figure 5.6, that is created.
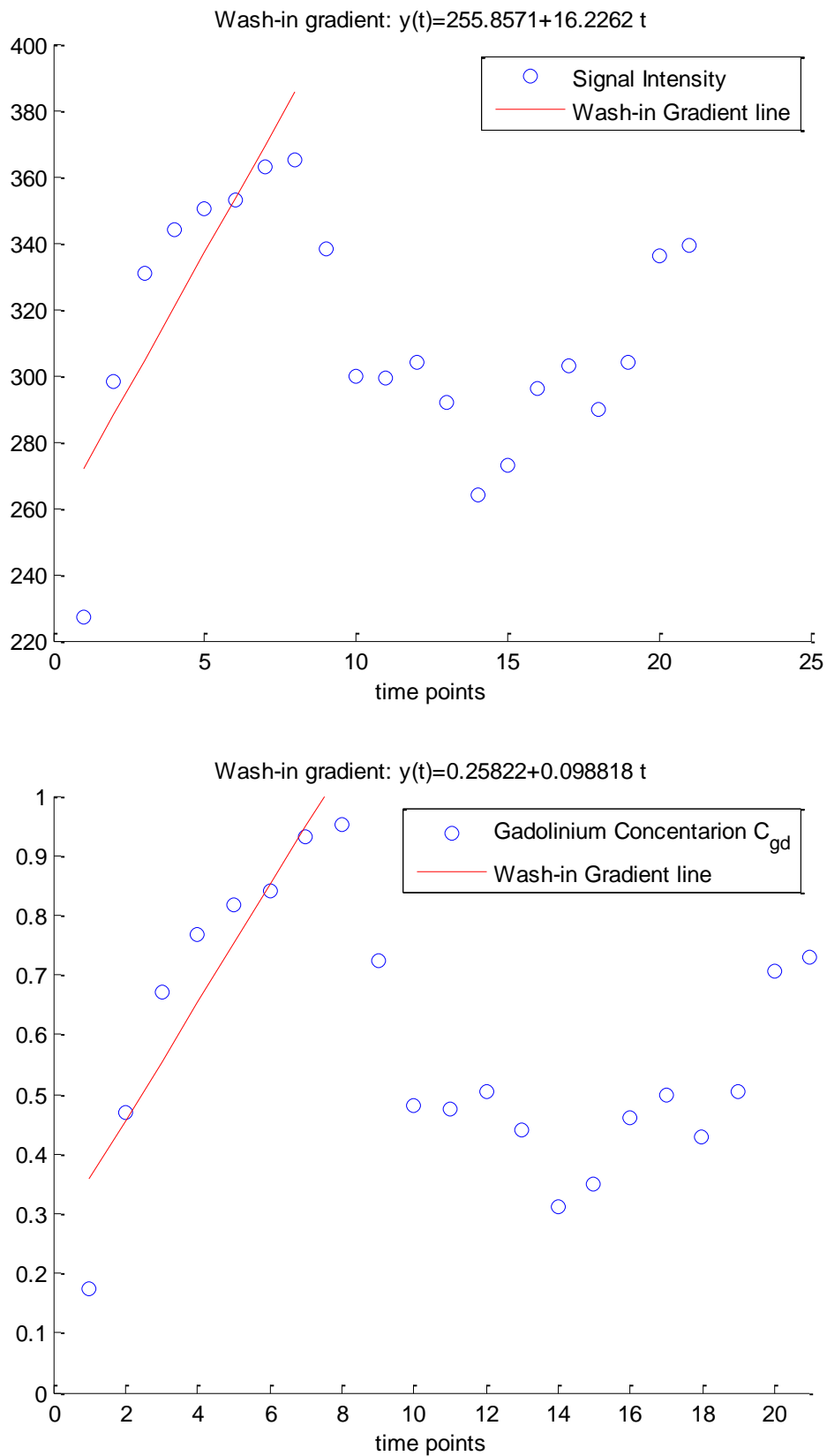
Figure 4.2: Explanation of Gradient Wash-in line, as the best line of the wash-in phase. The slope of the line, describes the parametric wash-in map that is created.

And also for the parameters based on integration (Initial Area Under the Curve, Final Area Under the Curve, Whole Area Under the Curve).
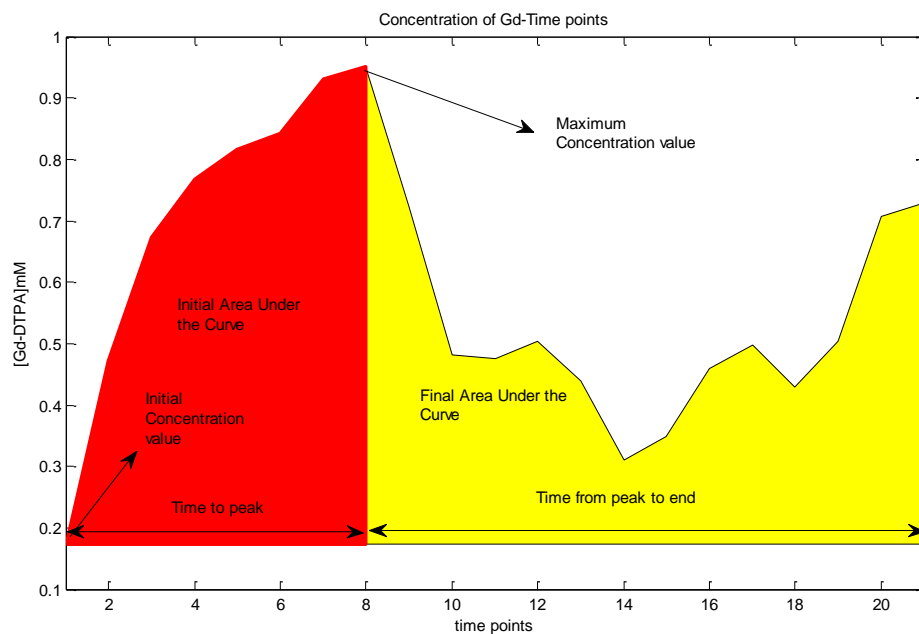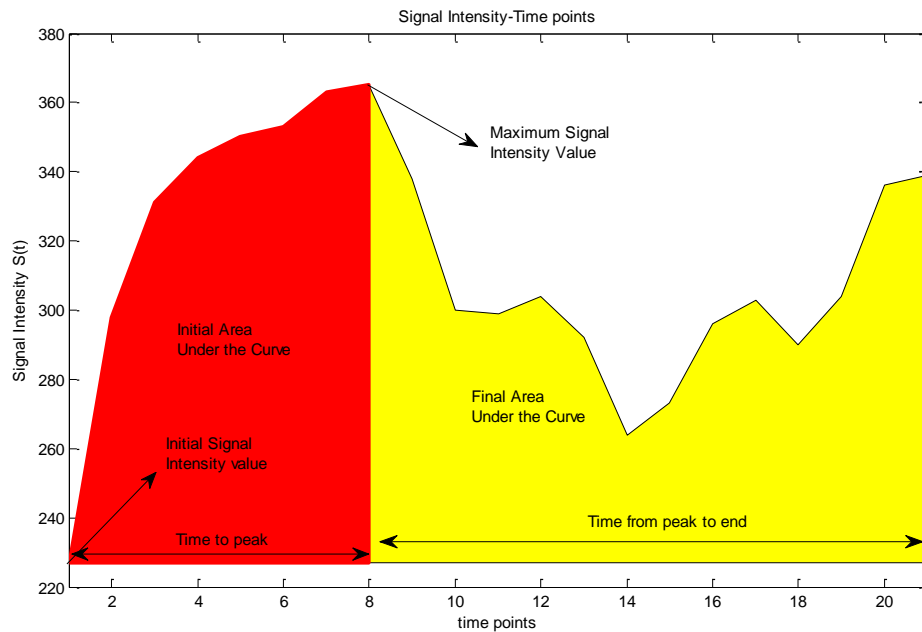

Figure 4.3: Explanation of integration based parameters: Initial, Final and Whole Area Under the Curve, for both Signal Intensity and Gadolinium Concentration.

Chapter 5

Results

The results, of this work, are cited below. The maximum upper bound for concentration, is set to be 1 mM. A map has been created, on the Region Of Interest (ROI), with the pre-contrast relaxation times. Also, maps for each Semi-quantitative parameter, are created, for both Signal Intensity and Gadolinium Concentration. The optimization results cited below, are for each one of the three types of curves, that we encounter, as mentioned in section 1.4.

5.1 Experimental Data

The data were given only for this study from University of Crete, Medical Physics Department, and they have been anonymized. They are composed of Dicom series, and were provided for both cervix-pelvis area, but also for brain region. The brain region has a role of validation for this study, because white matter and gray matter have typical values of relaxation times (T10). So we compare our predictions, with the reference values[2] of white matter (0.9s) and gray matter (1.2s). More about this part is discussed in section 5.4

The dicom series were given for each slice in different flip angle. Thus, we have a series of images in different slices for each of different flip angles Also, dicom series of perfusion, which means series of images for each slice and for each time point from the moment of injection of contrast agent, are provided. The above images, were converted intro 3D arrays, and 4D arrays, respectively, for a particular examined slice, via MATLAB. The above conversion, is essential in order to have the intensities in time and the intensities in angle gathered together. Consequently, we solve our optimization problem, for each voxel and we create a map of parameters, as described below. In this study, as contrast agent the gadopentetate dimeglumine (Gd-DTPA) was used for the data of cervix pelvis and Gadobutrol (Gd-BT-DO3A), for the brain data.

More specifically, for the cervix pelvis data we had 20 images slices for each one of the 7 different flip angle that was used and 30 images in time sequence. From the above, we examine the images for a specific slice (in this study we choose the 8 slice). Thus, for the examined slice we have 7 images in different flip angle and 30 images in time sequence. It must be noticed that

from the 30 images of time, we hold only the images without baseline (figure 1.1), that means images with contrast agent arrival.

Equivalently, for the brain data we have 24 images slices for each one of the 7 different flip angle that was used and 34 images in time sequence. From the above, we examine again the images for a specific slice (in this study we choose the 12 slice). Thus, for the examined slice we have 7 images in different flip angle and 34 images in time sequence. It must be noticed that from the 34 images of time, we hold only the images without baseline (figure 1.1), that means images with contrast agent arrival.

For the *pathological area of uterus*, the region of interest which is examined after an indication for the data, is an area of 49x39, which contains 1233 nonzero voxels. In the case of the *non pathological area of uterus*, the region of interest which is examined, is an area of 18x26, which contains 468 nonzero voxels.

Equivalently, for the *brain data in the case of validation*, an area of 24x24 which contains 576 voxels is examined. Also, for the *non pathological area of brain*, the region of interest of 19x22 area which is examined contains 418 nonzero voxels.

The examined slice of interest, for the case of pelvis-cervix (where angiogenesis was found) is the following:
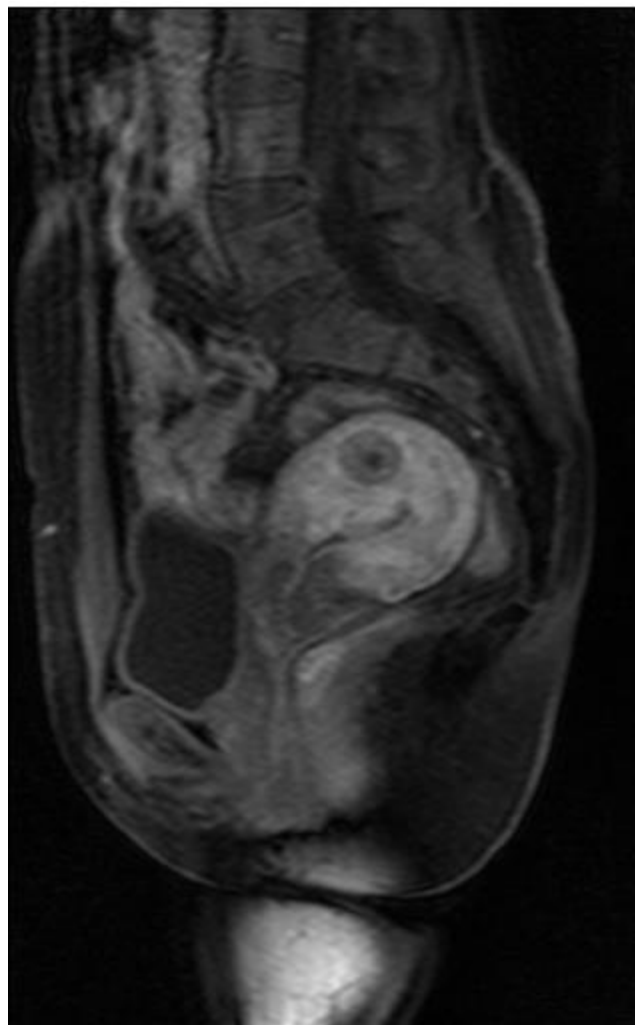

Figure 5a: Examined Slice of the cervix-pelvis image

Thus, after an indication for the data, the Region Of Interest is:
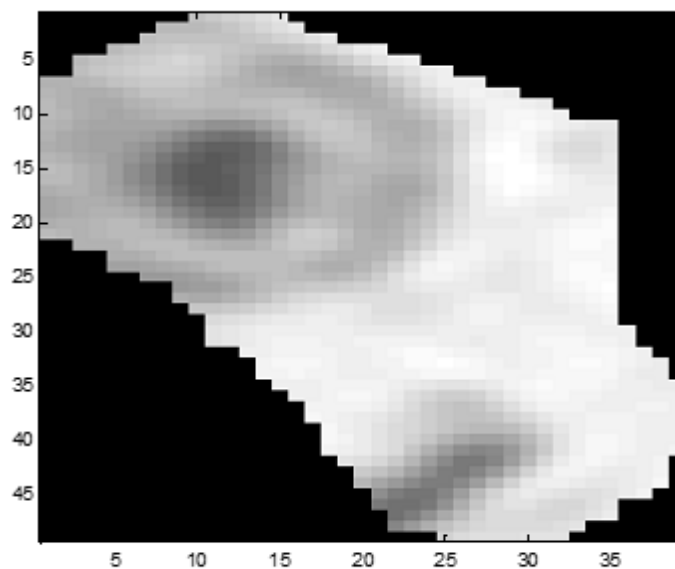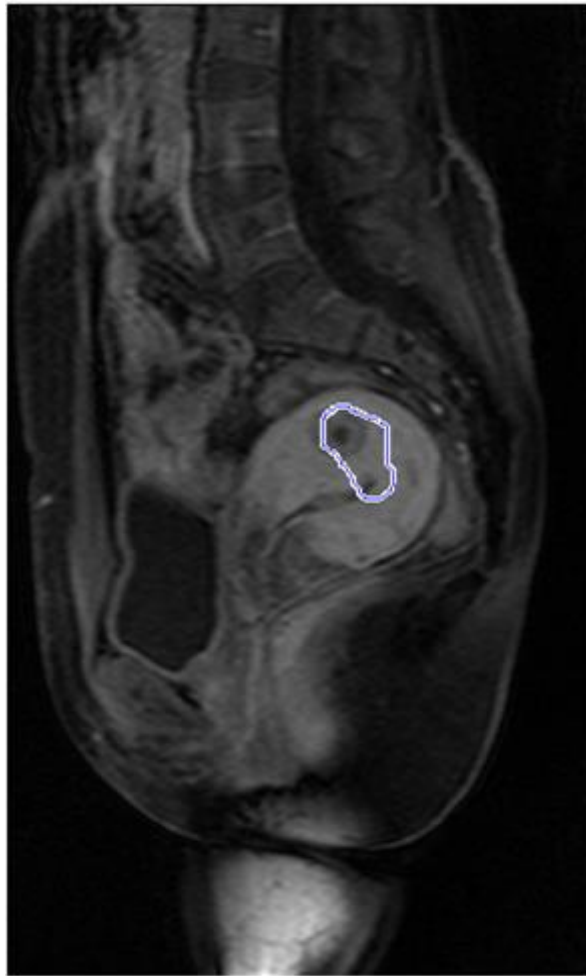
Figure 5b: The Region Of Interest, pathological, in the examined slice of uterus

The following optimization-concentration results, are for the image of *pathological* ROI. For the case of concentration (section 5.2), we cite three results on the three typical curves (Type I-

III), that we encounter. It must be noticed, that the last flip angle (60°), is used most of the times, for angiography.

For the cases of *perfusion descriptors*, we cite in section 5.3, the parametric maps, we extracted.

In section 5.4, the curves that we extracted from the optimization, for the *non pathological* ROI, and the parametric map of T10, are cited.

For the case of *validation*, we cite in section 5.5, the T10 map and the concentration-optimization results for Gray and White Matter.
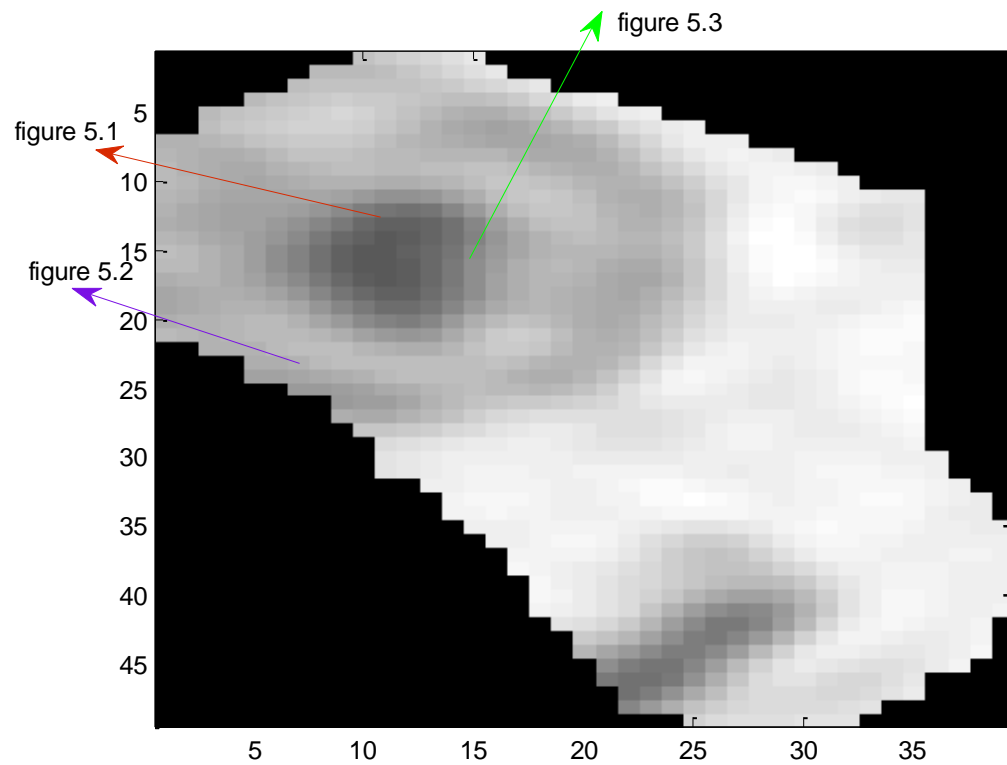
Figure 5c: The position of the figures 5.1, 5.2, 5.3 in the examined slice of pathological uterus data.

5.2 Concentration & Optimization Results

For the pathological Region Of Interest in uterus, the results of the three typical curves, that we encounter:
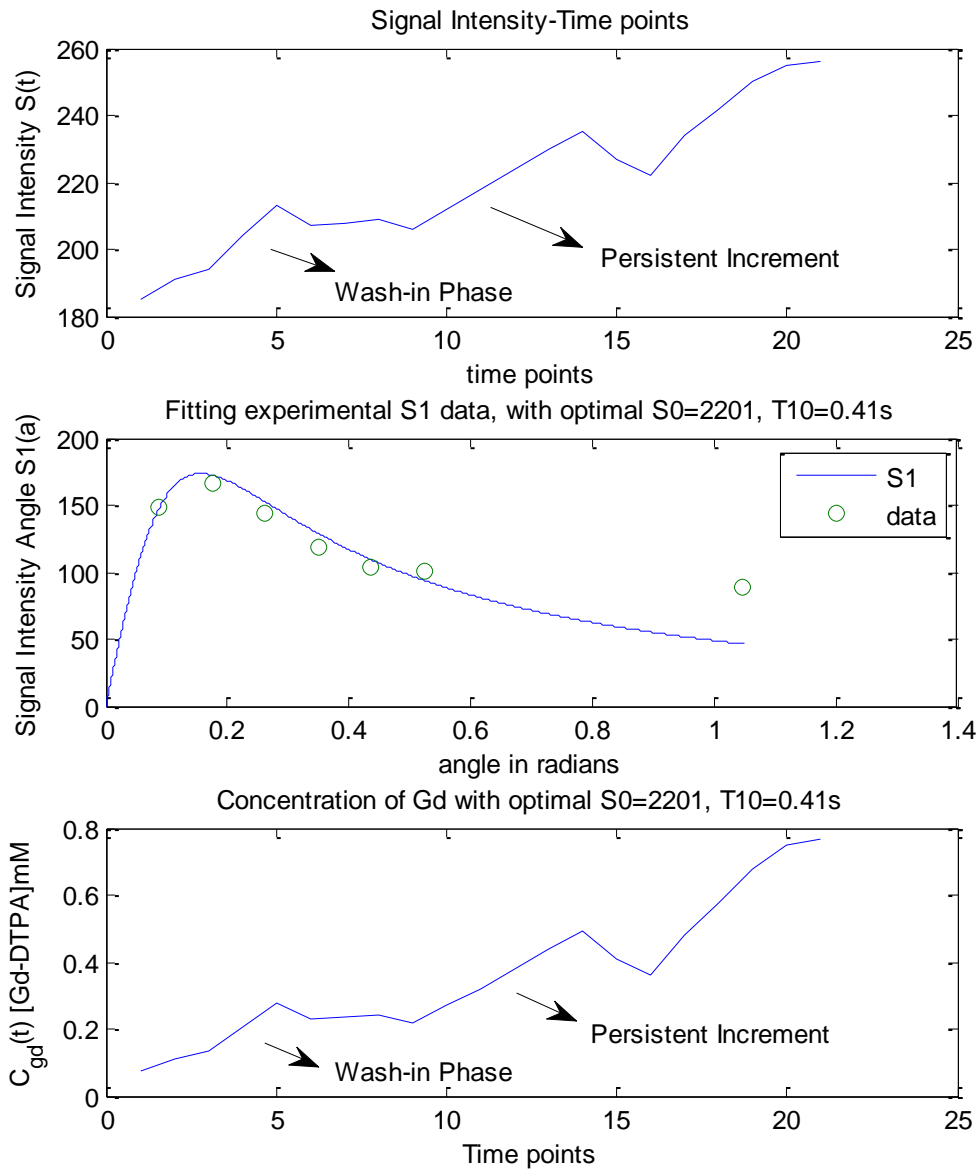

Figure 5.1: Concentration and Optimization Results for the type I of curve. In the first figure, we can see the Signal Intensity per Time. In the second figure, the fit to the experimental data [149 166 144 118 103 101 89], is shown, with the optimal values of S0, and T10. Finally, in the third figure, the curve of the Gadolinium Concentration is shown, with the optimal S0 and T10.
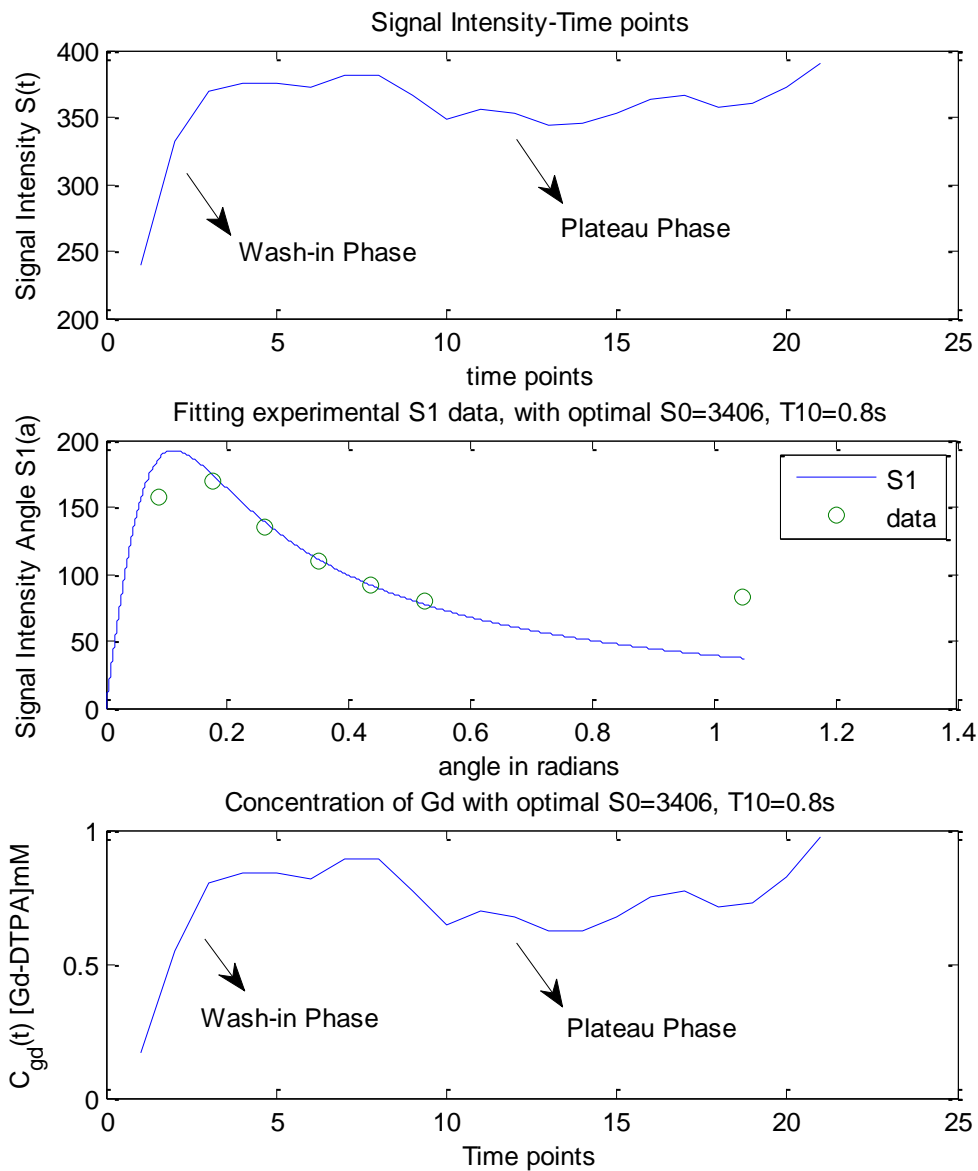
Figure 5.2: Concentration and Optimization Results for the type II of curve. In the first figure, we can see the Signal Intensity per Time. In the second figure, the fit to the experimental data [157 169 135 109 92 80 83], is shown, with the optimal values of S0, and T10. Finally, in the third figure, the curve of the Gadolinium Concentration is shown, with the optimal S0 and T10.
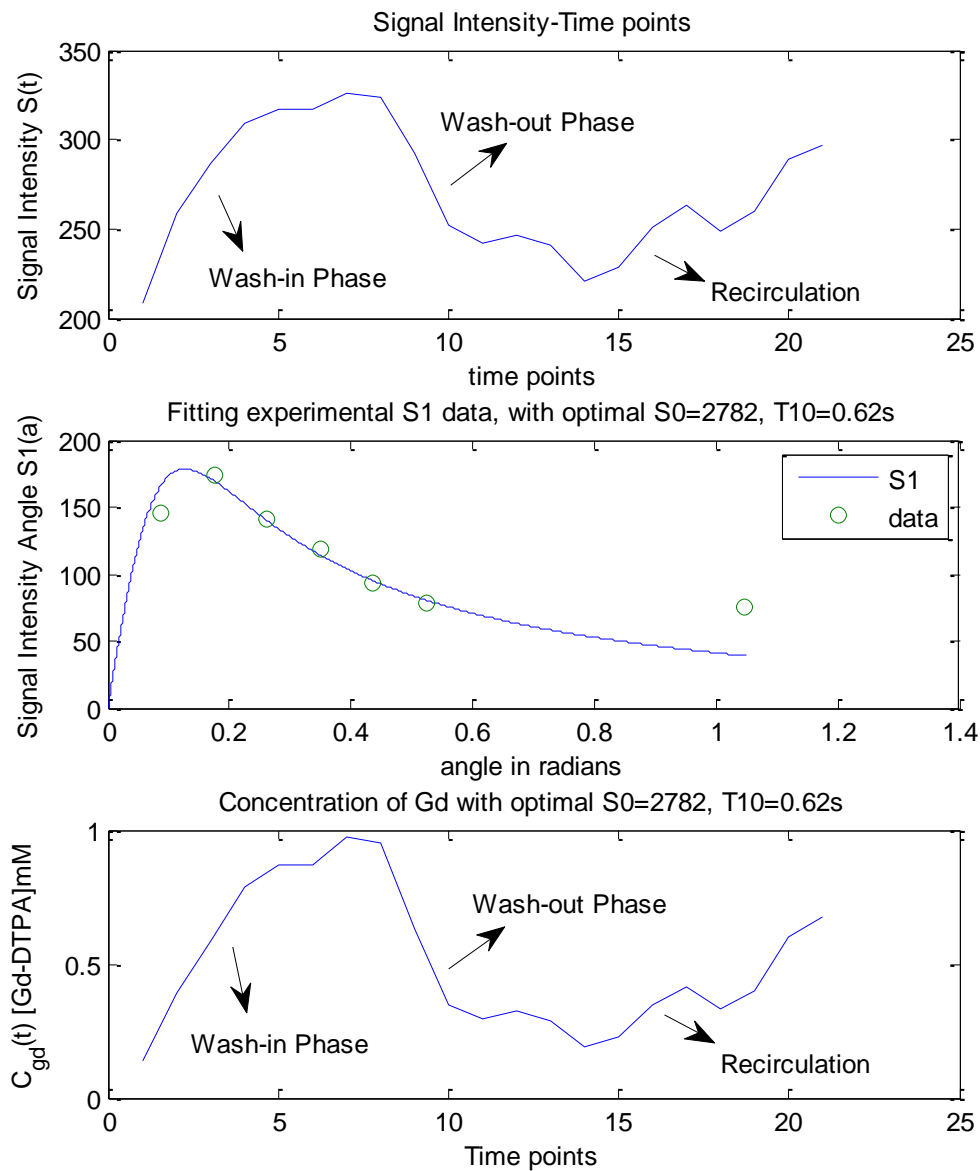
Figure 5.3: Concentration and Optimization Results for the type III of curve. In the first figure, we can see the Signal Intensity per Time. In the second figure, the fit to the experimental data [146 174 141 118 93 79 75], is shown, with the optimal values of S0, and T10. Finally, in the third figure, the curve of the Gadolinium Concentration is shown, with the optimal S0 and T10.

5.3 Perfusion Estimation Results

The results of the semiquantitative parameters that we used are shown below. We present T10 map, Maximum Signal Intensity, Maximum Intensity Time Ratio, Gradient Wash-in. Also, Initial Area Under the Curve, Final Area Under the Curve and Area Under the Curve Ratio are cited.

In the map of *T10*, (Figure 5.4), the shape of the ROI of cervix-pelvis is recognizable, and the areas with different contrast in image can be seen. The possible carcinoma is in the range of 0.8-0.9s and can be identified easily.

Figure 5.5 is the map of *Maximum Signal Intensity*, where higher values are located in the center of the ROI image. The shape of the cervix pelvis region of interest is also recognizable. The area in the center has higher maximum signal intensity than in the area in the top, which means that there is possibly high blood distribution in the centre. The possible carcinoma has a ring enhancement as it can be observed with a specific range of values.

For the *Maximum Intensity Time Ratio* (Figure 5.7 i, ii), there is a discrimination between the lesion and the other areas. This semiquantitative parameter, as the ratio of maximal signal change $S_{max} - S_1$ to the interval time, in the examined region appears higher in the center and lower in the area of possible lesion.

The *gradient wash-in* map (Figure 5.6 i,ii), has a similar, behavior to the result of Maximum Intensity Time Ratio. The pathological area has a different range of values, comparing to the normal areas. This parameter examines the slope of the gradient of upsweep of enhancement and we can observe a similar range of values in the region of possible carcinoma along with the ring enhancement of the lesion. The region in the center of the ROI has higher gradient, which correspond to higher perfusion.

Area under the whole curve, (AUC Figure 5.8), discriminates not in detail the lesion and the rest normal areas, by having different range of values. It measures the absorption of contrast agent from the time of arrival until the total wash-out.

In the figure 5.9(i-ii), *Initial Area Under the Curve*, describes the permeability of the tissue of interest, and the phase of wash-in, that means the phase until the signal reaches each maximum value. Also, it represents the early leakage of contrast agent into the Extracellular Extravascular Space (EES). This descriptor, provides a good result about the discrimination of lesion and the normal areas. IAUC measures the initial arrival of contrast agent that reflects blood flow, vascular permeability and the fraction of interstitial space [7]. So as it can be observed the possible carcinoma area has increased value, which means high leakage of contrast agent. Also the area in the bottom of the ROI has high IAUC, which is expected because it correspond to the end of the cervical of the uterus and we have increased vascularity.

In the figure 5.10(i- ii), *Final Area Under the Curve*, does not give enough information about the pathological area. Increased values of FAUC, are explained by increased EES, which means decreased tumor cellularity and less tissue damage [7]. Simply, this parameter is more essential in order to compute the parameter below. In the FAUC results we can observe the area in the center of the ROI to have increased FAUC values, which means we have less tissue damage. On the other hand, in the top of the uterus, the ring enhancement of tumor has lower values, which is equivalent to more tumor cellularity.

Figure 5.11(i-ii), *Area Under the Curve Ratio*, shows a good result about the pathological area, with the lesion to have considerably different values from the normal areas and can be identified. As a quotient of IAUC, and FAUC, it consists [7] the rate constant between the EES, and the blood plasma. The area in the bottom of the parametric map, has high value, possibly because it is the end of the cervical, where we have increased vascularity.

Comparing the above descriptors, MITR (figure 5.7) and Gradient wash-in (figure 5.6) have similar results. The area of possible carcinoma, in both cases, has similar range of values.

On the other hand, IAUC (figure 5.9) and AUCR (figure 5.11), indicate the area of most interest, with higher values than the others. Especially, in AUCR (figure 5.11) the possible carcinoma, has considerably different values from the normal tissue and can be identified easily.

The above descriptors are applied for both Signal Intensity, and Gadolinium Concentration, and the Parametric Maps are almost the same about the discrimination of the different areas.

Finally, in the histogram of figure 5.12, we see the distribution of the T10 values, and so the number of voxels for each different kind of tissue.

From the above perfusion descriptors, the *Maximum Signal Intensity* simply gives the level of the signal intensity with the largest enhancement by the contrast media from $S_{max} = \max S(t)$ [6] so it has low computational requirements. Similarly, in the case of *Maximum Intensity Time Ratio,* as the ratio of maximal change $S_{max} - S_1$ (or $C_{max} - C_1$) in the interval time t_{max} has not increased computational requirements. On the other hand, the estimation of the initial gradient of the upsweep of enhancement curve is based upon the least square fitting of the best line during the wash-in phase as described in Chapter 4 figure 4.2, so the computational requirements are increased. For the integration based parameters such as *Initial Area Under Curve, Final Area Under Curve and Area Under the Whole Curve,* the integration was achieved using Trapezoidal role and was calculated via MATLAB. The graphical equivalent of these integrations are seen in the figure 4.3. The integration increases the computation requirements of these parameters comparing to the other stated previously. Moreover, the *Area Under the Curve Ratio,* as the quotient of Initial Area Under Curve and Final Area Under the Curve requires a division between the two images in voxel-by-voxel basis.

The above perfusion descriptors were calculated for both Signal Intensity and Gadolinium Concentration. When the calculation is based upon Concentration as it can be seen in the Block Diagram of figure 2.5, it is required an estimation of the optimal T10, S0 that satisfy our constraints, in order to measure the concentration over time. On the other hand, when the calculated perfusion descriptors are based on Signal Intensity, we measure directly the descriptors.

Furthermore, the descriptors based upon Signal Intensities are probably less sensitive comparing with the one based on Gadolinium Concentration. This is reasonable, because the estimated values of T10 and S0 which are essential in order to measure the contrast agent concentration change from region to region more easily than the Signal Intensities.

Concerning the efficiency of those parameters the *Area Under the Curve Ratio* in figure 5.11 gives the clearest result concerning the identification of lesion. *Initial Area Under the Curve* in figure 5.9 is efficient to discriminate areas with high leakage of contrast agent in EES with other areas. The possible carcinoma is also easily identified in that parameter. *Final Area Under the Curve* in figure 5.10 is not that efficient to observe the lesion, but more to identify the areas with less tumor cellularity. *Area Under the Whole Curve* in figure 5.8 gives a basic idea of the discrimination between the lesion and the normal tissue. In the case of *Maximum Intensity Time Ratio* (figure 5.7) and *Gradient Wash-in* (figure 5.6)*,* these parameters have the possible carcinoma in a specific range of values and can be identified but not in much detail as AUCR (figure 5.11) and IAUC (figure 5.9). Also, areas with high needs for blood have increased values. Finally, in the *Maximum Signal Intensity* map in figure 5.5, the lesion can be identified but not in detail as the above parameters.

One possible combination would be to calculate the average Area Under the Whole Curve over time, AUC/time in order to measure the average Gadolinium Concentration over the interval time.
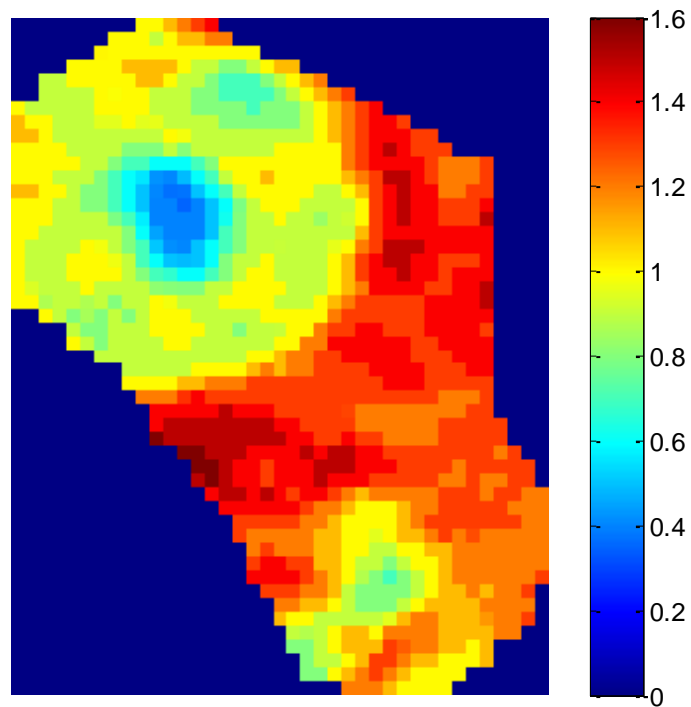
Figure 5.4: Parametric Map of pre-contrast relaxation time T10. The area of values higher than 1.2 possibly correspond to fluid or water based area. The lesion seems to have a range of values near 0.8s, but not to be a general behavior.
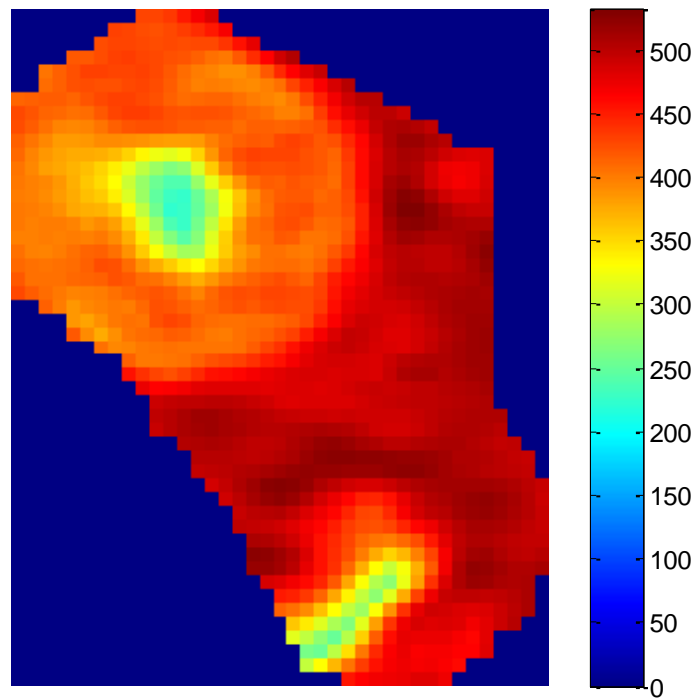
Figure 5.5: Parametric Map of Maximum Signal Intensity. This map describes the level of the Signal Intensity S(t) with the largest enhancement by the contrast media at each voxel [6].
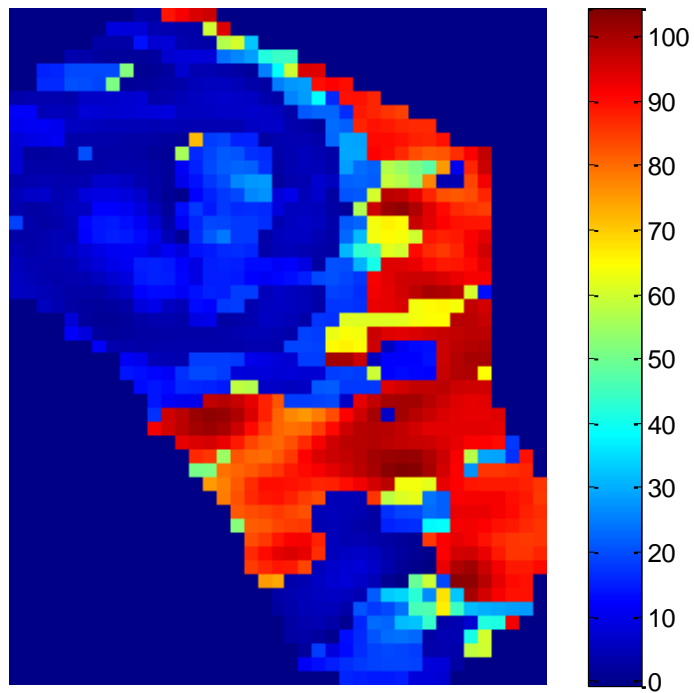
(i) Parametric Map of Gradient Wash-in for Signal Intensity
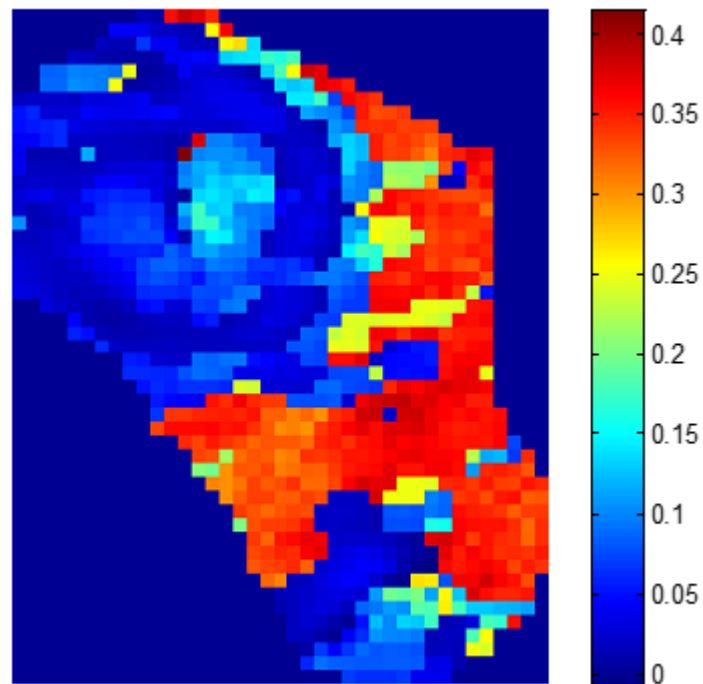
(ii) Parametric Map of Gradient Wash-in for Gadolinium Concentration

Figure 5.6: Parametric Map of Gradient Wash-in, for Signal Intensity and Gadolinium Concentration. The slope of the best fitting line of the wash-in phase, describes the parametric wash-in map for each voxel that is created [6].
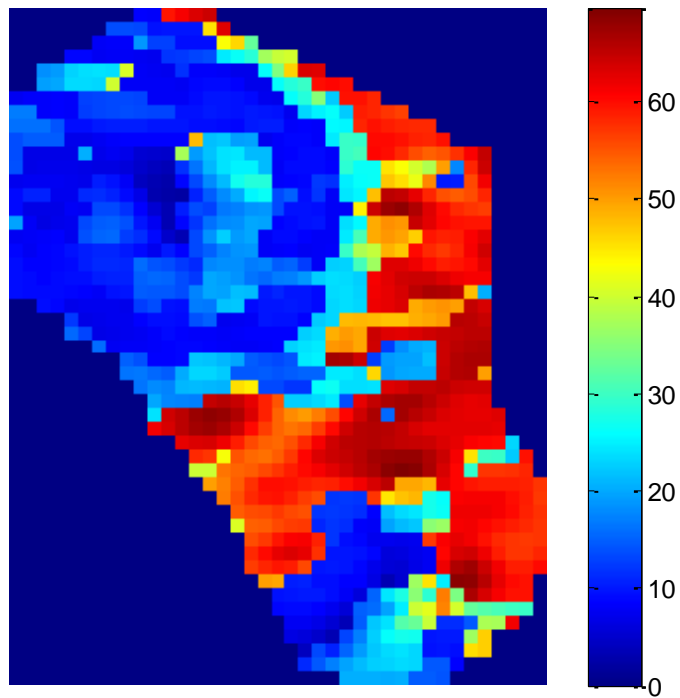
(i) Parametric Map of Maximum Intensity Time Ratio (MITR) for Signal Intensity
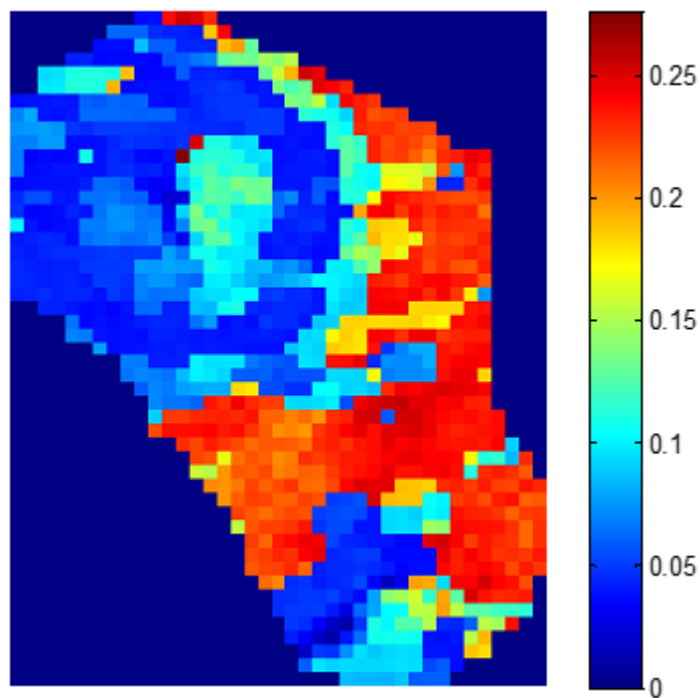
(ii) Parametric Map of Maximum Intensity Time Ratio(MITR) for Gadolinium Concentration

Figure 5.7: Parametric Map of Maximum Intensity Time Ratio (MITR), for both Signal Intensity and Gadolinium Concentration. MITR simply gives the ratio of maximal change $S_{max} - S_1$ (or $C_{max} - C_1$) in the interval time t_{max} for each voxel [6].
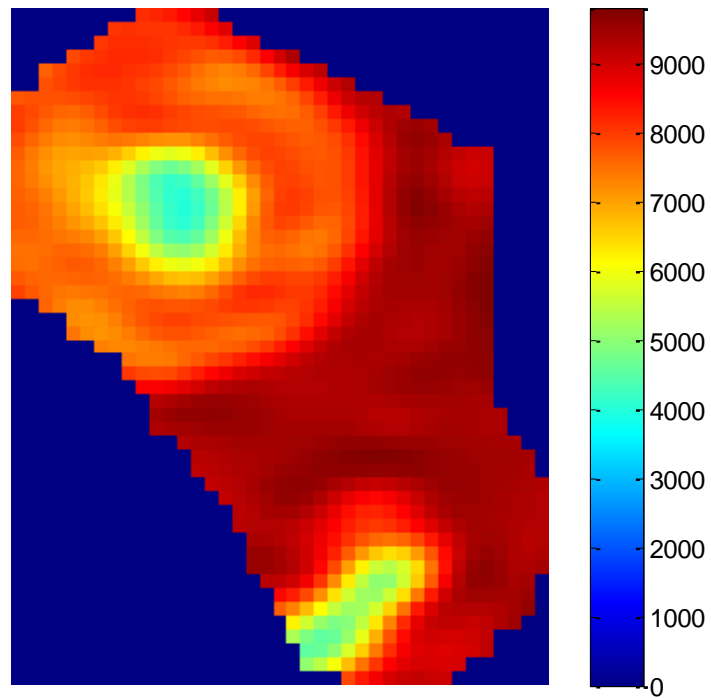
(i) Parametric Map of Area Under the Curve for Signal Intensity Curve (AUC)
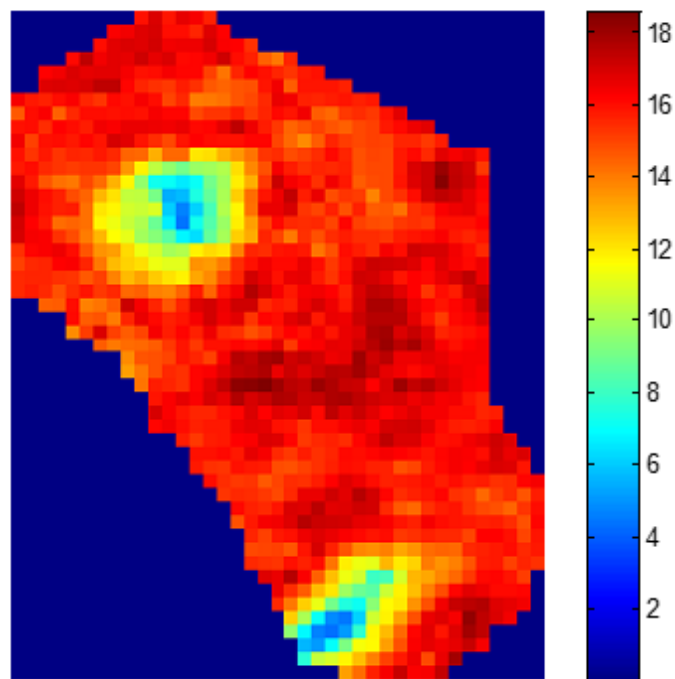

(ii) Parametric Map of Area Under the Curve for Gadolinium Concentration (AUC)

Figure 5.8: Parametric Map Of the whole Area Under the Curve (AUC), for both Signal Intensity and Gadolinium Concentration. It measures the absorption of contrast agent from the time of arrival until the total wash-out.
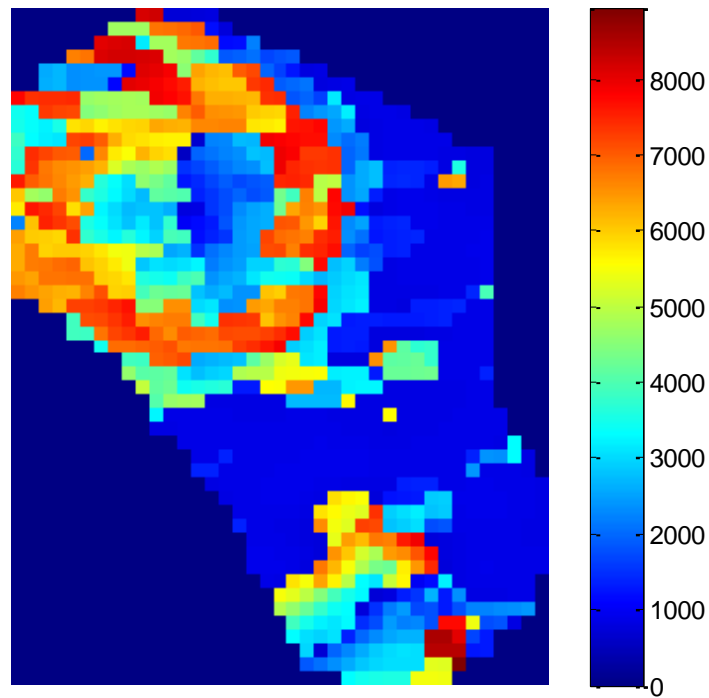
(i) Parametric Map of Initial Area Under the Curve for Signal Intensity (IAUC)
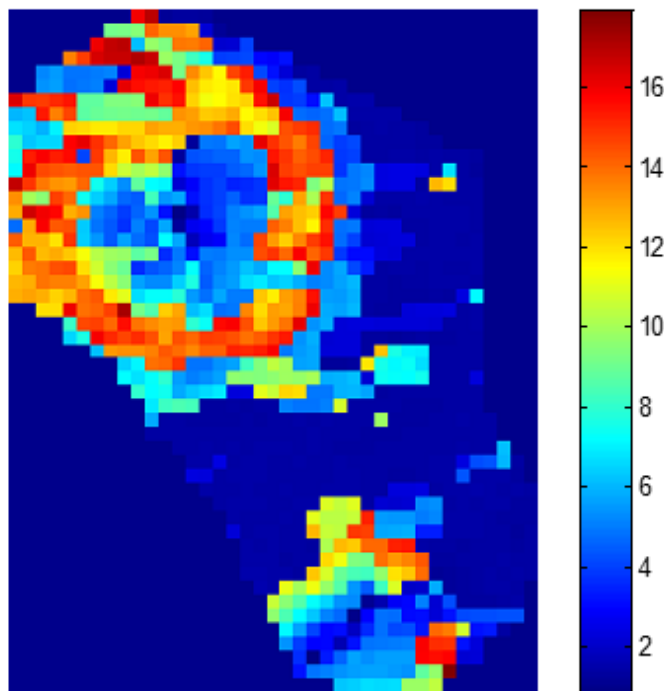
(ii) Parametric Map of Initial Area Under the Curve for Gadolinium Concentration (IAUC)

Figure 5.9: Parametric Map of Initial Area Under the Curve (IAUC), for both Signal Intensity and Gadolinium Concentration. IAUC measures the initial arrival of contrast agent that reflects blood flow, vascular permeability and fraction of interstitial space [7].
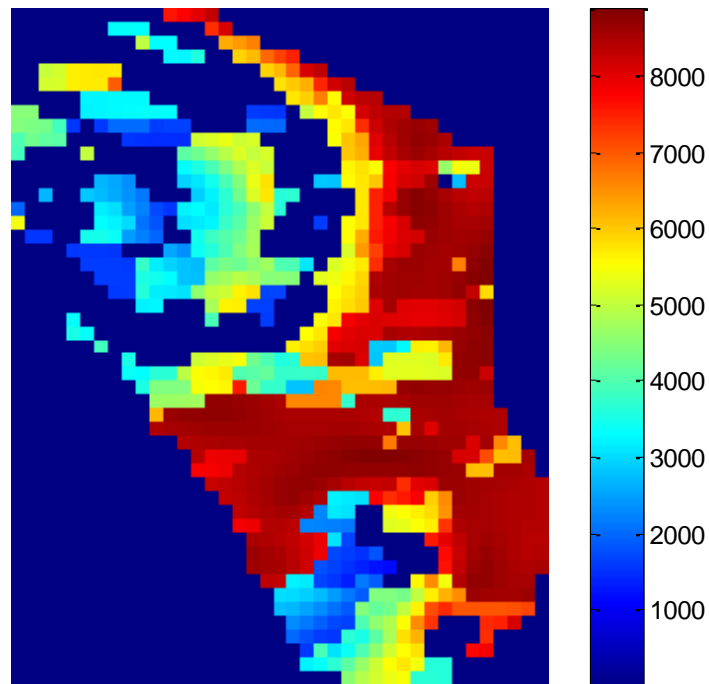
(i) Final Area Under the Curve for Signal Intensity (FAUC)
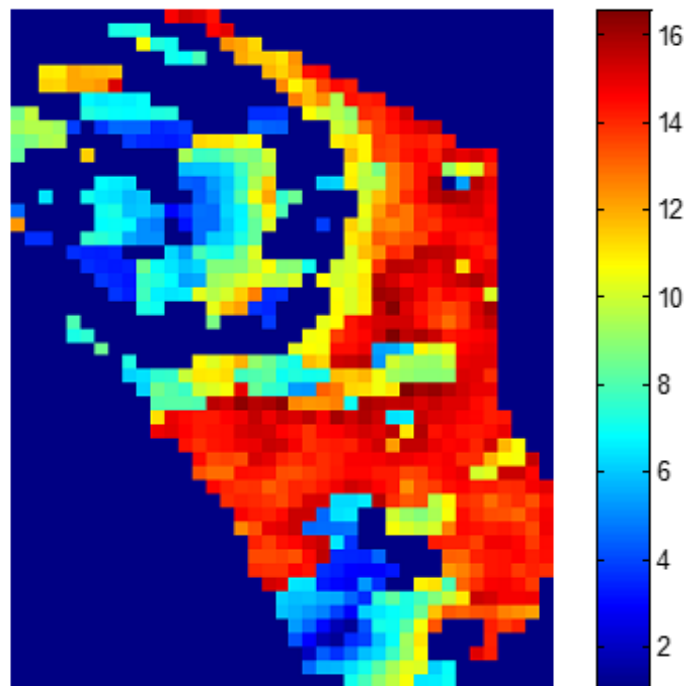
(ii) Final Area Under the Curve for Gadolinium Concentration (FAUC)

Figure 5.10: Parametric Map of Final Area Under the Curve (FAUC) for both Signal Intensity and Gadolinium Concentration. Increased values of FAUC, are explained by increased EES, which means decreased tumor cellularity and less tissue damage [7].
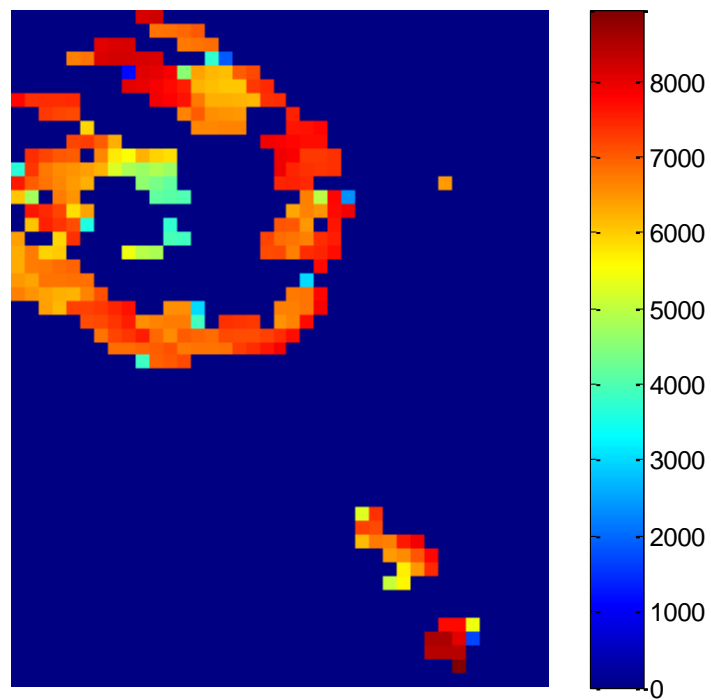
(i) Area Under the Curve Ratio for Signal Intensity (AUCR)
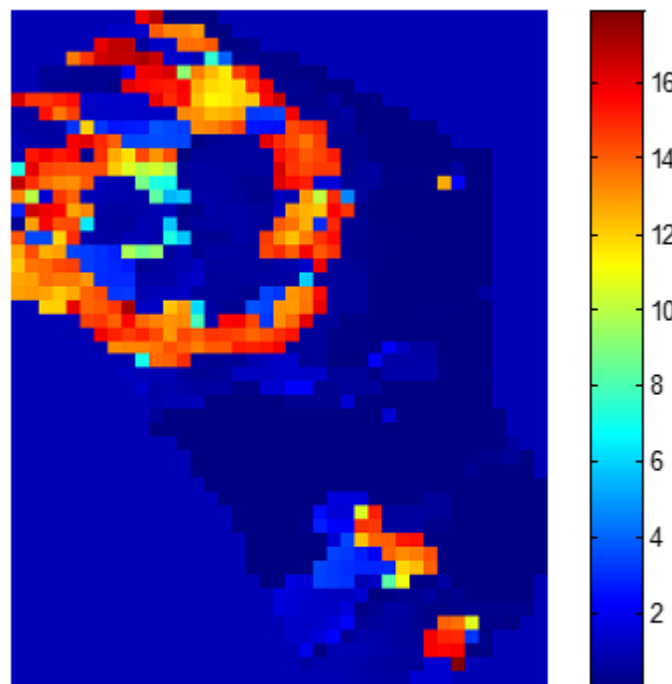
(ii) Area Under the Curve Ratio for Gadolinium Concentration (AUCR)

Figure 5.11: Parametric Map of Area Under the Curve Ratio (AUCR) , as a quotient of IAUC and FAUC, for both Signal Intensity and Gadolinium Concentration, it consists [7] the rate constant between the EES and the blood plasma.
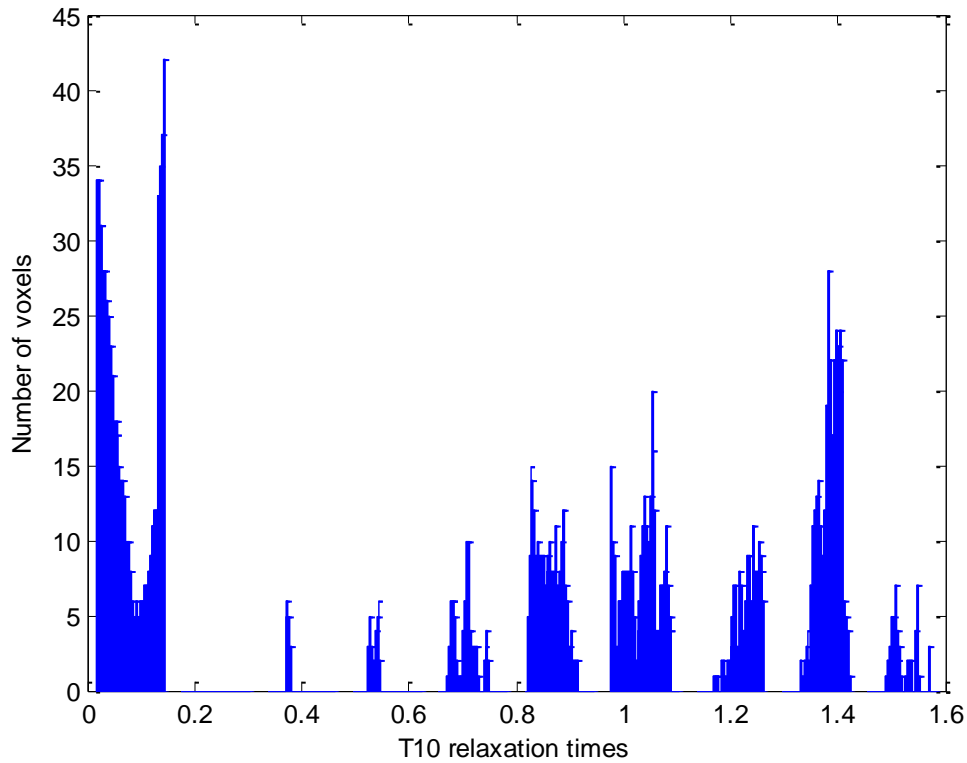
Figure 5.12: Histogram Of T10 Relaxation Times. The areas of no interest, have relaxation times equal to zero, so zero T10 values, correspond to areas with no particular interest.

It can be noticed that although we set our bound of estimation for T10, the range of $0.2 < T10 < 1.8s$, our maximum T10 value is 1.6s, which means that our upper bound is valid for the examined Region Of Interest.

Higher values (higher than 1.2s) of T10 relaxation times correspond to a more fluid area whereas values near 1.2s are most of the time water based tissues. Muscle usually has a relaxation time near 1s and fat a very low T10 value near 0.2s [26]. In our study, the possible carcinoma as can be observed in the AUCR results (figure 5.11) is the area in T10 map (figure 5.4) with values near 0.8s.

5.4 Non pathological areas results

In this section, we cite the concentration & optimization results for a non- pathological area, selected in the uterus data (figure 5.14, 5.15) but also on brain data (figure 5.17, 5.18). The parametric map of pre-contrast relaxation time T10 is cited as well (figure 5.13, 5.16), for each one of the ROIs.

Non-pathological Uterus Region

Thus, a Region Of Interest of a non cancerous area is examined in uterus data.
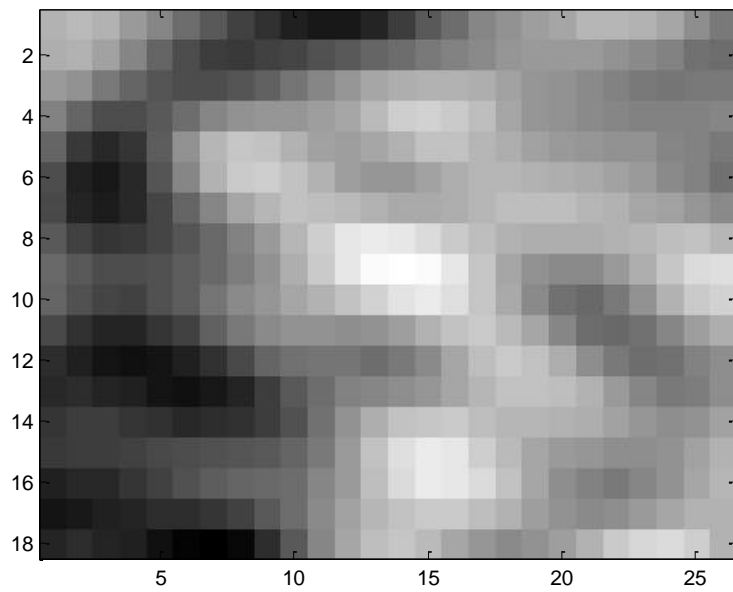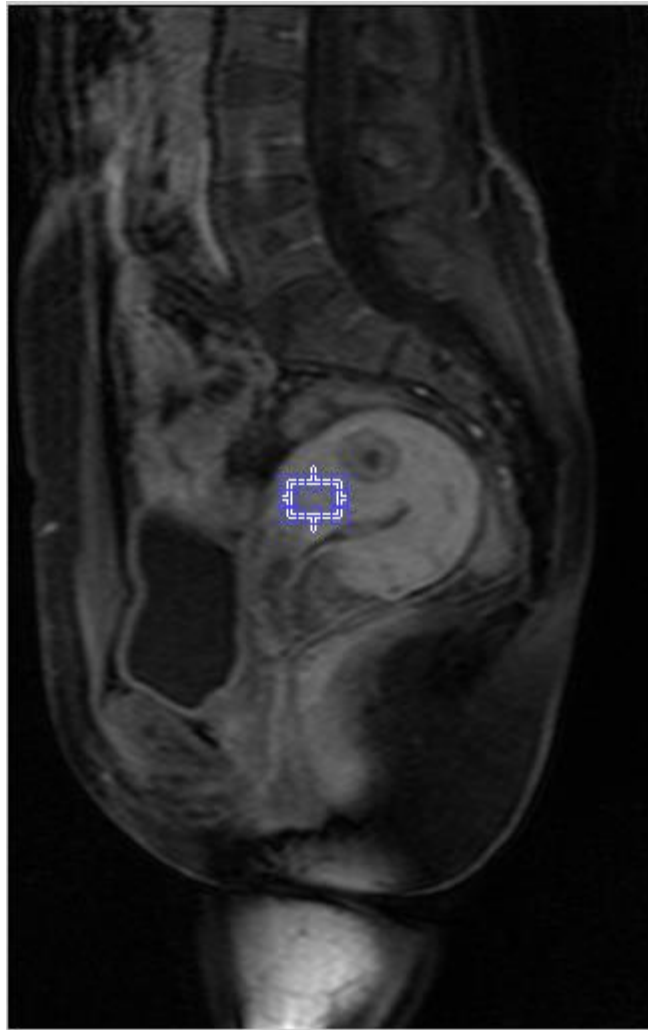
Figure 5d: The Region Of Interest, non pathological, in the examined slice of uterus

For the non-pathological Region Of Interest in uterus, the parametric map of T10 is:
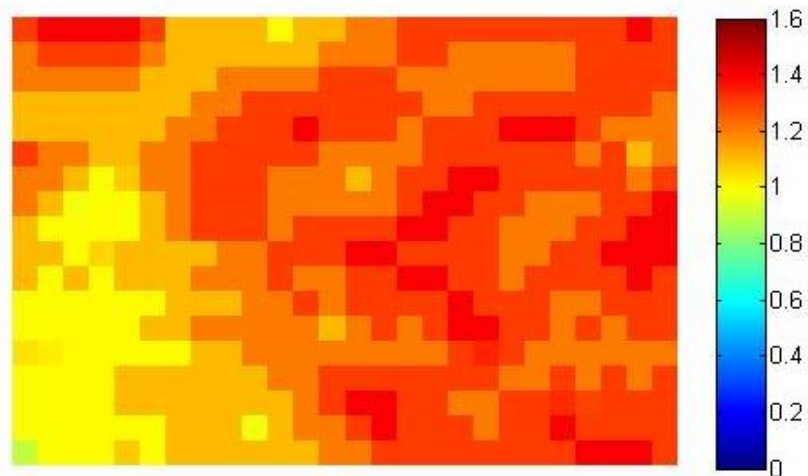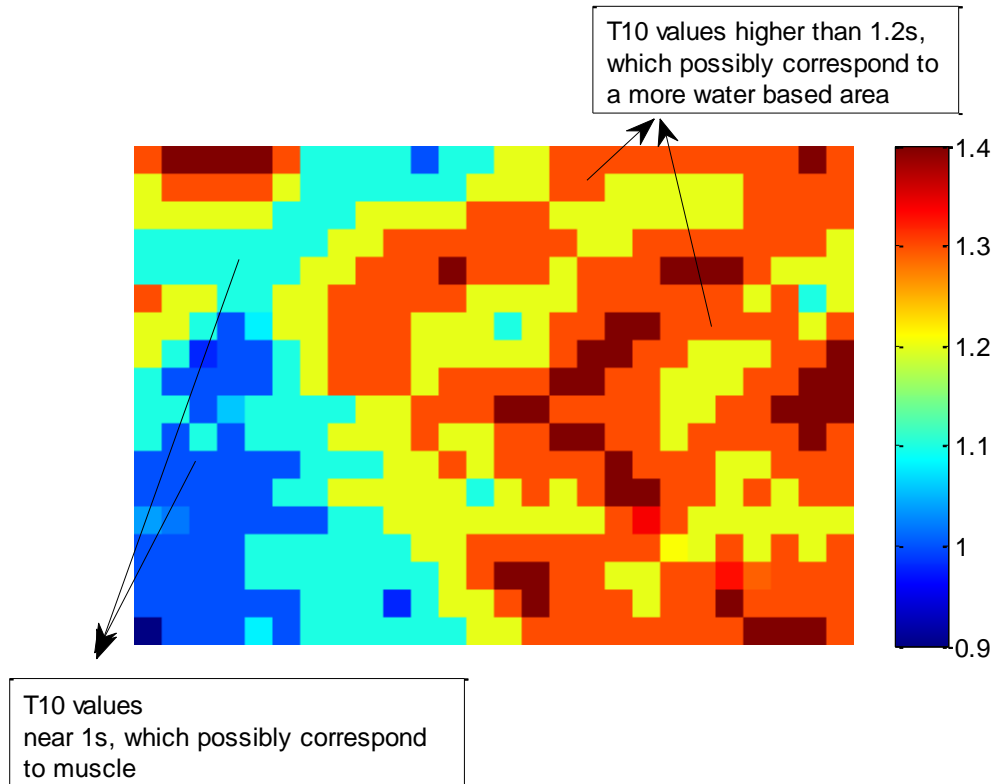

Figure 5.13: Parametric Map of pre-contrast relaxation time T10, for the non-pathological Region Of Interest in uterus. The first figure is the map with the colorbar of the extracted values only and the second figure is the map with the colorbar in the full range.

The curves that we extracted for two voxels are cited below (figure 5.14, 5.15).

For the selected ROI, we can observe that in the parametric map T10 (figure 5.13), there is a discrimination between higher values of T10, and lower values of T10. This is reasonable,

because the examined ROI, is selected near the muscle, in the top of uterus, and thus we have T10 values in the range of 1s, near in the muscle as it can be noticed, which is expected, comparing to the other area, where we have possibly more water-fluid element, and consequently increased T10.

We can see the plateau phase in both cases (figure 5.14, 5.15), which is expected, because the non-pathological areas, have most of the time, no significant reaction to the gadolinium arrival, so we can observe the wash-in, and then for the rest of the time, the stable phase. This stable phase also is interpreted as the saturation of capacitance in the Extravascular Extracellular Space and thus there is no space for more leakage of contrast agent. The difference, with the cancerous plateau in the optimization results of 5.2, is that in the non-pathological case (figure 5.14, 5.15), we have less steep wash-in phase, comparing to the pathological plateau case (figure 5.2).
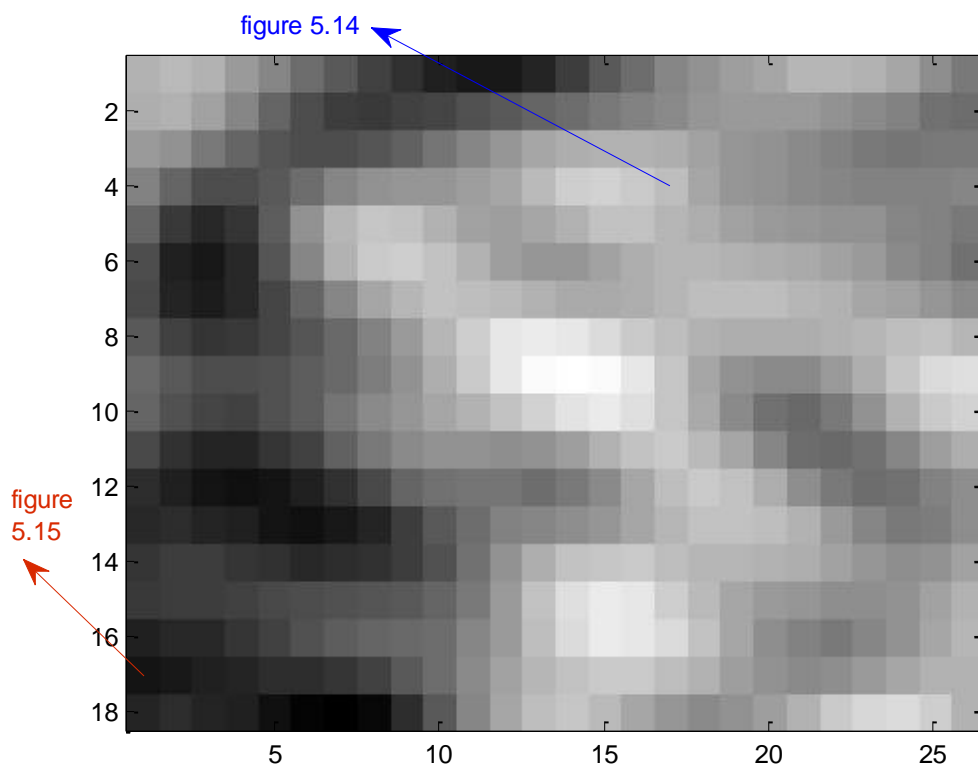

Figure 5e: The position of figures 5.14, 5.15 in the examined slice of non-pathological uterus region
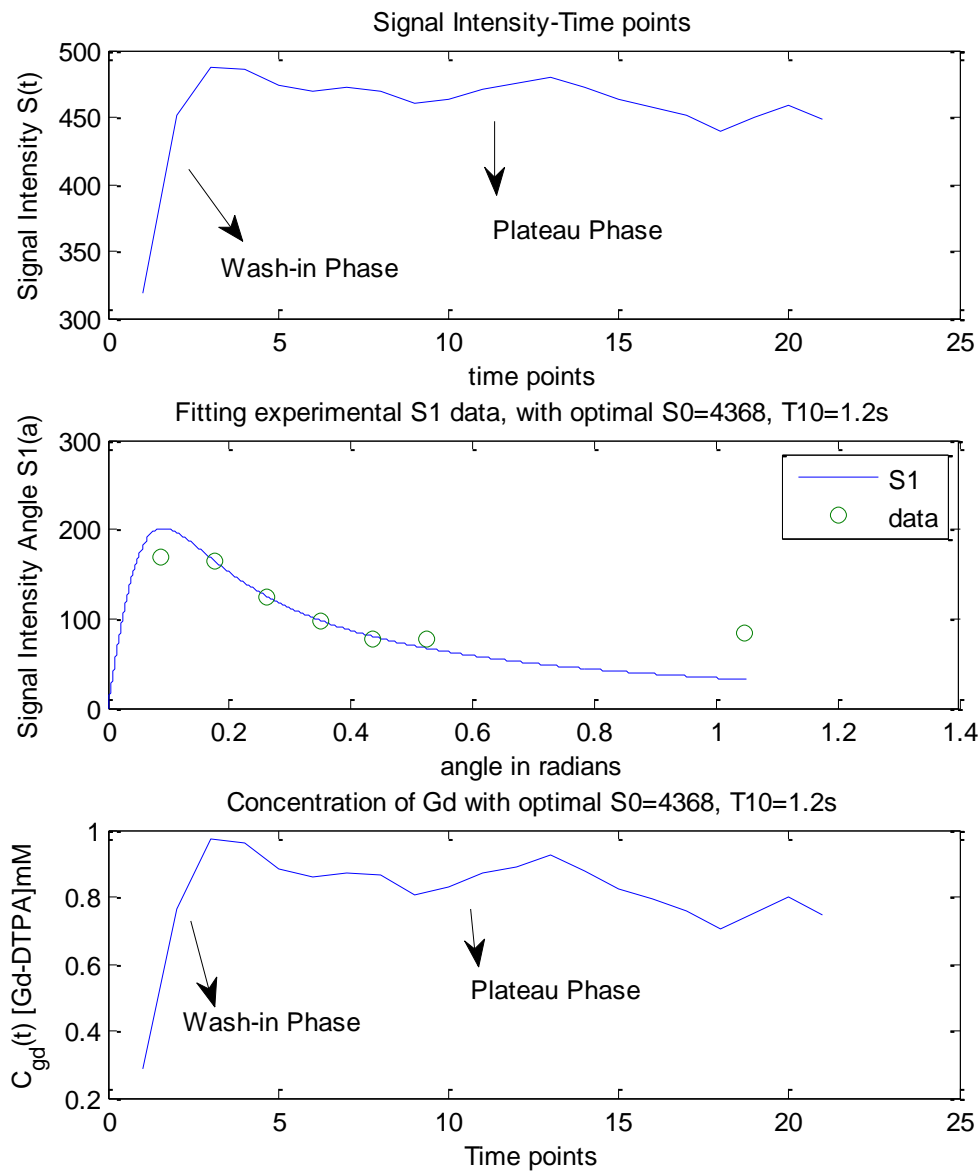
Figure 5.14: Concentration and Optimization Results for the non-pathological Region of Interest in uterus. In the first figure, we can see the Signal Intensity per Time. In the second figure, the fit to the experimental data [168 164 124 97 77 78 85], is shown, with the optimal values of S0, and T10. Finally, in the third figure, the curve of the Gadolinium Concentration is shown, with the optimal S0 and T10.
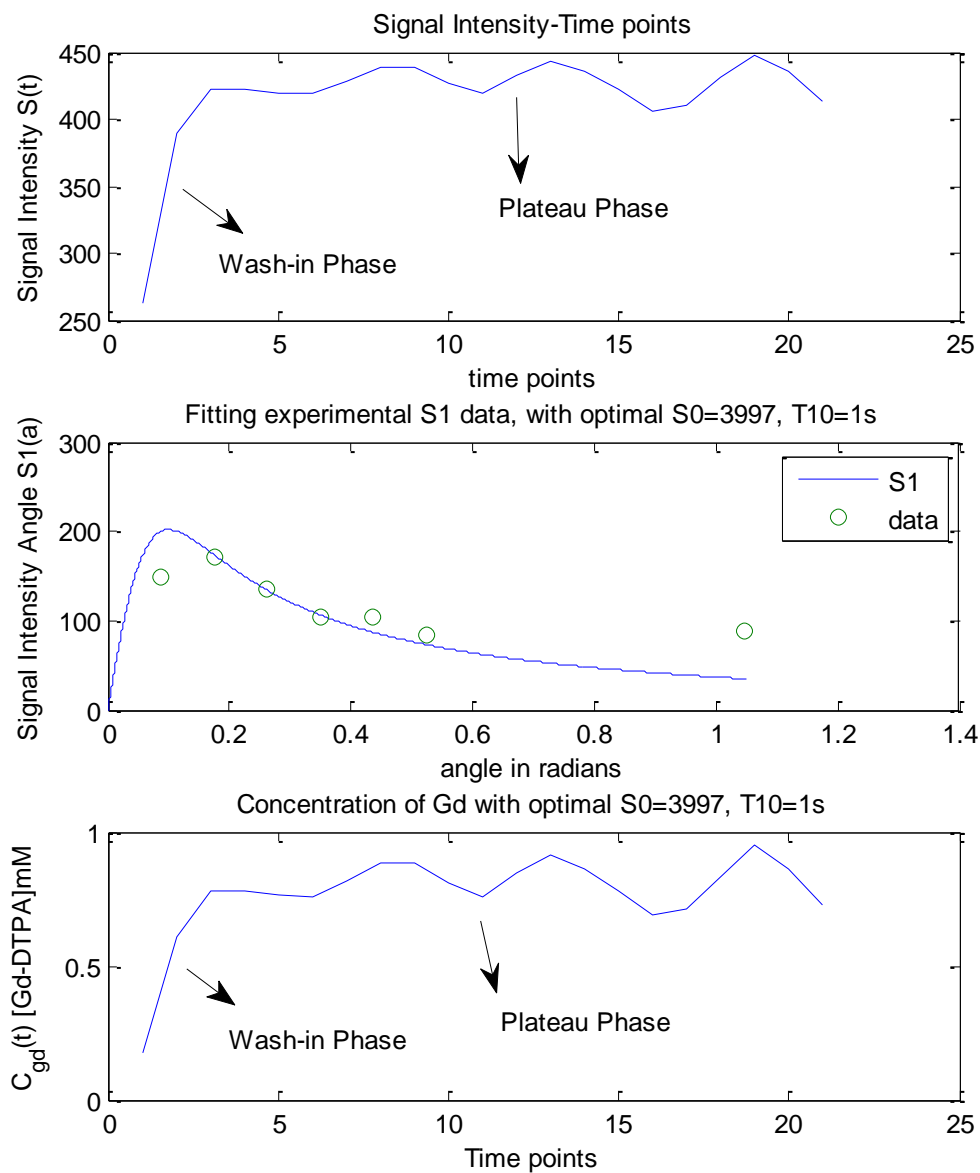
Figure 5.15: Concentration and Optimization Results for the non-pathological Region of Interest in uterus. In the first figure, we can see the Signal Intensity per Time. In the second figure, the fit to the experimental data [149 172 135 105 104 85 88], is shown, with the optimal values of S0, and T10. Finally, in the third figure, the curve of the Gadolinium Concentration is shown, with the optimal S0 and T10.

As we mentioned above, the brain data, has a role of validation in this study, but we also cite the extracted curves (figure 5.17, 5.18) and T10 map (figure 5.16) for a non-pathological Region Of Interest.

Non pathological Brain Region

Consequently, the examined slice of brain, at a specific time point is:
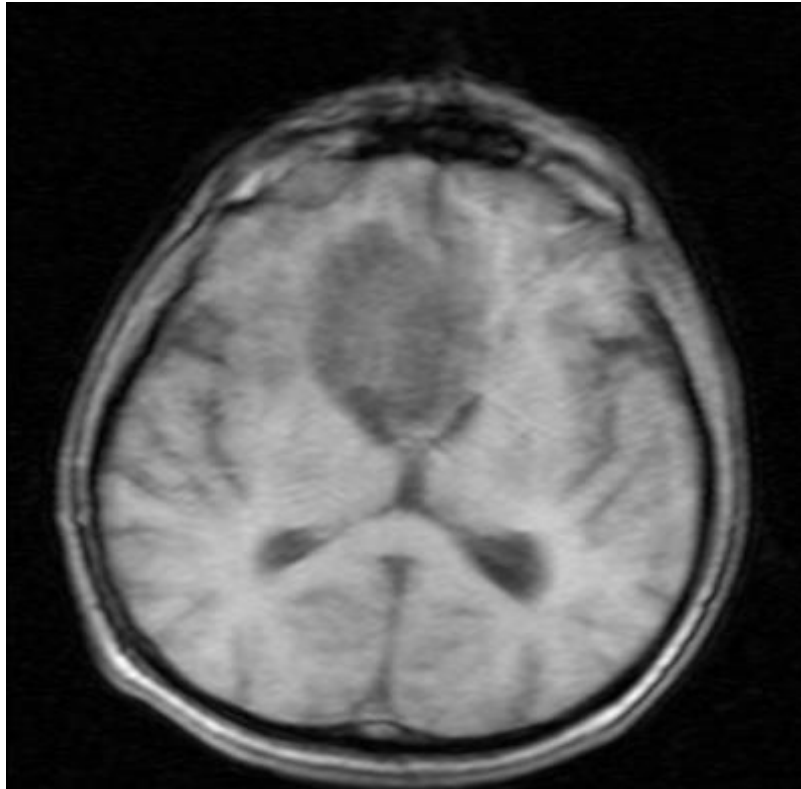
Figure 5f: Examined Slice of Brain Region

Selecting a non-pathological Region Of Interest in brain data, we cite the parametric map of T10.
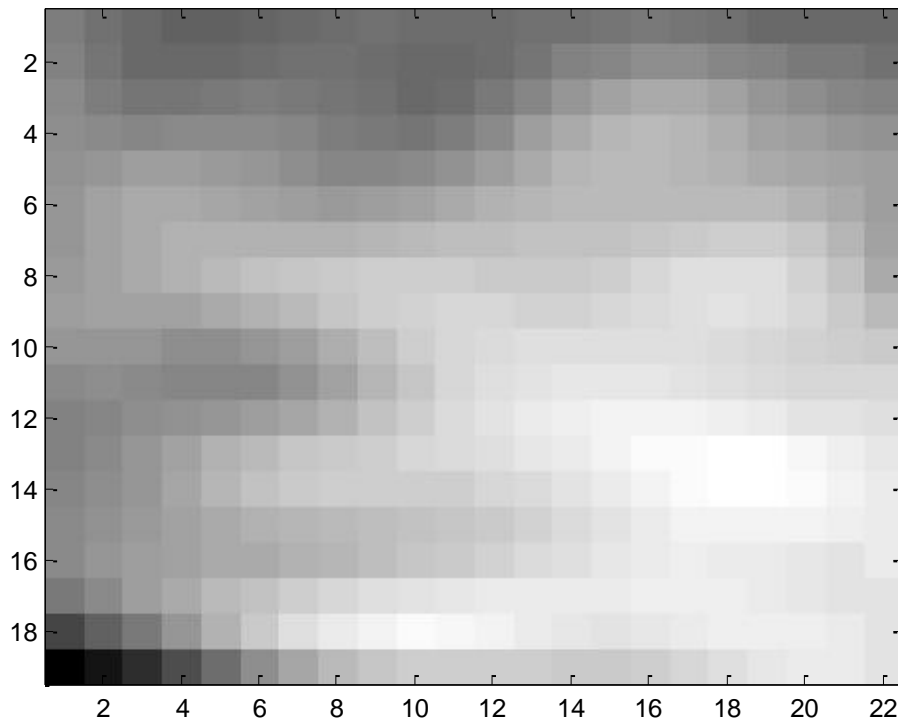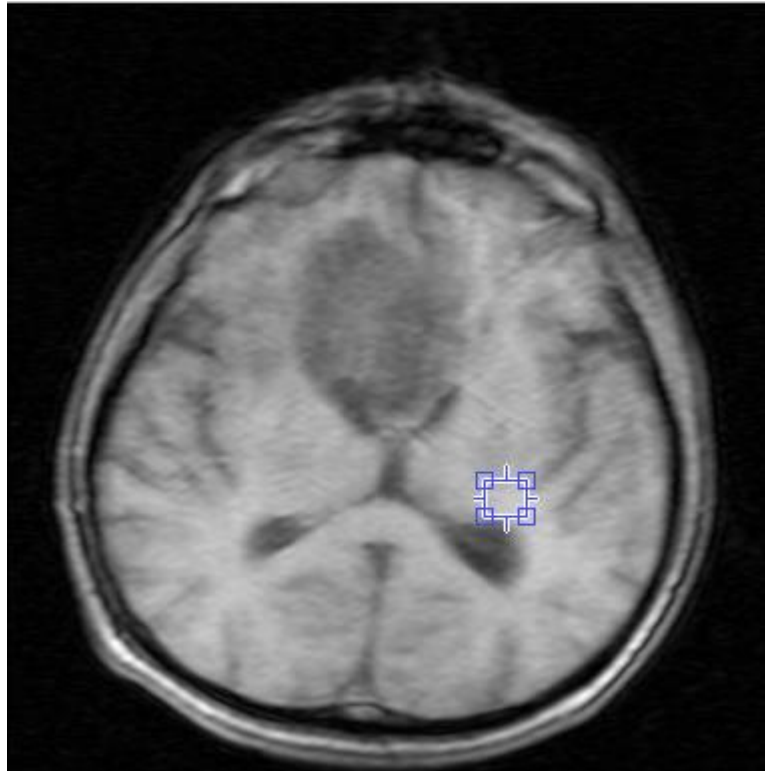
Figure 5g: The Region Of Interest, non pathological, in the examined slice of brain

Values of T10 near 0.8s that possibly correspond to White Matter

Area of higher values of T10 (more than 1.2s), that possibly correspond to a more dense regions and fibers as explained in figures 5h, 5i
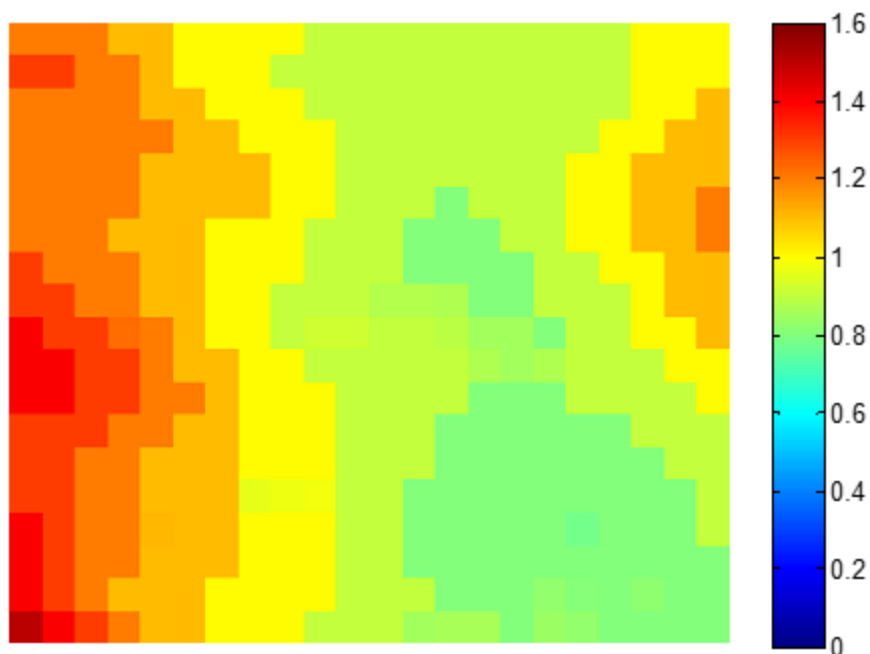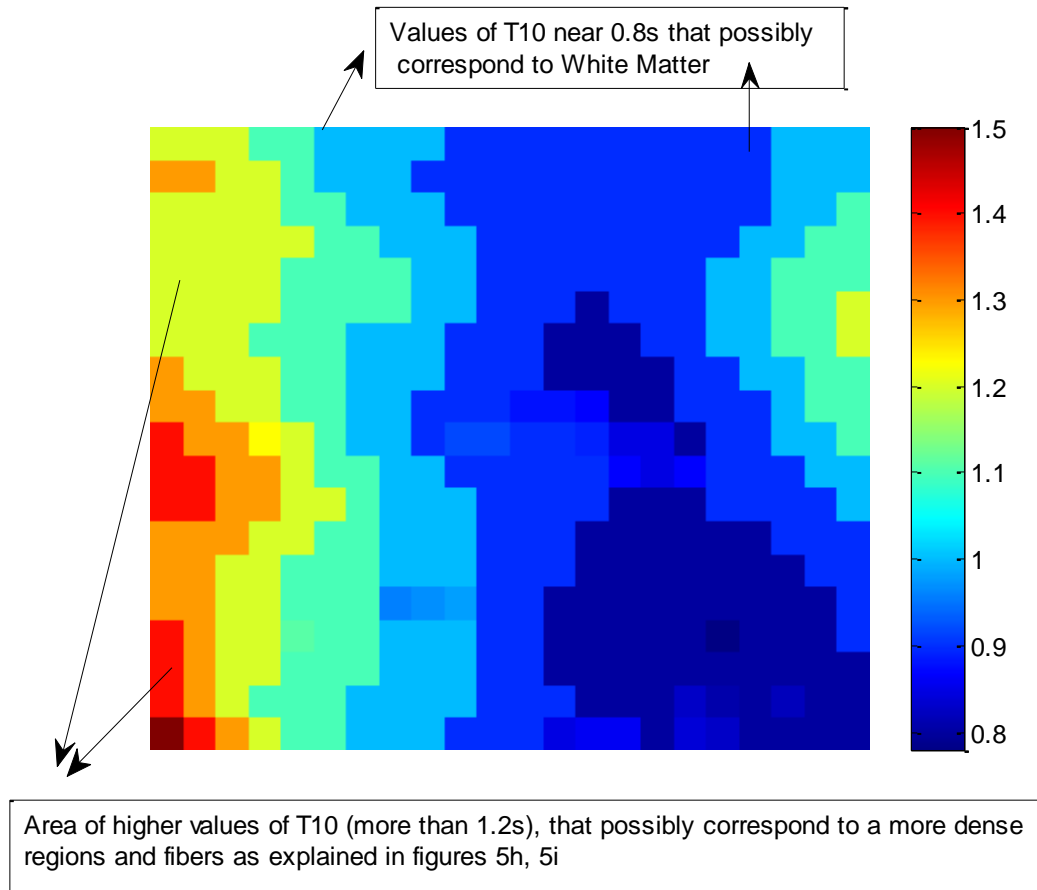
Figure 5.16: Parametric Map of pre-contrast relaxation time T10, for the non-pathological Region Of Interest in brain. The first figure is the map with the colorbar of the extracted values only and the second figure is the map with the colorbar in the full range.

In the selected Region Of Interest, we can observe some area of White Matter, which is the area with values near 0.8s in the parametric map of T10 (figure 5.16) and appear higher in the above ROI image (figure 5g). White Matter, is consisted mostly of myelin, and this is the main reason that appears whiter. The areas in the corners, correspond possibly to more dense regions, and fibers, and consequently we have increased T10 values.

This is explained in the following images, where in T2-weighted image (figure 5h), as an image for pathology, we can see more clearly the dense regions of the brain, and the water-based areas (such as cerebrospinal fluid (CSF)), and thus the fact that in the selected ROI, we have dense regions in the corners.

T2-Weighted FLAIR image (figure 5i), which is based on Inversion Recovery Sequence (section 1.2) is similar to the results of T2-weighted (figure 5h), but with suppressed CSF values, in order to bring out periventricular hyperintense lesions. In this image, we can notice that the selected region of interest, is non pathological because there are no values with high contrast.

Pathological Glioma has increased contrast in T2-Weighted

CSF as fluid element has increased contrast

Non pathological ROI with low contrast on T2-Weighted. Dense regions and fibers on the corner of our ROI.
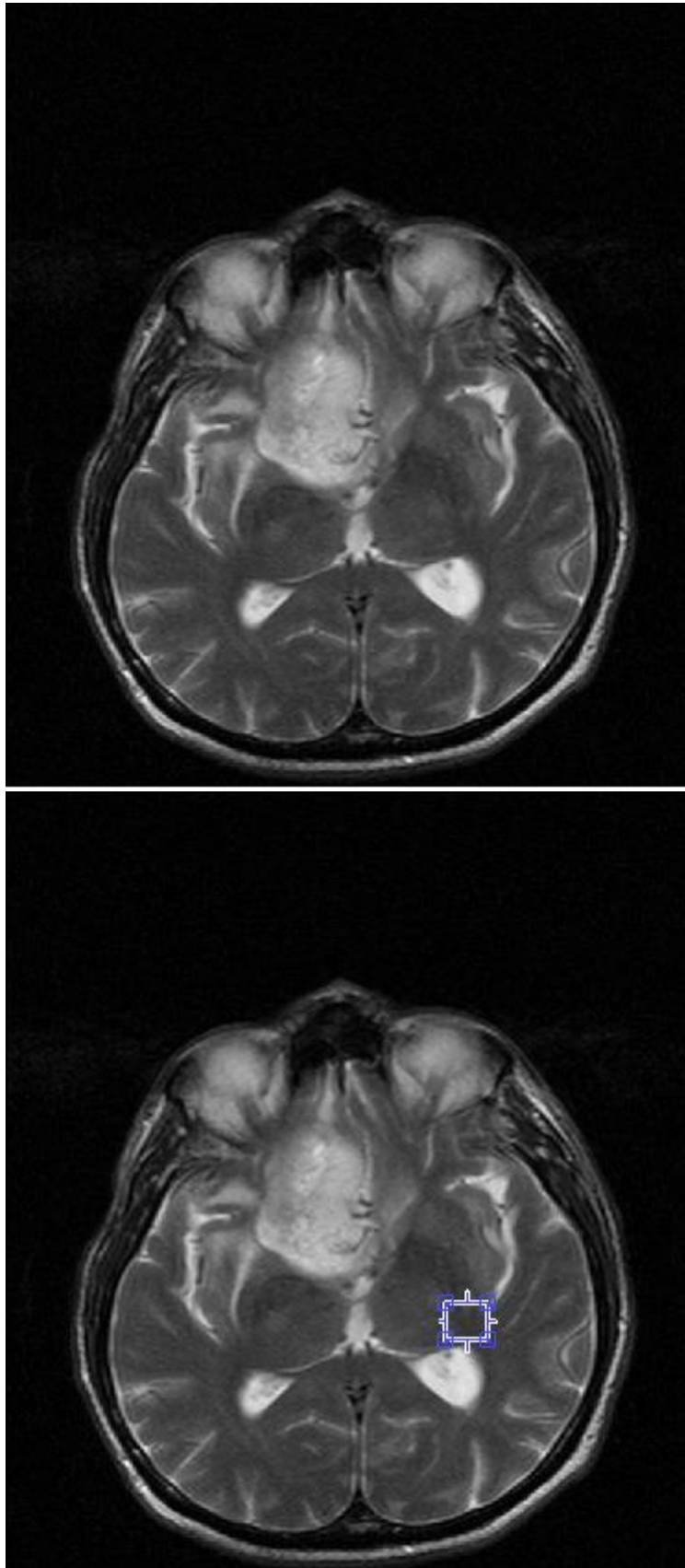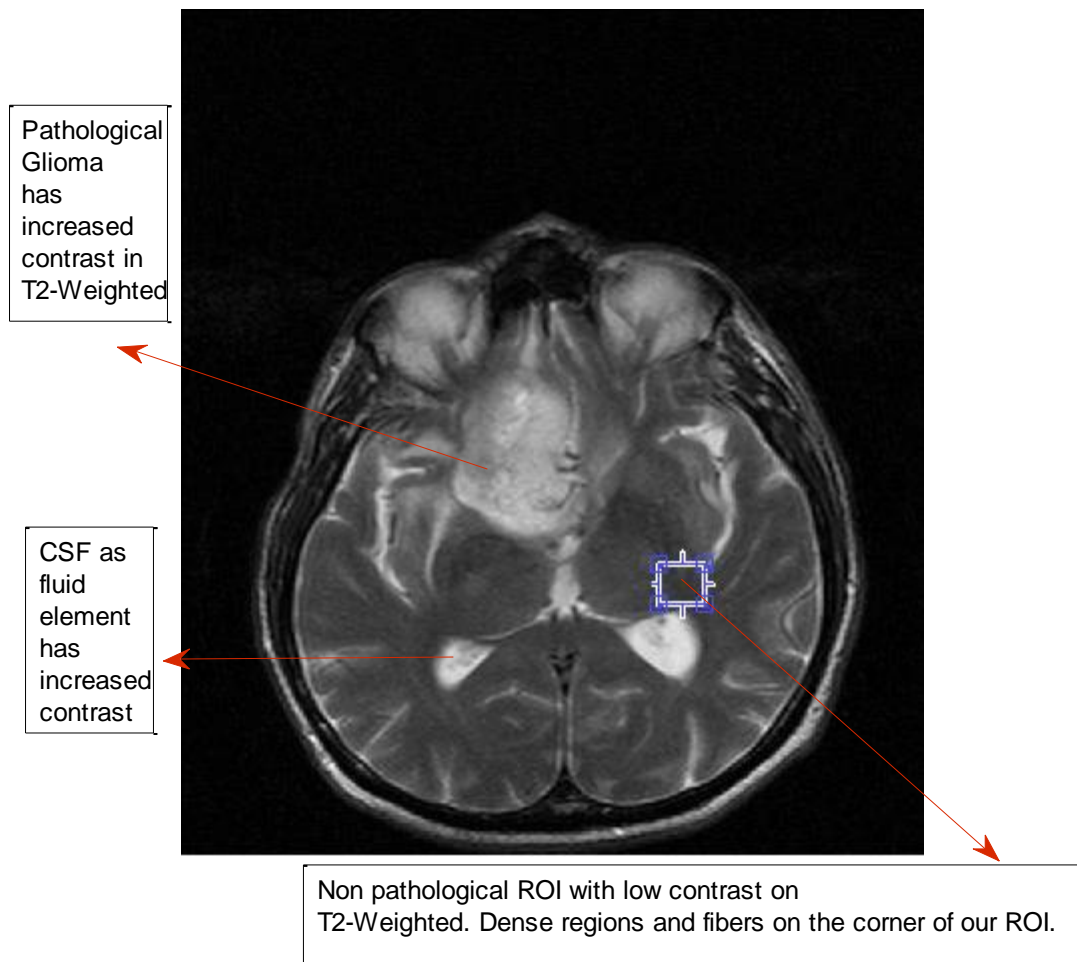
Figure 5h: T2-weighted Image for the examined slice in brain.
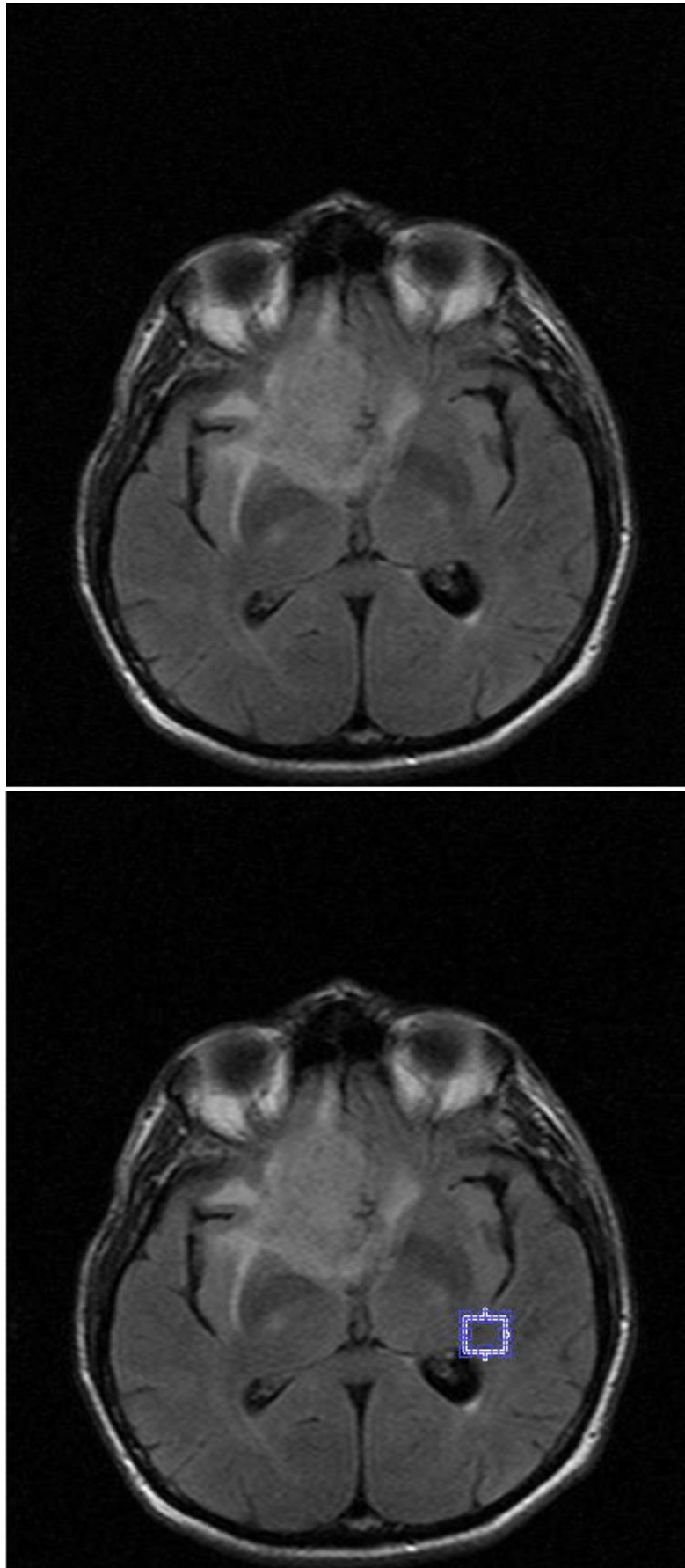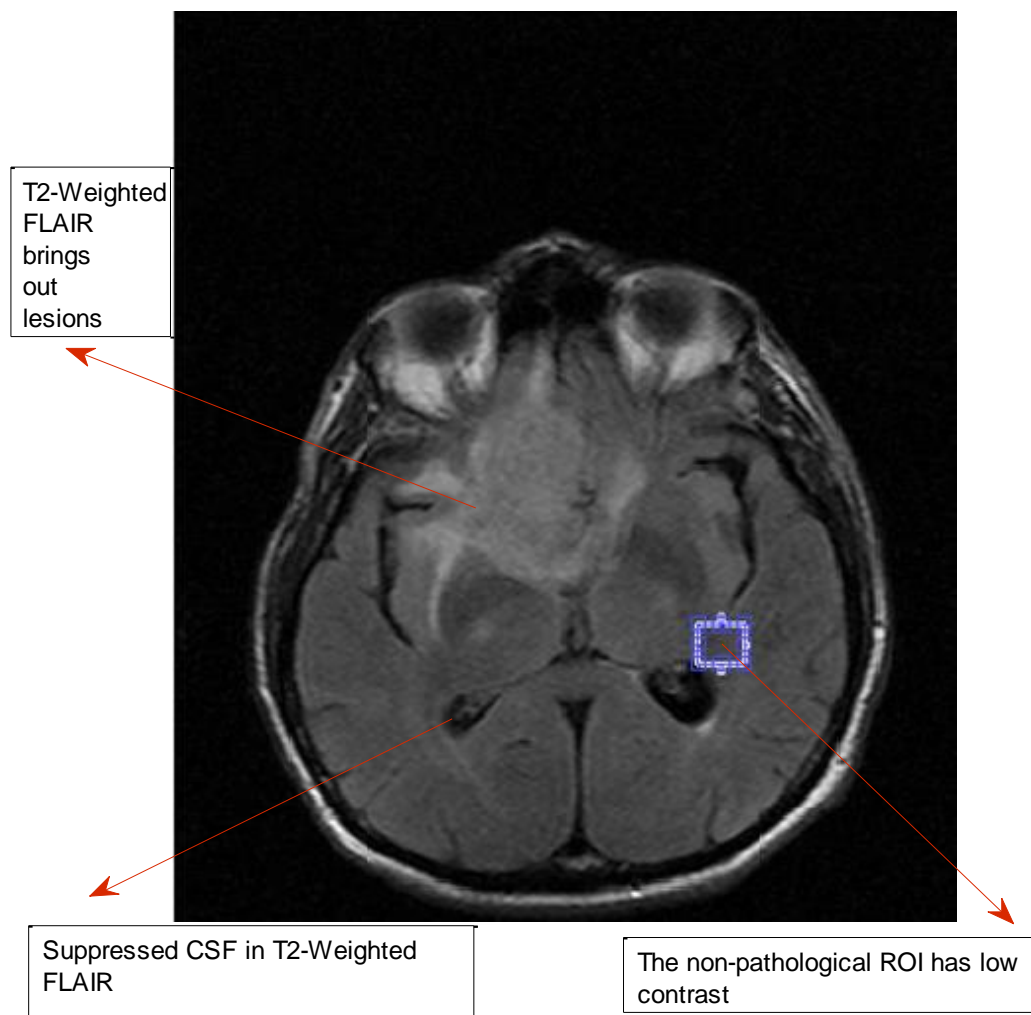
Figure 5i: T2-Weighted FLAIR Image, in the examined slice in brain.

and the curves that we extracted for two voxels are below (figure 5.17, 5.18).
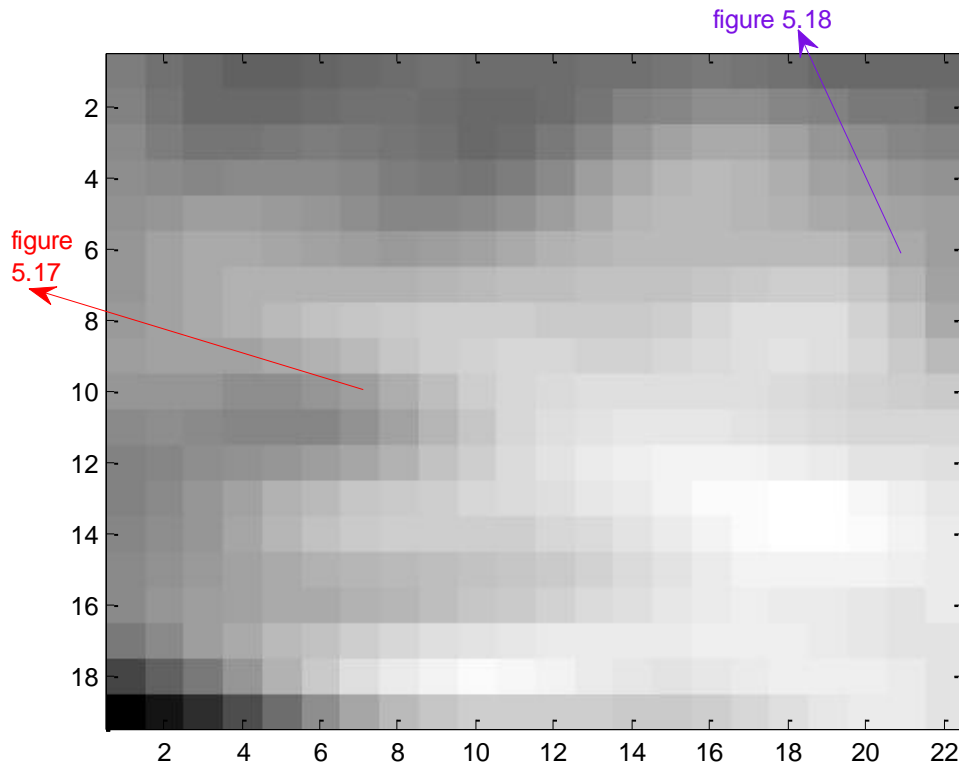
Figure 5j: The position of figures 5.17, 5.18 in the examined slice of non-pathological brain region.

We can observe again, the plateau phase in both cases (figure 5.17, 5.18), which is expected because the non-pathological areas, have most of the time no significant reaction to the gadolinium arrival, so we can observe the wash-in and then for the rest of the time, the stable phase. This stable phase also is interpreted as the saturation of capacitance in the Extravascular Extracellular Space and thus there is no space for more leakage of contrast agent. The difference, with the cancerous plateau in the optimization results of figure 5.2, is that in the non-pathological case, we have less steep wash-in phase, comparing to the pathological plateau case.
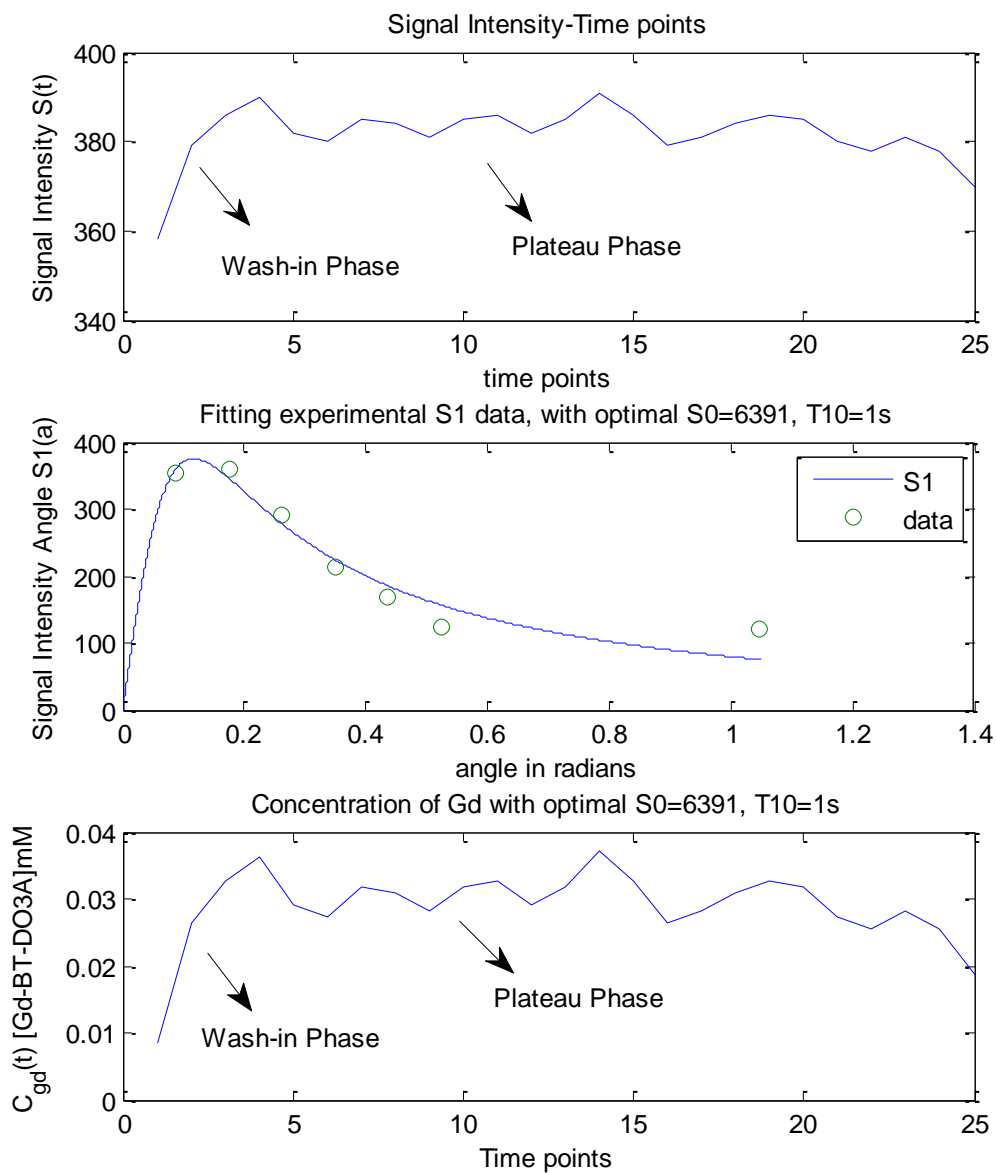
Figure 5.17: Concentration and Optimization Results for the non-pathological Region of Interest in brain. In the first figure, we can see the Signal Intensity per Time. In the second figure, the fit to the experimental data [355 360 290 213 170 123 122], is shown, with the optimal values of S0, and T10. Finally, in the third figure, the curve of the Gadolinium Concentration is shown, with the optimal S0 and T10.
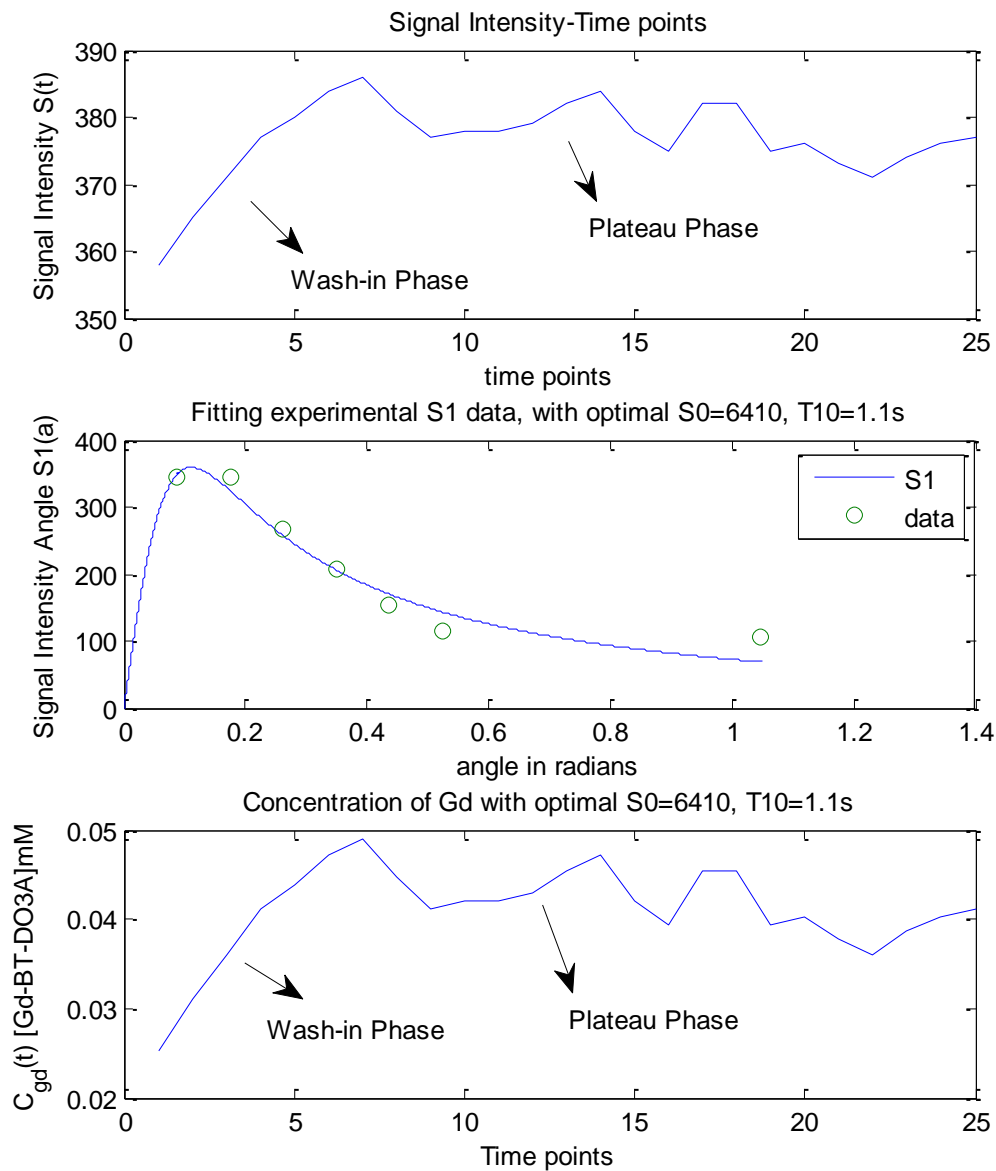
Figure 5.18: **Concentration and Optimization Results for the non-pathological Region of Interest in brain. In the first figure, we can see the Signal Intensity per Time. In the second figure, the fit to the experimental data [344 344 266 207 153 114 105], is shown, with the optimal values of S0, and T10. Finally, in the third figure, the curve of the Gadolinium Concentration is shown, with the optimal S0 and T10.**

Pathological (Glioma) Brain Region

It must be noticed that, in the specific brain data, in the Glioma region, the wash-in phase of the S1 experimental data starts in a lower angle (lower than 5°). This is because, glioma, is a very attacking tumor, and because of this, the used sequence in the hospital, which starts at 5° can not catch the wash-in phase, and thus it is unable to extract results for that region. A solution to the above problem, would be to set the sequence in the hospital, to start measuring in a lower angle (2°). With this setting, the sequence would catch the wash-in phase, and we would fit normally.

The figure below explains the above behavior:
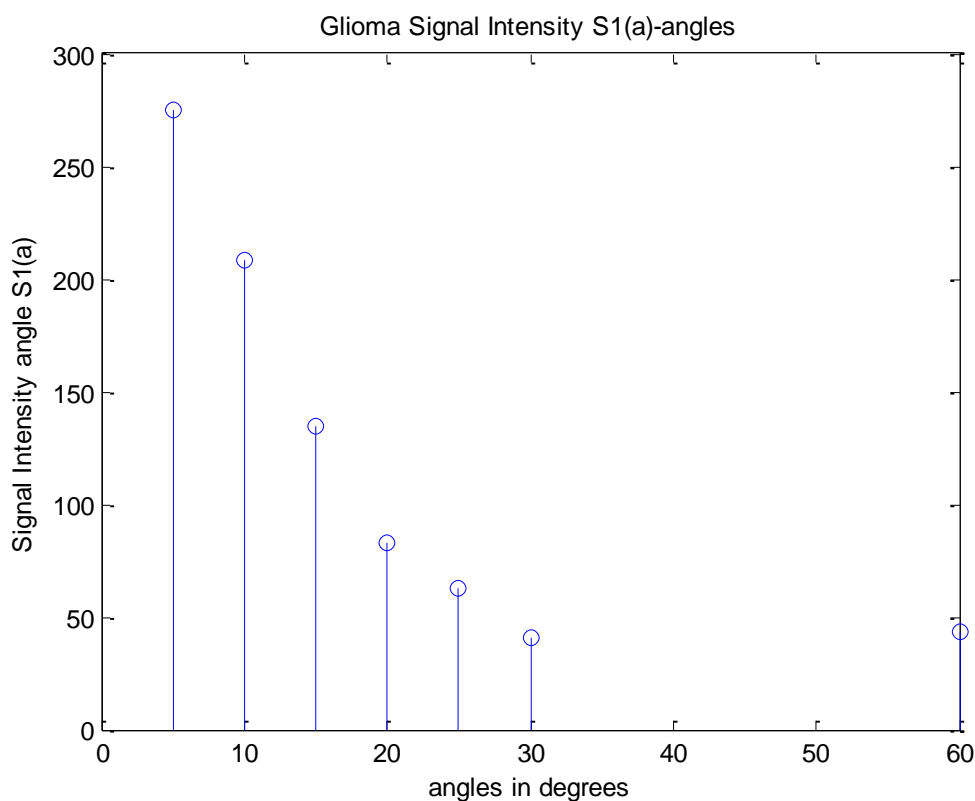
Figure 5.19: Explanation of the Glioma behavior in our data, on experimental S1(a) Signal Intensity angle.

We can observe that in the first angle (5°), we have the peak of enhancement, which is not valid, in order to fit with our function (3.2.3).

Comparison of Pathological and Non pathological results

To sum up, in the non-pathological results for both uterus (figure 5.14, 5.15) and brain data (figure 5.17, 5.18) we observed a plateau phase. This is expected because in the non-pathological regions, we have no tumor cellularity but a fixed structure of cells, considering there is no lesion. Thus, we have no considerable reaction to gadolinium arrival.

More specifically, in the uterus data in the pathological plateau (figure 5.2) we have a more steep wash-in phase comparing to the one of non-pathological (figures 5.14, 5.15).Similarly, in the brain data in the non-pathological case (figure 5.17, 5.18) the wash-in which is observed is not steep enough, which means we have no early leakage of contrast agent in this area, decreased blood flow and decreased vascular permeability.

Concerning the T10 relaxation times in the non-pathological uterus data (figure 5.13) we observed lower values of T10 in the left of uterus and higher in the rest of the region of interest. This is explained by the fact that the examined ROI is positioned as we mentioned above in the top of uterus near a possible muscle and thus we have T10 values near 1s. On the other hand, the area on the right has increased T10 values and correspond probably to a more water based area. The results of T10 tumor in the pathological ROI (figure 5.4) seem to have a range of values near 0.8s but this is not to be a general behavior of tumor. The area in the center has increased T10 values, which possibly correspond to water based tissues or fluid element.

We can notice that because pathological tissues usually have either edema or increased blood supply, their appearance can be seen as a mixture of water-based tissues and fluids. Also, fat tends to have high signal intensity at all contrasts, and so they can mask pathologies.[26].

5.5 Validation

As we mentioned above, in order to validate our estimations of pre-contrast relaxation time and thus the concentration of contrast agent, we used the brain region, where the values of T10, have a more standard behavior than the other body parts. Consequently, the white matter and gray matter have typical values, such as 0.9s and 1.3s respectively and we test how close are our predictions, with those theoretically [2] known values. Also, we are examining the ability of discrimination of those areas in the Parametric Map of T10 in figure 5.21. For the purpose of validation, we set the bound constraint of T10 up to $0.2 < T10 < 1.5$s.

In order to validate our results, we are examining the estimations of T10, by transferring the Region Of Interest in the area of Gray Matter and White Matter. Thus, we are selecting a ROI in figure 5k:
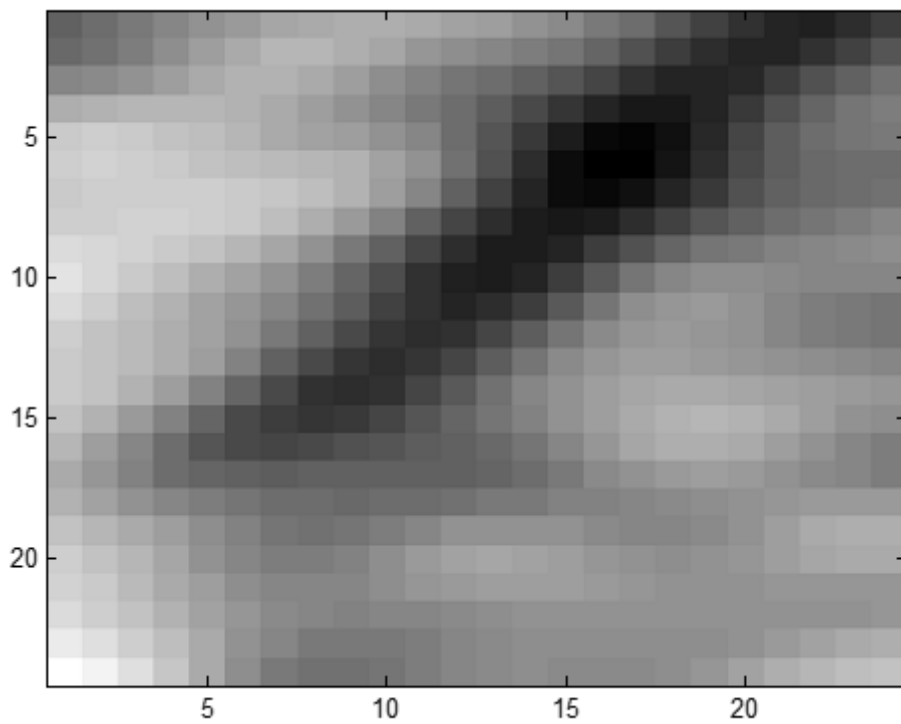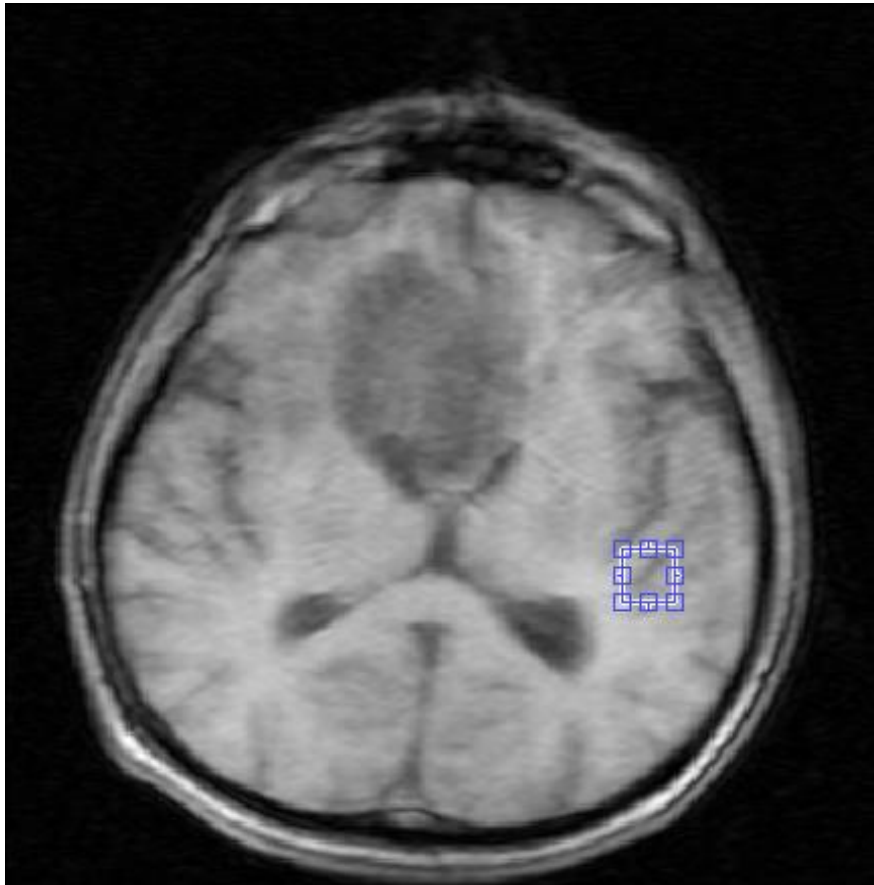
Figure 5k: The Region Of Interest, in the examined slice, for validation

And the parametric map of T10, is the following (figure 5.21):
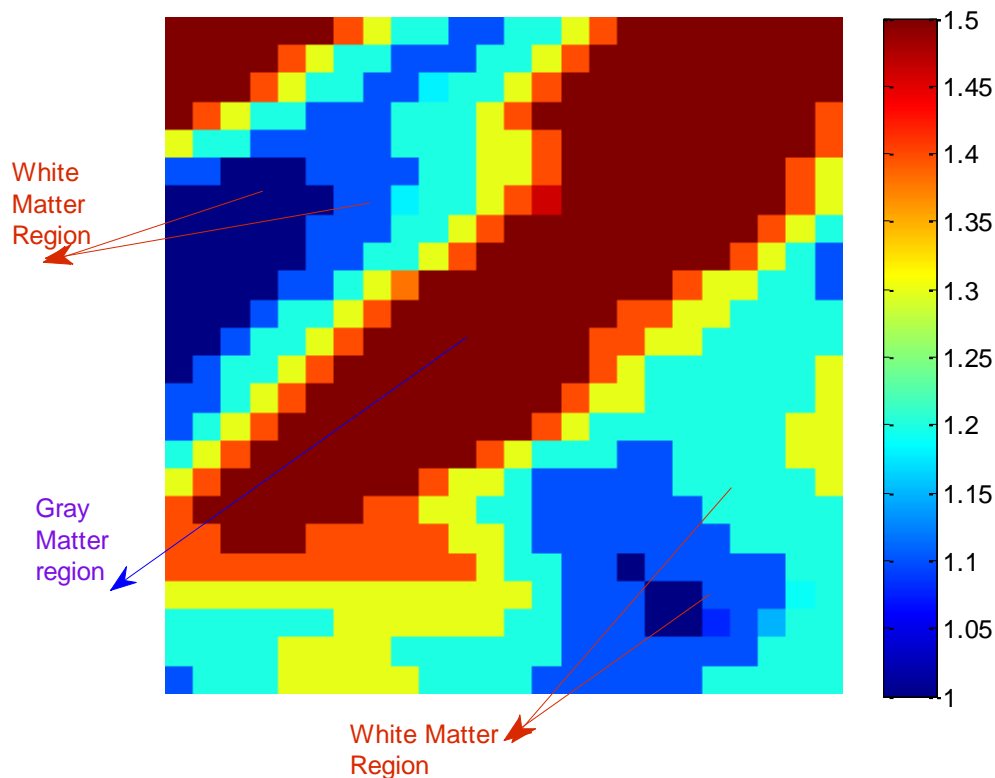
Figure 5.21: Parametric Map of pre-contrast relaxation time T10, for White and Gray Matter Region

It can be seen, that the estimated T10 for the case of Gray Matter (1.3-1.5s) are 0.3s higher from the T10 in the White Matter(1-1.2s), which is valid, according to the literature [2] measured in 37°C, where the T10 values are 1.2s for Gray Matter and 0.9s for White Matter. Consequently, we notice that the relaxation time of Gray Matter in literature is 0.3s higher than in the white matter. The T10 values in our study, are possibly affected by the glioma of the patient, and thus we have a small increment, on their range. The glioma may affects, the Signal Intensities of images in each of different flip angle S1(a). Also, the relaxation time T1 depends upon the age of the patient but also the temperature of the examined part of the body.

Consequently, having correct values for T10 according to the above, then the estimated Gadolinium Curve is valid along with the parametric maps we are extracting. Also, the discrimination between Gray Matter and White Matter is obvious in figure 5.21.

The concentration and optimization results, for Gray and White Matter are cited below (figures 5.22, 5.23):

In the case of Gray Matter curve (figure 5.22), we can see a steeper wash-in, comparing to the wash-in phase of White Matter (figure 5.23), which is expected, because Gray Matter is relative

to the thinking function of the brain, has increased vascularity, and consequently has higher needs for blood.
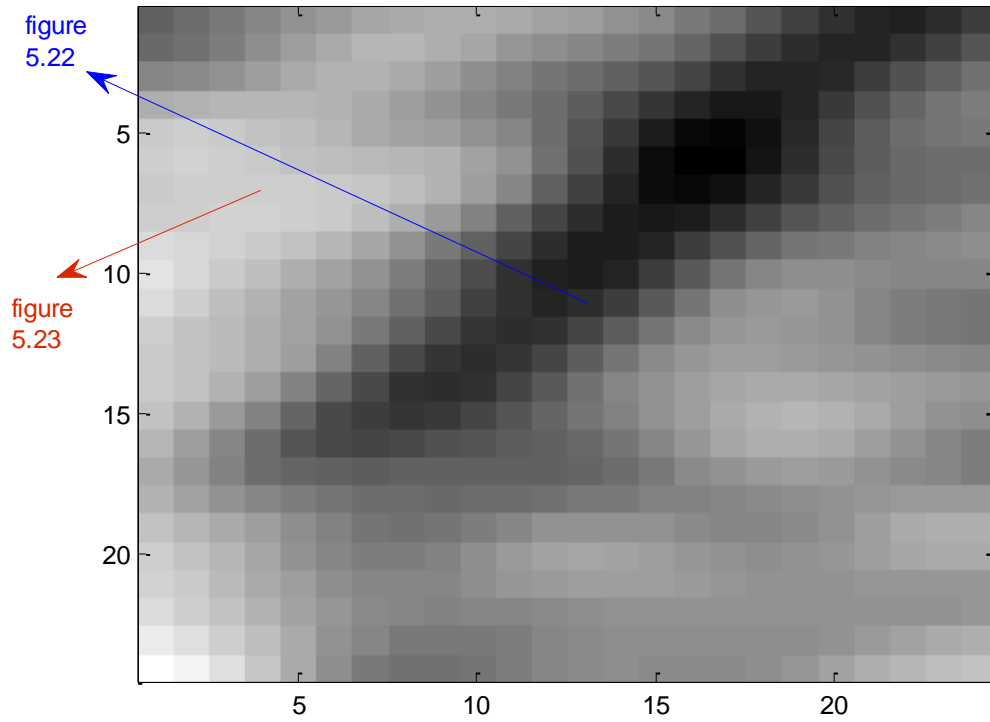
Figure 5l: The position of figures 5.22, 5.23 in the examined slice for validation on brain region.
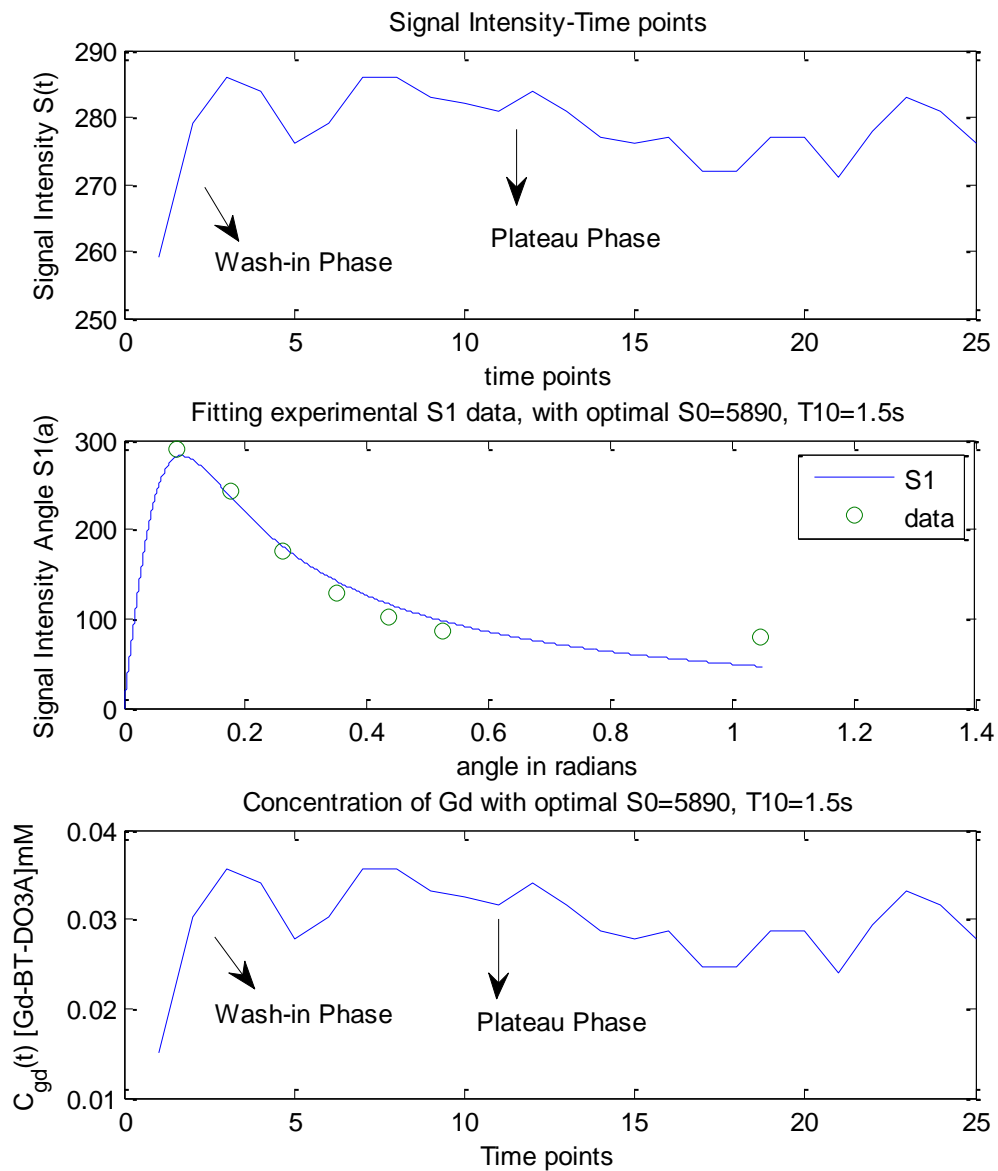
Figure 5.22: **Concentration and Optimization Results for Gray Matter. In the first figure, we can see the Signal Intensity per Time. In the second figure, the fit to the experimental data [290 242 176 129 102 87 80], is shown, with the optimal values of S0, and T10. Finally, in the third figure, the curve of the Gadolinium Concentration is shown, with the optimal S0 and T10.**
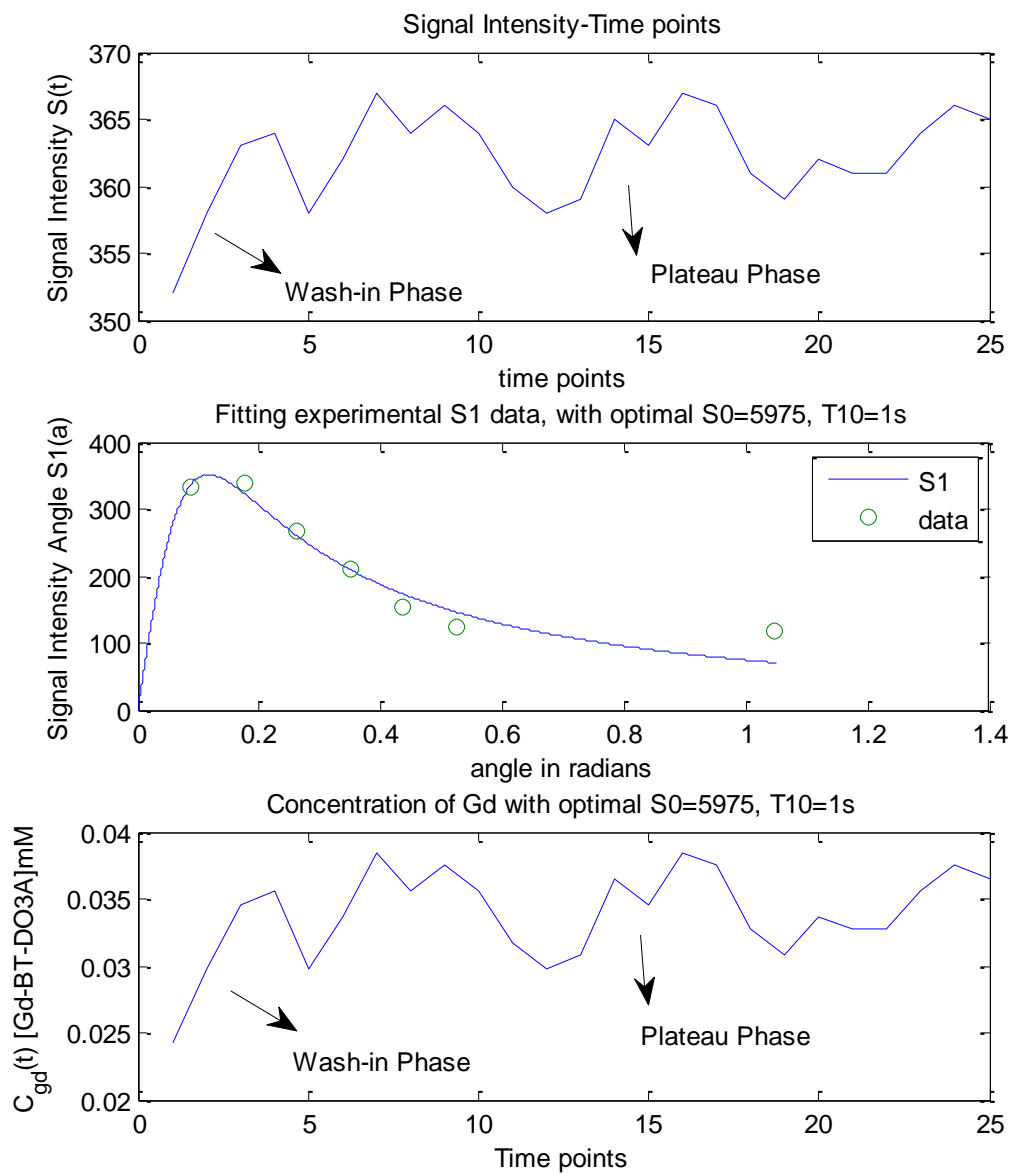
Figure 5.23: Concentration and Optimization Results for White Matter. In the first figure, we can see the Signal Intensity per Time. In the second figure, the fit to the experimental data [334 338 266 209 155 123 117], is shown, with the optimal values of S0, and T10. Finally, in the third figure, the curve of the Gadolinium Concentration is shown, with the optimal S0 and T10.

Chapter 6

Conclusion & Future Work

6.1 Conclusion

An analytical solution is proposed in this study, to estimate the pre-contrast relaxation time T10, and the equilibrium magnetization S0. Thus, as mentioned in section 3.2, we have an optimization problem, with non linear constraints to solve.

The results of this work, are for uterus. The brain region has a role of validation for this study, where we examine only the Region of White and Gray Matter, to validate our estimations of T10. The analytic solution, for the optimization problem, is performed for each voxel. Consequently for the uterus data, we created a map of parameters, such as T10 map, Maximum Signal Intensity, and for both Signal Intensity and Gadolinium Curve, we calculated maps of Maximum Intensity Time Ratio, Gradient Wash-in Area Under the Curve, Initial Area Under the Curve, Final Area Under the Curve, Area Under the Curve Ratio, and AUC of the whole Curve.

From the above maps, T10 map, Maximum Intensity Time Ratio, Gradient Wash-in, and IAUC, AUCR, show a good performance in the results, so that detection of abnormalities could be possible, comparing to normal tissue.

For the non-pathological part (section 5.4), we cited the parametric map T10, of the selected Region of Interest, for both uterus and brain data, but also the concentration-optimization results. In the same section, we discussed their results, and the anatomical and physiological background of them.

For the validation part (section 5.5), it can be seen that the estimated T10 values on Gray Matter, are higher from White Matter, in a range of 0.3s, which is valid. The T10 values, are possibly affected by the glioma of the patient, as explained in the same section and thus we have a small increment, on their range.

The outcome of this work can be split in two parts.

On the first part, estimation of pre-contrast relaxation T10 and equilibrium magnetization S0 was achieved and so the estimation of contrast agent concentration over time on a voxel-by-voxel analysis in a range of 0-1mM. This method can be used also to measure the contrast agent concentration in the plasma, simply by transferring the region of interest in the artery. Thus, having concentration in plasma and in tissue (this study) pharmacokinetic parameters k_{trans}, k_{ep}, v_e [6] can be extracted which take into account the physiology of the tissue and their result are more specific about the possible carcinoma.

On the second part, semiquantitative parameters were calculated based on the Signal Intensity and Gadolinium Concentration. These parameters can enhance and help the approach of diagnosis because as it can be observed in section 5.3 they can identify the area of the lesion and of possible carcinoma, especially in the result of AUCR (figure 5.11) so that the pathological area can be discriminated from the normal region.

6.2 Future Work

In this task, we consider each voxel, as a unique element, but it can be noticed, that neighbouring voxels, have similar behavior. We could add as a new constraint, in our optimization problem, a smoothness constraint, so that, we are looking a priori in a specific region for neighbouring pixels.

More specifically, [31:pg 42] the smoothness constraint is:

$$SM = \iint_a^b \overset{f}{\overbrace{(u_x)^2 + (u_y)^2 + (v_x)^2 + (v_x)^2}} \, dxdy$$

Where u=T10 and v=S0, are our parameters of optimization problem to estimate. The pointer, indicates the parameter in which we differentiate. The a,b are corresponding to the neighborhood,we are examining on the image. Adding this constraint to our minimization function, we could have:

$$E=CF+\lambda \cdot SM$$

where CF is our cost function, the least-square error, SM is the smoothness constraint, λ is a constant, which we define 0.1, and E is the new loss function. Thusly, we are examining the derivatives with respect to u $(\frac{\vartheta E}{\vartheta u})$ and v $(\frac{\vartheta E}{\vartheta v})$ again. The derivatives of CF are known from Section 3.3. The derivatives of the SM term, would be included in our gradients, and could be derived using Euler-Lagrange equations [31:pg 42] :

$$\frac{\vartheta f}{\vartheta u} = \frac{\vartheta}{\vartheta u}\frac{\vartheta u}{\vartheta x} + \frac{\vartheta}{\vartheta u}\frac{\vartheta u}{\vartheta y} = 2 \cdot u_{xx} \cdot u_{yy}$$

$$\frac{\vartheta f}{\vartheta v} = \frac{\vartheta}{\vartheta v}\frac{\vartheta v}{\vartheta x} + \frac{\vartheta}{\vartheta v}\frac{\vartheta v}{\vartheta y} = 2 \cdot v_{xx} \cdot v_{yy}$$

Therefore, having the new loss function E, we solve the same problem (Section 3.2), with those additional constraints, solving a differentiate equation. The complexity, though, of the problem is increased.

The new Lagrangian would have the form:

$$L(x, y, \mu1, \mu2, \mu3, \mu4) = E + \mu1\left(\frac{sin\theta - S_{min}/x}{sin\theta - cos\theta\frac{S_{min}}{x}} - e^{-\frac{TR}{y}}\right) + \mu2\left(-\frac{sin\theta - S_{max}/x}{sin\theta - cos\theta\cdot\frac{S_{max}}{x}} + \right.$$

$$\left. e^{-M\cdot TR - \frac{TR}{y}}\right) + \mu3 \cdot (0.2 - y) + \mu4 \cdot (y - 1.8)$$

where E is defined as

$$E = CF + \lambda \cdot SM = \sum_a \left(x \cdot \frac{sina\cdot\left(1 - e^{-\frac{TR}{y}}\right)}{1 - cosa\cdot e^{-\frac{TR}{y}}} - d\right)^2 + \lambda \cdot SM, \tag{6.1}$$

and we set to zero the derivatives $\frac{\vartheta L}{\vartheta u}$ and $\frac{\vartheta L}{\vartheta v}$, having the same Complementary Conditions as in Section 3.3.

Bibliography

[1] Ingrid S. Gribbestad, Kjell I. Gjesdal, Gunnar Nilsen, Steinar Lundgren, Mari H. B. Hjelstuen, and Alan Jackson. *An Introduction to Dynamic Contrast-Enhanced MRI in Oncology.* In Dynamic Contrast-Enhanced Magnetic Resonance Imaging in Oncology, page 3-22, Springer 2005.

[2] Greg J.Stanisz, Ewa E.Odrobina, Joseph Pun, Michael Escaravage, Simon J.Graham, Michael J.Bronskill, and R.Mark Henkelman.*T_1,T_2 Relaxation and Magnetization Transfer in Tissue at 3T*. Magnetic Resonance in Medicine, 54(3):507-512, 2005

[3] http://www.who.int/mediacentre/factsheets/fs297/en/

[4] Hiroshi. Yoshioka, MD, PhD, Philipp M. Schlechtweg, MD, Katsumi. Kose, PhD. *Magnetic Resonance Imaging.* In Imaging of Arhritis and Metabolic Bone Disease, Elsevier 2009.

[5] Denis Hoa, *Nucler Magnetic Resonance*, http://www.imaios.com/en/e-Courses/e-MRI/NMR

[6] Kakai Shen, *Parametric Image Formation of Human Prostate Cancer Vascularisatiom from MRI Perfusion Data.* Master's Thesis*, University of Burgundy,* 2008

[7] C.H. Suh, H.S. Kim, Y.J. Choi, N. Kim, and S.J Kim. *Prediction of Pseudoprogression in Patients with Glioblastomas Using the Initial and Final Area Under the Curves Ratio Derived from Dynamic Contrast-Enhanced T1-Weighted Perfusion MR Imaging*, 10.3174/ajnr.A3634, 2013.

[8] http://www.thedcetool.com/scientific

[9] David L.Buckley, Robert W. Kerslake, Stephen J. Blackband, Antony Horsman. *Quantitative Analysis of Multi-Slice Gd-DTPA Enhanced Dynamic MR Images Using an Automated Simplex Minimization Procedure*. Magnetic Resonance in Medicine, 32(5):645-651,1994.

[10] Melanie Heilman, Fabian Kiessling, Marta Enderlin and Lothar R.Schad. *Determination of Pharmacokinetic Parameters in DCE MRI. Consequence of Nonlinearity Between Contrast Agent Concentration and Signal Intensity,* Investigate Radiology, 41(6):536-543, 2005

[11] Mei-Lin W.Ah-See and Anwar R.Padhani. *Dynamic Magnetic Resonance Imaging in Breast Tumours.* In Dynamic Contrast-Enhanced Magnetic Resonance Imaging in Oncology, pages 145-174, Springer 2005.

[12] David L.Buckley and Geoffret J.M.Parker. *Measuring Contrast Agent Concentration T1-Weighted Dynamic Contrast-Enhanced MRI.* In Dynamic Contrast-Enhanced Magnetic Resonance Imaging in Oncology, pages 69-80, Springer 2005.

[13] National Cancer Institute Web site http://cancer.gov/cancertopics/understandingcancer

[14] Fang Cao, Olivier Commowick, Elise Bannier, Jean-Christophe Ferre, Gilles Edan, and Christian Barillot. *MRI Estimation of T_1 Relaxation Time Using a Constrained Optimization Algorithm*, MBIA 2012, LNCS 7509, pp. 203–214, Springer-Verlag Berlin Heidelberg 2012

[15] A.R.Padhani. *Dynamic contrast-enhanced MRI in clinical oncology: Current status and future directions.* Journal of Magnetic Resonance Imaging, 16:407-422,2002.

[16] Paul S.Tofts talks: *Methods for quantitative relaxation parameter mapping: measuring T_1 and T_2.* ISMRM Hawaii, 2009

[17] Fernando Calamante, Evert-jan P.A Vonken, and Matthias J.P van Osch. *Contrast Agent Concentration Measurements Affecting Quantification of Bolus-Tracking Perfusion MRI*, Magnetic Resonance in Medicine 58:544-553, 2007.

[18] Cuenod CA, Balvay D. *Perfusion and vascular permeability: Basic concepts and measurement in DCE-CT and DCE-MRI.* Diagnostic and Interventional Imaging (2013), http://dx.doi.org/10.1016/j.diii.2013.10.010

[19] Xiangyu Yang and Michael V.Knopp *Quantifying Tumor Vascular Heterogeneity with Dynamic Contrast-Enhanced Magnetic Resonance Imaging: A Review,* Journal of Biomedicine and Biotechnology, 2011, http://dx.doi.org/10.1155/2011/732848

[20] Tobias Heye, Daniel T.Boll, Caecilia S. Reiner, Mustafa R. Bashir, Brian M. Dale, and Elmar M. Merkle. *Impact of Precontrast T_{10} Relaxation Times on Dynamic Contrast-Enhanced MRI Pharmacokinetic Parameter: T_{10} Mapping Versus a Fixed T_{10} Reference Value*, Journal of Magnetic Resonance Imaging, 2013

[21] Sean C.L. Deoni, Brian K.Rutt, and Terry M. Peters *Rapid Combined T_1 and T_2 Mapping Using Recalled Acquisition in the Steady State,* Magnetic Resonance in Medicine 49:515-526 (2003)

[22] Fernando Calamante, Evert-jan P.A Vonken, and Matthias J.P van Osch. *Contrast Agent Concentration Measurements Affecting Quantification of Bolus-Tracking Perfusion MRI,* Magnetic Resonance in Medicine 58:544-553 (2007)

[23] A.Jackson *Analysis of dynamic contrast enhanced MRI,* The British Journal of Radiology,77 (2004).

[24] JPB O' Connor, A.Jackson, GJM Parker, and GC Jayson, *DCE-MRI biomarkers in the clinical evaluation of antiangiogenic and vascular disrupting agents,* British Journal of Cancer, 189-195, 2007.

[25] Denis Hoa, *NMR Signal and MRI contrast* http://www.imaios.com/en/e-Courses/e-MRI/MRI-signal-contrast

[26] Donald W. McRobbie, Elizabeth A. Moore, Martin J. Graves, Martin R. Prince *MRI From Picture to Proton*, pages 30-46, Cambridge University Press, 2006.

[27] Denis Hoa, *Improving MRI contrast: Contrast agents*, http://www.imaios.com/en/e-Courses/e-MRI/Improving-MRI-contrast-Contrast-agents

[28] Liuquan Cheng , Xiru Li *Breast magnetic resonance imaging: kinetic curve assessment, Gland Surgery* 2013;2(1):50-53, doi: 10.3978/j.issn.2227-684X.2013.02.04

[29] Sofie Isebaert, Frederic De Keyzer, Karin Haustermans, Evelyne Lerut, Tania Roskams, Ilse Roebben, Hendrik Van Poppel, Steven Joniau, Raymond Oyen. *Evaluation of semi-quantitative dynamic contrast-enhanced MRI parameters for prostate cancer in correlation to whole-mount histopathology,* European Journal of Radiology 81:217– 222, 2012.

[30] Stephen Boyd, Lieven Vandenberghe, Convex Optimization, Cambridge University Press, 2009.

[31] Guido Gerig Lecture, CS 6320, Optical Flow I, University of Utah, Spring 2012 http://www.sci.utah.edu/~gerig/CS6320-S2012/Materials/CS6320-CV-S2012-OpticalFlow-I.pdf

[32] Steuard Jensen, An introduction to Lagrange Multiplier, 2009 http://www.physics.smu.edu/olness/ftp/misc/6321/NOTES/lag2.pdf

[33] Jan A.Snyman Practical Mathematical Optimization. An introduction to basic Optimization Theory and Classical and New Gradient-Based Algorithms,Springer 2005

[34] S.Dong MIT Internal Publications(Course Project) 18.086 Mathematical Methods for Engineers II,2006 *http://web.mit.edu/dongs/www/publications/projects/2006-05-23_18.086_ConstrainedOptimization.pdf*

[35]http://www.csc.kth.se/utbildning/kth/kurser/DD2427/bik11/DownloadMaterial/Lectures/LagrangeMult.pdf

[36] http://www.onmyphd.com/?p=kkt.karush.kuhn.tucker

[37] A. Ozdaglar, *Pseudonormality and a Lagrange Multiplier Theory for Constrained Optimization,* Ph.D. Thesis, January 2003, MIT, EECS Department.

[38] Denis Hoa, MRI Sequences http://www.imaios.com/en/e-Courses/e-MRI/MRI-Sequences

[39] Y.Xue, J. Yu, M. A. Rosen, R. Rengan, H. S. Kang, S. Englander, R. Mick, and H. K. Song *Enhanced perfusion measurement accuracy in DCE-MRI via improved baseline signal estimation,* Proceeding of the International Society of Magnetic Resonance in Medicine, 2011.

[40] http://www.spincore.com/T1IR/